ELASTIC DEFORMATIONS AND INSTABILITIES IN THIN FIBERS AND FILMS

Elastic Deformations and Instabilities in Thin Fibers and Films

By Adam Fortais, B.Sc, M.Sc

A Thesis Submitted to the School of Graduate Studies in the Partial Fulfillment of the Requirements for the Degree Doctor of Philosophy

McMaster University
Doctor of Philosophy (2021)
Hamilton, Ontario (Department of Physics and Astronomy)

TITLE: Elastic Deformations and Instabilities in Thin Fibers and Films
AUTHOR: Adam Fortais B.Sc, M.Sc (McMaster University)
SUPERVISOR: Dr. Kari Dalnoki-Veress
NUMBER OF PAGES: xi, 103

Abstract

Systems across nearly all length scales can experience elastic deformations. The details of how a system deforms is generally determined by i) the way stresses and loads are applied, ii) size, shape, geometry, and physical constraints, and iii) the material properties of the system. Although the physical forces causing deformations are often simple in origin, the interplay between these forces and the physical constraints of these systems can produce *instabilities* – situations where small changes in loading can cause large and sometimes surprising mechanical effects. From an application-based perspective, These effects can lead to interesting and useful techniques as well as sometimes beautiful patterns and features reminiscent of complex, natural systems. This thesis centres on three research manuscripts, each concerning different elastic instabilities observed in slender elastic fibers.

In the first paper (Chapter 3, published in the European Physical Journal E) we explore the effect of tension, compression, and torsion on slender fibers, and explain the looping and twisting behaviour observed with a simple linear elasticity model.

The second paper (Chapter 4, published in Physical Review Letters), presents a novel interaction between slender elastic fibers and liquid-air bubbles on the surface of a liquid bath. We find that for certain combinations of fiber and bubble (depending on size, thickness, material, etc), a fiber may partially penetrate and spontaneously wrap around the bubble at its liquid-air interface.

In the third paper (Chapter 5, to be submitted), considers the elastic response of coupled elastic systems with incompatible strains. In this case a thin film is pre-strained before a slender fiber is affixed to its surface, acting like a strut or support. Then, biaxial tension and/or compression is applied to the film, causing the fiber to buckle and rotate in and out of the plane of the film in, ultimately, predictable and controllable ways.

Lastly, an appendix is included, featuring several examples of the science writing I have done for less technical audiences, broadly related to the themes presented in this thesis.

Acknowledgements

Thus, I tend to compare our community of soft-matter theorists to the amateur painters of a hundred years ago - spending their Sunday afternoons in the park, and capturing a few simple scenes - involving their friends, their children, and those they love. I see no better style. - Pierre Gilles de Gennes

I had big plans for this section of the thesis. Of course I couldn't have done any of this without the help of my lab-mates, classmates, and TA-mates. Of course I couldn't have survived without the love and support of my family and friends (there is a lot of overlap in these thank-yous by the way, please see the Supplemental Information for a Venn Diagram). Of course I'd like to give each of you your own thank-you chapter, but unfortunately it looks like you'll all have to share this one page. Sorry (and thank you, of course)!

Now, for the serious, emotional part. As I look back on the path I walked over the last seven years, there were some very difficult moments. Reflecting on these times, I asked Kari, "Kari, when I look back on the path I walked over the last seven years, there were some very difficult moments. I see our footprints together and am grateful for the times you've been there for me, but I also see times where there were only one set of footprints. Why did I have to go through those times alone?" And to this, Kari said, "Adam, have you learned nothing about granularity? Look at the depth of the prints, those are the times I gave you a piggyback ride. Also, just look at the size, those clearly aren't your shoes..." "Oh yeah, that was awesome! Thanks!"

Kari, I wish I could thank you in some way proportional to the support and guidance you've given me, but I'm afraid that would not be possible. Thank you for taking a chance on me and not looking too closely at my grades coming out of undergrad. Thank you for indulging me in all of my weird pursuits and phases. Thank you for being a teacher and supervisor, but moreover, thank you for being a friend.

Thank you, all of you.

Contents

Abstract iii

Acknowledgements v

1 Introduction 1

1.1 Elasticity Theory: Extension, Compression, and Shear 4

1.1.1 Hooke's Law and Forces 4

1.1.2 Poisson Effect 7

1.1.3 Hooke's Law and Energy 10

1.1.4 Shear 12

1.2 Elasticity Theory: Bending and Twisting 14

1.2.1 Bending Moment 14

1.2.2 Bending Energy 18

1.2.3 Torsion 19

1.3 Elasticity Theory in Three-Dimensions 21

1.3.1 Hooke's Law in Three-Dimensions 22

1.3.2 Slenderness and Plane Stress 24

1.4 Capillarity and Other Forces 25

1.4.1 Surface Tension, Capillarity, and Interfacial Energy 26

1.5 Comparing Forces at Different Scales 32

1.5.1 Surface Tension and Gravity 33

1.5.2 Elasticity and Surface Tension 34

1.6 Elastic Instabilities 36

1.6.1 Buckling of Slender Structures: Critical Load and Stability . 38

1.6.2 Energy Methods 40

2 Experimental Methods 43

2.1 Sample Preparation 44
2.1.1 Polymers 44
2.1.2 Fibers 44
2.1.3 Films 48
2.2 Experimental Methods 50
2.2.1 Manipulating Fibers 50
2.2.2 Manipulating Films 50
2.3 Sample Measurements 51
2.3.1 Imaging 51
2.3.2 Measuring Forces 52

3 Energy release by twisted, compressed fibers via hockling and writhing 55

4 Spontaneous elastocapillary winding of thin elastic fibers in contact with bubbles 65

5 Buckling of elastic fibers confined to a thin elastic film 73

6 Discussion and Conclusions 81

A Science Writing 87

List of Figures

1.1 A rectangular prism extends by Δx in response to a force F applied to one end. 6

1.2 A rectangular prism undergoes extension in response to an applied stress. It contracts in the directions perpendicular to the extension according to its Poisson ratio. 8

1.3 A rectangular prism with height l and cross-sectional area A experiences a shearing force F on its top surface, resulting in a deformation that reaches a maximum magnitude of Δx at its top surface. 13

1.4 a) A beam before bending. b) The beam has width $2r$ and length L, and can be thought of as a series of uniformly spaced plates with a neutral axis passing through the mid-line of the beam. c) Upon bending, the spacing of the plates above the neutral axis (the convex side) increases while the spacing of the plates below the neutral axis (the concave side) decreases. The curvature at any point along the beam can be defined by its curvature κ or its radius of curvature ρ, causing an internal bending moment M (red arrows). 15

1.5 A "cantilever" beam with length L and arbitrary cross-sectional area A has been bent by a force F applied at its end causing a deflection $w(x)$. 16

1.6 A beam with arbitrary cross-sectional area A has been bent by a force F into an orientation with curvature κ that varies along its arclength s 18

1.7 A cylindrical beam with cross-sectional radius r and length L experiences a torsional force τ, causing one end beam to twist by θ radians relative to the other end. 19

1.8 A schematic of the intermolecular interactions of liquid molecules within the bulk of the liquid compared to the surface. The molecules at the surface of the bath are in an energetically unfavorable state compared to the ones in the bath. 26
1.9 A three-sided wire frame and a movable bar of length L support a liquid film. A force F is required to move the bar and increase the surface area of the liquid film by $2Ldx$. 28
1.10 A liquid droplet sits atop a flat, smooth, non-deformable solid surface. In the absence of other forces, the droplet takes on the shape of a spherical cap with contact angle θ_y defined by the competition of interfacial energies. 29
1.11 Elastocapillary deformations at different scales. a) Even stiff or thick solids can experience capillary-based shear, though the characteristic length scale of these deformations l_s may be small and isolated to the surface of the solid. Softer materials experience larger deformations. b) Compliant materials (which are not necessarily soft, but are thin) can experience stretching with characteristic strains S or c) bending with a length scale l_B. 35
1.12 An elastic beam buckles in response to being subjected to a compressive force F. 38
1.13 A schematic plot of the elastic energy in a fiber as a function of tension/compression for its initial twisted state (U_i) and final bent state (U_f). By calculating $\Delta U = 0$ (circled) we can predict at what point it becomes energetically favorable for the fiber to deform into its bent orientation. 41

2.1 A micropipette is dipped into a liquid polymer and pulled out, resulting in thin fiber. 46

2.2 a) A thin polymer film is made by placing a polymer solution on a mica substrate and spun at several thousand revolutions per minute. b) The resulting polymer film is dipped into a water bath trapping water between the polymer film and the mica. c) The polymer sample is placed film-side-down on a new substrate. The mica is lifted away from the new substrate, leaving behind the polymer film which is now adhered to the new substrate. 49
2.3 A polymer fiber is attached to two posts. The left post can be translated and rotated. The right post is a force transducer that deflects as a response to tension in the fiber. 51
2.4 a) Top-down view of the biaxial strain device. An X-shaped elastic sheet with a hole in the centre is connected to four translational stages. A thin film adheres to the sheet and a polymer fiber adheres to the film. b) The translational stages allow for tunable biaxial stress. 52
2.5 Side view of the biaxial strain device with rotating camera lens. The rotating lens can image the polymer film sample at multiple angles. 53

6.1 A polymer fiber with intrinsic curvature. A mm-scale ruler is included for scale. 84

Chapter 1

Introduction

"Science" is used in all sorts of ways. Some refer to science as a domain of study which includes biology, chemistry, physics (and many other fields), often contrasted with the "Arts". I like to think of it as a system or a set of philosophical techniques designed to understand the natural world, such that "science" is less a *thing* and more a *process*. Sometimes, informally, people may use it as a verb (though slang usage like "sciencing a set of samples" is usually abandoned early during a young scientist's career). But regardless of how one thinks of it, I believe most people would agree that the purpose of scientific inquiry is to uncover Nature's hidden machinery by discovering the way things work. Compared to other branches of science though, physics can seem a little bit different – funny, even. On one hand, physics could be considered the science of everything. By knowing the universe of matter, energy, and forces on the most fundamental level, one could argue that physics could explain how *everything* works. In practice though, such a theory would be preposterously complicated and probably not as useful as one would hope. What tends to be more useful is assuming the system has a certain level of complexity (for example, in this thesis we will generally treat liquids and solids as bulk materials, not collections of individual molecules or atoms), and apply the techniques of physics in order to understand the system's behaviors.

In this thesis I will make reference to a wide range of systems that aren't always thought of as the domain of "physics". As I alluded to above, physics alone is not always the right tool for the job. DNA replication is a lot easier to understand if we make the assumption that fundamental particles can form atoms which can form

the molecules that make up the rungs of the DNA ladder. But science can be funny. Parallel fields of science may have grown out of an attempt to simplify certain types of questions and make our collected knowledge more useful, but sometimes there are problems that resist being solved with the tools of that field. In times like this, trimming away reality's excess (like gravity, friction, air resistance, chemistry, etc) can shed new light on a problem. At its core, this is what this thesis is about – finding the key physical details that bring these complicated problems into focus.

Consider again, a strand of DNA. The "double-helix" shape is perhaps one of the most iconic symbols of biological research, evoking ideas of genetic sequencing and cloning for many people. But in some ways, it's not the most accurate way to think of deoxyribonucleic acid. Another representation of DNA could have you imagining it as a microscopic tangle of spaghetti noodles. In its natural state, DNA is incredibly long ($\sim$ 3 m) compared to the diameter of the nucleus it's usually confined to ($\sim$ 6 μm) [1, 2]. The trick to packing it all in is to form tangles and snarls of spaghetti-like globules [3–10]. And what is perhaps more surprising is that the way the molecule tangles actually determine how it codes for different proteins [11–13]. How DNA functions is a complicated question that may seem like a purely biological or chemical problem. Yet, how DNA molecules (and other strand-like systems like plant tendrils, tangled cables, yarn ply, etc. [14–23]) mechanically bend, twist, and wind is an aspect of the problem that physics is well suited to, and is related to the results presented in Chapter 3.

When it comes to identifying the parts of a physical system to incorporate into a model, it is useful to consider how the system's scale influences its mechanics. When engineers build large structures, they need to consider how the structure will respond to the stresses caused by gravity. As the scale of the structure decreases, the influence of gravity typically decreases as well. On small enough scales (like the experiments contained in this thesis), the force of gravity is small enough to be inconsequential to the mechanics of the system. Likewise, at certain scales, forces that would usually be negligible can become significant. Elastocapillarity has emerged as an exciting and active field over the last few years, focusing on the competition between elastic forces and surface tension effects [24–29]. In day-to-day scenarios, discussion of surface tension often begins and ends at liquids. For

example, surface tension is what lets insects skate across the surface of a pond, defines the shape of liquid droplets, and causes the meniscus often seen in glasses of water [30–32]. But on small scales or coupled with soft solids, surface tension can cause measurable and significant elastic deformations as well [29,33–35]. Thin elastic sheets have been shown to bend, fold, crumple, and stretch in interesting and ultimately predictable ways [36–46]. Hairs and fibers can be made to clump together or even coil and wind spontaneously under the influence of surface tension [47–54]. In fact, many small biological systems are overwhelmingly defined by surface tension [17, 55, 56]. Chapter 4 focuses on such a system, exploring the surprisingly dynamic interaction between thin elastic fibers and liquid bubbles.

Of course, natural systems do not *decide* what scale they develop on – nature does what it will and scientists are left to make sense of it all. But scientists can take inspiration from nature and apply what we learn to new technologies. For instance, the push to smaller and smaller devices and the promise of "lab on a chip" technologies has made microfluidics, self-assembled structures, and flexible electronics attractive areas of development, but fabricating tiny devices is only one piece of the puzzle [57–62]. Manipulating these devices on small scales is also a challenge. Taking advantage of elastic instabilities and elastocapillarity, researchers have been able to create self-propelled nano-robots, micropatterning techniques, moisture collection tools, and unique, self-actuating structures [63–67]. With this in mind, Chapter 5 explores the way deformations to thin elastic membranes can be controlled with fiber-based elastic instabilities.

The research contained in this thesis draws inspiration from many natural and human-made systems, and even though these systems may span different size scales and can be made of many different materials, all of the experiments are linked by a common thread. All of these systems exhibit similar behaviour to simple elastic objects under stress. When applied to the right natural system, the results within this thesis can provide predictions based on theoretical and experimental evidence that will hopefully help future researchers understand more complicated real-life phenomena. The work in this thesis is presented in a "sandwich" format, where the original, peer-reviewed research resulting from my graduate studies is presented in between introductory and supporting information, and concluding remarks on

the presented work. The first chapter is intended to introduce the relevant physics and theoretical techniques used throughout the thesis. The second chapter presents the experimental techniques used in the following studies, and elaborates on some of the details that could not find space in the peer-reviewed manuscripts. The next three chapters comprise the centerpiece of the thesis and contain the original research performed in support this degree. The final chapter culminates with suggestions for possible directions this research can go, and ways to expand the contained results. Lastly, an appendix is included, featuring several examples of the science writing I have done for less technical audiences, broadly related to the themes presented in this thesis.

1.1 Elasticity Theory: Extension, Compression, and Shear

Much of the theory in this section and indeed in this thesis is derived from introductory elasticity. Because humanity has always had a need to apply mechanical forces to objects, introductory texts on the subject are numerous. For the reader completely new to the physics of elasticity who is inspired to learn more about the subject, any first-year physics textbook will have several chapters devoted to the study. Beginning here will provide a typical learning path typical of an undergraduate education. However, a more committed reader may find Timoshenko's *Theory of Elasticity* to be a more complete and comprehensive starting point [68]. In this thesis I attempt to find a middle ground between the two approaches while incorporating the results of modern research that more directly inspired the work presented here.

1.1.1 Hooke's Law and Forces

Hooke's law is a phenomenological model that relates extension (or compression) to the force required to affect such an extension (or compression) and in a sense, is the centrepiece of this thesis. It was originally published in 1676 by British

physicist Robert Hooke in the form of a Latin anagram [1], "*ceiiiinosssttuv*" [69]. Two years later he provided the unscrambled theory, "*ut tensio, sic vis* " which means "as the extension, so the force". A more explicitly (and less cryptic) version of Hooke's law can be written as such:

$$F = k\Delta x. \tag{1.1}$$

In this equation, F is the applied force, k is a stiffness constant that depends on the size, shape, and material properties of the object in question, and Δx is the change in length of the object when F is applied. Notice that in this equation, the extension of the object is linearly related to the force being applied, doubling F doubles Δx. As the extension, so the force. Likewise, the equation does not differentiate between extension or compression and is also valid when $\Delta x < 0$.

The proportionality constant, k, is typically presented in units of Newtons per meter, and relates extension to force. It is often called the stiffness constant, or spring constant, and quantifies how difficult it is to stretch or compress the object in question. Since k can vary from object to object, k is often determined experimentally. However, it is possible to calculate k by considering the object's size and shape, and the intrinsic stiffness of the material that it is made from. Determining k, or the stiffness of materials, will be a recurring theme throughout this thesis so we will not discuss it in detail now.

It is worth noting some of the simplifications inherent in using Equation 1.1 to describe a system. First, it assumes that F is linear with respect to Δx. In reality, most materials exhibit some stiffening or softening when they are stretched, and particularly during large deformations. This detail can be added to Equation 1.1 in a number of different ways but often this assumption will hold for elastic materials undergoing small extensions. Perhaps the biggest simplification made within Equation 1.1 though, is how it deals with the size and shape of the object. Equation 1.1 is essentially a 1-dimensional theory that can be applied to three-dimensional objects; it only describes the absolute distance of extension or

[1] Apparently staking claim to a theory was important to 17th century scientists, but sharing the theory was not; hence the practice of publishing work in the form of a secret code was common.

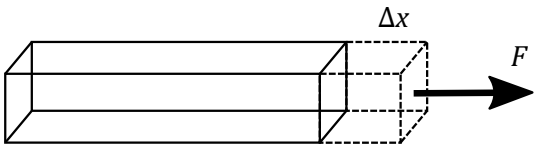

FIGURE 1.1: A rectangular prism extends by Δx in response to a force F applied to one end.

compression in one dimension, treating k as a phenomenological constant (a term that is fit into the model based on experimental observations). However, k can be related to real, measurable properties of elastic materials, like its geometry and intrinsic stiffness, which we now properly identify as the material's Young's modulus, E.

To quantify an object's E, we can relate the force required to deform the object to the object's size and shape. Consider a rectangular prism made of some unknown elastic material with length x_0 and cross-sectional area A_0. A stress $\sigma_x = F/A_0$ normal to A_0 is applied to the ends of the prism. As a reaction to σ_x, the length of the rectangular prism increases by Δx, and we can define the strain as,

$$\varepsilon_x = \Delta x / x_0. \tag{1.2}$$

Relating stress to the strain it causes gives the following relationship:

$$\sigma_x = E\varepsilon_x. \tag{1.3}$$

Through dimensional analysis, we can see that E has units of $\mathrm{N/m^2}$ or Pa, and is an intrinsic property of the material the object is made of. With this in mind, we can re-write Equation 1.1 in terms of E,

$$F = EA_0\varepsilon_x. \tag{1.4}$$

What we have done so far is start with a simple model of elasticity and added features to bring the model more in line with our real-life observations. Specifically, the observation that two objects made from the same material won't respond in the same way to the same force if they have different sizes and shapes. There

is another simple observation we can make while stretching or compressing an elastic material that has so far not been included in this model. Were you to stretch an elastic band, what you would find is that in addition to an extension, the elastic band also experiences a contraction perpendicular to the applied force. This phenomenon is known as the Poisson effect and is considered next.

1.1.2 Poisson Effect

When a stress is applied to a material, it will experience a strain and become deformed. For example, if a block with a volume $V_0 = L \times W \times H$ is subjected to a force along the direction of L, its length will change by $\Delta L = \varepsilon L$, resulting in a new length $L' = L + \Delta L$ and its volume will also change accordingly: L, $V' = L' \times W \times H$. While some materials (like cork and some types of foam mattresses) appear to follow this behavior, other materials (like polymers and waterbeds) will experience additional deformations in order to minimize the system's changes in volume. In fact, real materials exhibit the full range of behaviors when stressed, from decreasing in volume, maintaining a constant volume, and in rare cases even increasing in volume [70, 71]. This kind of volumetric change in response to strain is called the Poisson Effect, and is often a result of a material's molecular structure.

Consider again our compressed block. If we do not know what material it's made from, we cannot tell if $\Delta V = V' - V_0$ will be positive, negative, or zero. But what we can say is the mass of the block will remain the same. So, for our block to exhibit a change in volume, it must also experience a change in density; a property related to the packing of the molecules that make up the material. In many cases (especially throughout this thesis) we wish to ignore molecular properties and treat our systems as being made of a continuous bulk material. So instead of considering what is happening at the molecular level, we can instead use an experimentally determined material property – the Poisson ratio [2].

[2] Like many scientific concepts, this one was named after a prolific European mathematician. In this case, French mathematician Siméon Denis Poisson, who was active during the turn of the 19$^{\text{th}}$ century. Despite being a pioneer in the study of fluid mechanics and having the name "Poisson", he was not a fish.

The Poisson ratio ν of a material is a unitless parameter defined by the negative change in strain in the directions perpendicular to an applied stress (transverse: $\varepsilon_{\text{trans}}$) as a function of the strain in the direction of the applied stress (axial: $\varepsilon_{\text{axial}}$):

$$\nu = -\frac{\mathrm{d}\varepsilon_{\text{trans}}}{\mathrm{d}\varepsilon_{\text{axial}}}. \tag{1.5}$$

By inspection, we see that if the axial and transverse strains are independent, $\nu = 0$. If a compression in the axial direction causes an expansion in the transverse directions (or if an extension in the axial direction causes a compression in the transverse directions), $\nu > 0$. Of course, we can also use ν quantitatively to determine how the dimensions of an object is affected by an axial strain.

FIGURE 1.2: A rectangular prism undergoes extension in response to an applied stress. It contracts in the directions perpendicular to the extension according to its Poisson ratio.

If a stress σ_x is imposed on our block that results in a strain ε_x, we can describe its new dimension in the $\hat{x}$-direction as $L' = L + \Delta L = L\varepsilon_x$, and the change in length of an infinitesimal slice of our block is $\mathrm{d}L = L\mathrm{d}\varepsilon_x$. Likewise, the response of our block in the transverse directions can be described by $W' = W + \Delta W$ and $H' = H + \Delta H$ and $\mathrm{d}W = W\mathrm{d}\varepsilon_y$ and $\mathrm{d}H = H\mathrm{d}\varepsilon_z$ respectively. Note that we will assume the Poisson effect in each of the transverse directions is identical. Then, from Equation 1.5 we can relate ε_y and ε_z to ε_x:

$$-\nu \int_{L}^{L+\Delta L} \frac{\mathrm{d}x}{x} = \int_{W}^{W'+\Delta W} \frac{\mathrm{d}y}{y} = \int_{H}^{H'+\Delta H} \frac{\mathrm{d}z}{z}, \tag{1.6}$$

where we have already used the fact that $\mathrm{d}x = x\mathrm{d}\varepsilon_x$ in each direction. Performing these integrals and exponentiating our result gives,

$$(1+\varepsilon_x)^{-\nu} = 1 + \varepsilon_y = 1 + \varepsilon_z. \tag{1.7}$$

Finally, making an approximation consistent with our small strain, linear elasticity requirements,

$$-\nu\varepsilon_{\text{axial}} \approx \varepsilon_{\text{trans}}. \tag{1.8}$$

Returning to the volume of our block under a stress σ_x, we find (to a first-order approximation),

$$\frac{\Delta V}{V} = (1 - 2\nu)\varepsilon_x. \tag{1.9}$$

Now we can finally put some real numbers to our qualitative discussion at the beginning of this section. An object whose strains in three-dimensions are completely independent will have $\nu = 0$, and the new volume corresponding to a strain ε_x is $V' = V(1+\varepsilon_x)$. On the other hand, a material that conserves its volume perfectly results in $\nu = 0.5$.

Various polymers are used throughout this thesis, all of which exhibit a Poisson ratio of $\nu \approx 0.5$, which puts them in a class of materials considered "incompressable" [68, 72]. Incompressibility is an approximation often used in fluid mechanics to describe liquids experiencing low to moderate stresses, and can be justified by comparing the mobility of liquid molecules to the ability to change the molecule's packing density [32]. With many liquids, the molecules that make them up are usually mobile – many are made up of small molecules held together by relatively weak inter-molecular interactions (this will be further explained in Section 1.4.1). This weak adhesion between molecules and their high mobility also means that molecules are relatively free to find conformations that optimize the balance of attractive and repulsive forces between molecules. In cases like this, it is more difficult to reduce the material's inter-molecular spacing than it is for the molecules to re-organize and find free volume to occupy (flow). In this sense, polymers can be a lot like liquids (and at high enough temperatures, are liquids). Compared to something like a crystal, polymer molecules can be quite mobile, exhibiting both liquid-like and solid-like properties. Depending on the polymer, small deformations can be accommodated by flow and reorientation of the polymer molecules, much like a liquid.

Materials with more regular and rigid inter-molecular spacing (like metals or

crystals) however, are often much less mobile, often held together by strong chemical bonds. In this case, an applied stress is more likely to flex and strain the network of bonds holding the material together, which can increase or decrease the distance between these bonds. Exactly how these materials respond varies, but many metals have Poisson ratios around $\nu \sim 0.33$, exhibiting some coupling between perpendicular strains, potentially causing changes in intermolecular density and volume.[3]

Depending on the geometry of the system and the magnitude of the strain, the Poisson effect may be small, but it can also significantly affect the deformations experienced by an object [60, 73–75]. In Chapter 5, an ultra-thin elastic film undergoes biaxial strain where all four sides of the pseudo-two-dimensional sheet are held fixed at their edges. When the sheet is stretched along one axis, the Poisson effect would have the other axis contract. However, being fixed on all four sides hinders the contraction, increasing the stress in the axis perpendicular to the applied strain instead. In a way, this acts like a stiffening that a sheet otherwise un-fixed on its sides would not experience.

1.1.3 Hooke's Law and Energy

So far we have considered stress and strain in the context of forces. Force is an intuitive starting point, but much of the analysis contained in the following chapters uses the concept of potential energy and work. We will now consider how energy can be stored and released in an elastic system.

If a stress is applied to a *perfectly elastic* material and it is deformed via some strain ε, we assume it will return to its original shape once the source of stress is removed. Energy is put into the material through work (applied stress) which is stored as elastic potential energy. When the stress is removed, the elastic potential

[3] I mentioned cork and foam mattresses previously as materials with $\nu \approx 0$. This is less about inter-molecular interactions and more about the microscopic structure of these materials. Cork and foam are materials permeated by many air pockets. Stresses applied to such materials can deform these air pockets in one direction without causing much distortion in the transverse directions. A useful property when corking wine bottles and trying not to disturb a sleeping partner.

energy is released, restoring the material to its original dimensions. Under the assumption of a perfectly elastic material, we can exactly equate the work performed on the material W to the change in elastic energy stored by the material,

$$W = \Delta U, \tag{1.10}$$

where $\Delta U = U_\mathrm{f} - U_\mathrm{i}$ is the difference between stored elastic energy before and after work has been done on the system. We can find ΔU by integrating the applied force F along the distance that the material is strained, defined by ε,

$$\Delta U = \int_{\varepsilon_0}^{\varepsilon} \int_A \sigma \mathrm{d}A' \mathrm{d}\varepsilon', \tag{1.11}$$

where $\sigma \mathrm{d}A' = \mathrm{d}F$ is the force applied to each increment of area $\mathrm{d}A'$ that the force is applied over. A few things we can see immediately is that the geometry, as well as the elastic modulus of the material, will influence the work required to strain the material, and how much energy the material will store elastically for a given strain. This makes sense, since we would expect a larger, stiffer material would be harder to deform than a smaller, softer one. However, we can also see that it is possible σ may not be uniformly applied over A. This idea can be developed to model the forces and energies related to bending and will be covered is Section 1.2.1. In the mean time, if we assume σ is constant with respect to A' and $\sigma = E\varepsilon$,

$$\Delta U = \int_{\varepsilon_0}^{\varepsilon} EA\varepsilon' \mathrm{d}\varepsilon'. \tag{1.12}$$

Performing the integral with respect to strain gives,

$$\Delta U = \frac{1}{2} EA(\varepsilon^2 - \varepsilon_0^2). \tag{1.13}$$

Hooke's law is an astoundingly simple model that does a remarkably good job of describing a wide range of systems. This might not be all too surprising given the constraints we've placed on the systems we use Hooke's law to model. Knowing when these constraints are satisfied is crucial to understanding when Hooke's law is valid, so it is worth restating them here:

- Force is linear with respect to extension/compression (as the extension, so the force);
- Extensions/compressions are relatively small and perfectly elastic.

As a final example of the ubiquitous nature of Hooke's law, a reasonable approximation of a solid's elastic modulus can be calculated by applying Hooke's law to the intermolecular interactions making up the solid. The attraction between molecules or even entropically unfavorable stretching of polymers can be described by many different potential energy functions, but for small deformations, many of these functions can be approximated as being Hookean [31,76,77]. In other words, Hooke's law can be used on a microscopic level to approximate the stiffness constant required when using Hooke's law on a macroscopic scale. Of course, this is just a consequence of Hooke's law having a simple (linear) mathematical form. In the next section we will continue treating our materials as Hookean, but expanding the types of deformations we impose on our materials.

1.1.4 Shear

Place the palms of your hands together and rub them back and forth, like you are trying to warm them up. That is shear. A standard analogy used in many engineering textbooks to describe shear is that of a deck of cards being forced to slide past one another such that they extend in a direction parallel to the plane of the cards. In both of these examples, we are considering discrete objects with some amount of friction between them. For our purposes though, it is more useful to think of these discrete slices as being glued together and having friction replaced by the internal elasticity of the glue that resists deformation. The force per unit area required to create this extension then, is called the shear stress and is defined as $\tau = F/A$, where A is the area parallel to the direction of τ. However, notice in Figure 1.3 that while the change in length Δx from shear stress is constant across A, it varies with l. Put into terms of our deck of cards, each card will experience the same displacement relative to the card below it, but a different displacement relative to the bottom card. Like with linear stress and strain, we would like to be able to quantify shear stress and strain in terms of material stiffness, independent

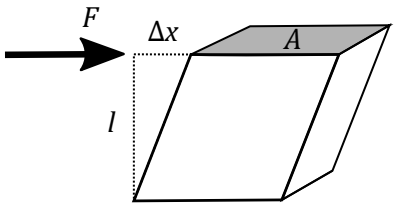

FIGURE 1.3: A rectangular prism with height l and cross-sectional area A experiences a shearing force F on its top surface, resulting in a deformation that reaches a maximum magnitude of Δx at its top surface.

of geometry. In this case, we can define the shear strain,

$$\gamma = \frac{\Delta x}{l}. \tag{1.14}$$

Referring again to Figure 1.3, we can see that γ is constant regardless of where along l or A we look.

We can enact a similar strategy with F, scaling it by the surface area over which it acts,

$$\tau = F/A. \tag{1.15}$$

τ is called the shear stress, and like linear stress, τ has units of $\mathrm{N/m^2}$.

Finally, we can relate γ to τ like we did in the case of extension and compression,

$$\tau = G\gamma, \tag{1.16}$$

where G is the shear modulus; a parameter analogous to the elastic modulus E. Though E and G have the same units and represent material stiffness, they are not the same. However, they are closely related via the material's Poisson ratio [68],

$$G = \frac{E}{2(1+\nu)}. \tag{1.17}$$

For many polymer materials with $\nu \approx 0.5$, this gives the relation $G = E/3$.

Although we can consider compression/extension and shear independently, it is more typical for real systems to experience some combination of these stresses.

Additionally, these stresses can vary over the cross-sectional area of an object, leading to more complicated deformations. We cover these deformations next.

1.2 Elasticity Theory: Bending and Twisting

So far we have spent a considerable amount of time focusing on stress and strain in the form of compression, extension, and shear, but of course there are other modes of deformation that a material can experience. In this section we will consider bending and twisting within the linear, elastic regime. We will apply these results to model systems similar to those featured in Chapter 3, Chapter 4, and Chapter 5. Later we will see how the geometry and material properties of our systems along with the way we apply stresses to them, can result in interesting, useful, and sometimes counter-intuitive deformations. Where possible, we will relate these interesting behaviors to the real-life systems and phenomena in nature and engineering which motivate the later chapters. But before we get too far ahead of ourselves, let's start with bending.

1.2.1 Bending Moment

Bending has a lot in common with extension and compression. In fact, if we limit our scope to small deformations within the realm of linear elasticity, we can model bending as the sum of linear strains that vary along the cross-sectional area of the object we are bending.

We can visualize the relationship between bending and extension/compression by considering an elastic beam of length L and width $2r$. If a load were applied to the beam such that it formed a circular arc with constant curvature κ, the strain within the beam varies from positive to negative along the cross-section of the beam, as shown in Figure 1.4. If we think of our beam as a sequence of thin cross-sectional slices, we can consider the strain in terms of small distances $\mathrm{d}s$ between adjacent slices. When the beam is unbent, $\mathrm{d}s$ is constant along the beam's length as well as over each slice's area. If the beam is bent, we can define an axis passing through the centre of the slices as a "neutral axis". This is a length passing through our beam such that small curvatures neither increases nor

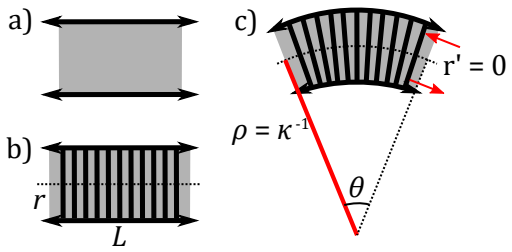

FIGURE 1.4: a) A beam before bending. b) The beam has width $2r$ and length L, and can be thought of as a series of uniformly spaced plates with a neutral axis passing through the mid-line of the beam. c) Upon bending, the spacing of the plates above the neutral axis (the convex side) increases while the spacing of the plates below the neutral axis (the concave side) decreases. The curvature at any point along the beam can be defined by its curvature κ or its radius of curvature ρ, causing an internal bending moment M (red arrows).

decreases its length. If we were to define an axis slightly above the neutral axis (tending toward the convex side of our bent beam), we would see an increase in length ($\varepsilon > 1$). Likewise, below the neutral axis (on the concave side) we would expect a decrease in length ($\varepsilon < 1$). The exact amount of strain experienced by any axis we draw through our bent object will then be defined by the curvature κ and the distance it is from the neutral axis, r',

$$\varepsilon = \frac{(r' + \rho)\theta - \rho\theta}{\rho\theta} = \frac{r'}{\rho} = r'\kappa. \tag{1.18}$$

We can think of Equation 1.18 as describing the linear extension or compression at a particular point along the length of an infinitely thin fiber.[4] More commonly though, we will be considering objects with finite thickness such that $\varepsilon(r') = r'\kappa$ needs to be evaluated over the cross-sectional area A of the object. Note that despite $\varepsilon(r')$ taking on a range of values from positive to negative over A, it will generally cause an elastic restoring force (proportional to the elastic modulus E) that acts to unbend the object, regardless of where along A one looks. In particular, the restoring force acts as a rotational force acting around the neutral

[4]It is worth noting that for large κ, "shearing" may become significant within the object, in which case a more comprehensive description of elasticity is required. This will be commented on later in this section, but for a more detailed discussion on non-linear elastic theory and large deflections, one can refer to Theory of Elasticity by Timoshenko [68].

axis, as shown in Figure 1.5. Therefore, this restoring force can be calculated by integrating the torque around the neutral axis caused by ε,

$$M = E \int_A r'^2 \kappa \mathrm{d}A'. \tag{1.19}$$

Although κ and A can vary along the length of the object, for any particular location along the objects length we will assume these values are constant, allowing us to find,

$$M(x) = E\kappa \int_A r'^2 \mathrm{d}A', \tag{1.20}$$

where the leftover integral is a parameter often referred to as the second moment of area I of an object. I describes the distribution of matter around the neutral axis and, conveniently, has been computed and tabulated for many common geometries such that it is usually easy to look up [78]. Thus, we arrive at a convenient and compact expression for the bending moment of an object,

$$M(x) = EI\kappa. \tag{1.21}$$

The bending moment $M(x)$ is an important and useful quantity as it is essentially

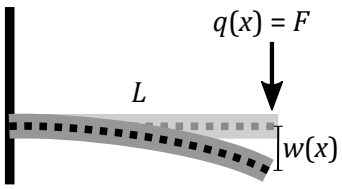

FIGURE 1.5: A "cantilever" beam with length L and arbitrary cross-sectional area A has been bent by a force F applied at its end causing a deflection $w(x)$.

Newton's third law for bent, elastic objects. Recognizing that Equation 1.21 describes the bending forces *internal* to the object in the absence of external forces, we can consider the response of an object, like the beam shown in Figure 1.5, to an external load $q(x)$ applied perpendicular to the neutral axis of the object. For example, a beam of length L held fixed at one end, subjected to a perpendicular load $q(L) = F$ applied perpendicular at its end will undergo some deflection. In

equilibrium, the applied load will be compensated by $M(x)$ such that,

$$\frac{\mathrm{d}^2 M(x)}{\mathrm{d}x^2} = q(x). \tag{1.22}$$

In much of this thesis, we will make the assumption that curvatures are small, deformations are perfectly elastic, and beams are uniform. This leads to the Euler-Bernoulli beam equation,

$$EI\frac{\mathrm{d}^4 w(x)}{\mathrm{d}x^4} = q(x), \tag{1.23}$$

where we've approximated the curvature $\kappa = \mathrm{d}\theta/\mathrm{d}x \approx \mathrm{d}^2 w/\mathrm{d}x^2$. Solving this differential equation and inserting the relevant boundary conditions allows us to solve for the deflection $w(x)$ along the beam, and in the case of the cantilever in Figure 1.5, results in a maximum deflection where the force is applied,

$$w(L) = \frac{FL^3}{3EI}. \tag{1.24}$$

The technique demonstrated above is one of the more simple cases of balancing the internal and external bending moments. Part of what makes this example so simple are the approximations and assumptions we have included in the solution, like linear elasticity, pure bending, and small deformations. For more complicated systems, the strategy can be expanded to include rotational inertia (first introduced by Rayleigh) as well as shear (Timoshenko-Ehrenfest beam theory) by adding an additional (coupled) differential equation to Equation 1.22,

$$\frac{\mathrm{d}w}{\mathrm{d}x} = \phi - \frac{1}{KAG}\frac{\mathrm{d}}{\mathrm{d}x}\left(EI\frac{\mathrm{d}\phi}{\mathrm{d}x}\right), \tag{1.25}$$

where K is called the Timoshenko shear coefficient, G is the shear modulus, and ϕ is the angular deflection that the plane of A experiences. In general, the effect of introducing the extra mode of deformation to the system is to lower the stiffness of the beam. However, if G is taken to be arbitrarily large, the object can become fully resistant to shearing effects and we recover the Euler-Bernoulli equation.

Though Euler-Bernoulli beam theory can be too simple to describe some systems, the experiments in this thesis are in fact well described by this more basic

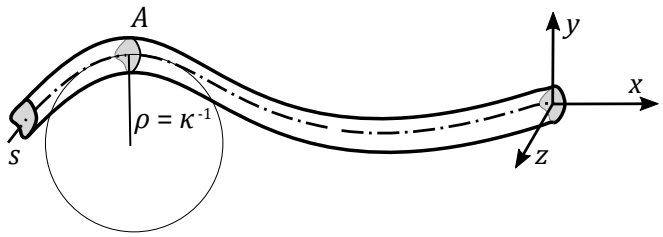

FIGURE 1.6: A beam with arbitrary cross-sectional area A has been bent by a force F into an orientation with curvature κ that varies along its arclength s

model, addressing explicitly the times when the basic model appears to fail.

Naturally, if extension and compression can store elastic potential energy in a system, so can bending. Next we will consider the elastic potential energy stored in (or work required to illicit) the bends in our system.

1.2.2 Bending Energy

In Section 1.1.3 we calculated the stored elastic energy in a material as a function of its geometry, elastic modulus, and strain. In that section, we took advantage of the assumption that strain is uniform throughout the material. In the case of bending, we know the strain over an object's cross-sectional area varies (see Section 1.2.1), but it is of course also possible that the curvature changes along the length of the material like in Figure 1.6.

The strategy then, is to essentially use Hooke's law to determine the total strain energy over each infinitesimally thin slice of cross-sectional area. This is actually easier than it may sound, since we did most of the hard work while calculating the bending moment $M(x)$. Rather than calculating the torque around the neutral axis $r' = 0$, we can first find the strain energy in a thin slice by integrating $U_B = 1/2(EA\varepsilon^2)$ over the cross-sectional area,

$$\mathrm{d}U_B = \frac{1}{2}\int_A E\varepsilon^2 \mathrm{d}A'. \tag{1.26}$$

Using the result from Equation 1.18 we find,

$$\mathrm{d}U_B = \frac{1}{2}E\kappa^2 \int_A r'^2 \mathrm{d}A' = \frac{EI\kappa^2}{2}. \tag{1.27}$$

The final step, then, is evaluating Equation 1.27 along the length of our object. In the case of an object with constant curvature, this ends up being a matter of multiplying $EI\kappa^2/2$ by the object's length. Otherwise, if κ varies with the object's arclength s, the solution will require evaluating κ^2 at each point along s.

1.2.3 Torsion

Just as a description of bending could be derived from differences in strain across an object's cross-sectional area, torsion can be described as a type of shear deformation that also varies across the cross-sectional area of our material. In this section we will develop a description of torsion for a uniform, elastic beam in terms of shear.

A uniform, elastic beam of length L and radius r is shown in Figure 1.7. A torque τ is applied to one end of the beam such that the one end is rotated an angle θ relative to the other end. Taking just a thin, circular slice of our beam,

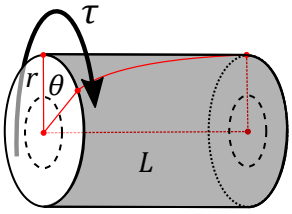

Figure 1.7: A cylindrical beam with cross-sectional radius r and length L experiences a torsional force τ, causing one end beam to twist by θ radians relative to the other end.

we can calculate its shear strain relative to an adjacent thin slice. Since the beam rotates about its long axis, each point that is at a the same distance r' from the rotational axis will experience the same γ,

$$\gamma' = r'\frac{\theta}{L}. \tag{1.28}$$

Since the strain is uniform for a specific r', we can calculate γ for the full strip with radial thickness $\mathrm{d}r'$,

$$\mathrm{d}\gamma = 2\pi r'\gamma'\mathrm{d}r', \tag{1.29}$$

$$\mathrm{d}\gamma = 2\pi r'^2\frac{\theta}{L}\mathrm{d}r'. \tag{1.30}$$

We can calculate the twisting moment T for a cross-sectional slice of the beam – a parameter analogous to the internal bending moment M from Section 1.2.1 – by integrating $\mathrm{d}\gamma$ over its area,

$$T = \frac{JG\theta}{L}, \tag{1.31}$$

where $J = \pi r^4/2$ is the polar moment of inertia of a cylindrical beam. Like the second moment of area I, J has been solved for many different geometries and is easy to look up [78].

Like bending, elastic energy can also be stored in a system through torsion. The amount of work required to twist a system with constant T by an angle $\Delta\theta$ is just $U_T = T\Delta\theta$, but for something like a beam or fiber from Section 1.2.1, T varies with $\Delta\theta$. In this case, it's more informative to think about the elastic energy being stored between each successive slice of cross-sectional area A,

$$\mathrm{d}U_T = \int_{\Delta\theta/L} JG\phi'\mathrm{d}\phi' = \frac{JG(\theta_f^2 - \theta_i^2)}{2L^2}, \tag{1.32}$$

where ϕ' is rotation per unit length, informing how much one slice has rotated in reference to an adjacent slice. If we make the assumption that T is uniform along the length of the object, evaluating $\mathrm{d}U_T$ along the full arclength of is simply,

$$U_T = \frac{JG(\theta_f^2 - \theta_i^2)}{2L}. \tag{1.33}$$

Like the results from Section 1.2.1, Equation 1.33 represents the first level of complexity as far as a description of elasticity and torsion are concerned. Critically, θ/L must remain small in order for our linear, Hookean elasticity description to

be valid. But this doesn't mean θ must be small, provided the length is long. We take advantage of this detail in Chapter 4 where we explore the bending, buckling, and twisting of long, slender fibers subjected to large degrees of twist.

1.3 Elasticity Theory in Three-Dimensions

Throughout Chapter 1 we have considered elasticity, one facet at a time. We have developed Hookean descriptions of stresses and strains related compression, extension, bending, and shearing, but so far we have only considered these modes in isolation. In general, an object can experience more than one of these stresses at any one time, and in more than one direction. In many cases, we can use our intuition to identify the most important stresses within a system and focus only on those, picking and choosing which results from the previous sections to use. But a full description of the system should account for all of the stresses throughout the body of our object. A succinct way of doing this is with mathematical tensors [68].

Some advanced treatments of elasticity theory may choose to begin with tensor notation. There is merit in this approach, but as this is my thesis, I have decided to treat it as an aside. I've decided to do this to reflect my own approach to studying these systems, while acknowledging that a section explicitly linking the work in this thesis to the wider literature is important.

Hooke's law in one-dimension is one of the first things taught in physics and engineering, and much of what follows is a sort of ad-hoc addition to the one-dimensional description. By the time I encountered the elasticity matrix description, my physical intuition had become coloured by the more simplistic, piecemeal version of elasticity described above. In some ways, this has been to my detriment. In some ways, I see it as an advantage. From a mathematical perspective, the matrix formulation is far superior as all of the above expressions and many more relationships follow from just a few dense equations. This, paired with numeric simulations and computer modelling, provides an incredibly powerful tool for investigating all sorts of elastic phenomena. On the other hand, thinking of all of these modes of deformation individually has pushed me to seek simple, intuitive, and easily applied descriptions of elastic phenomena. If developing a model is like

painting, I've specialized in expressionism. But nature is realism. The deepest understanding comes from the union of both[5].

1.3.1 Hooke's Law in Three-Dimensions

The three-dimensional form of Hooke's law incorporates the normal and shear stresses in one dimension, for each Cartesian coordinate. This means a full three-dimensional description will include the extension/compression in the normal direction, two equations that account for the Poisson effect in the perpendicular directions, and shear. Let's first consider normal stresses.

If a stress σ_x is applied to a material in the $\hat{x}$ direction, we can calculate the resulting strains in the perpendicular directions σ_y and σ_z;

$$\varepsilon_{x,x} = \frac{1}{E}\sigma_{x,x}, \tag{1.34}$$

$$\varepsilon_{x,y} = -\frac{\nu}{E}\sigma_{x,x}, \tag{1.35}$$

$$\varepsilon_{x,z} = -\frac{\nu}{E}\sigma_{x,x}. \tag{1.36}$$

It is important to note that here we have assumed an isotropic material, so $\varepsilon_{i,j} = \varepsilon_{j,i}$. The calculation same can be done in the $\hat{y}$ and $\hat{z}$ directions, and combining the all of these expressions gives,

$$\begin{bmatrix} \varepsilon_{x,x} \\ \varepsilon_{y,y} \\ \varepsilon_{z,z} \end{bmatrix} = \frac{1}{E}\begin{bmatrix} 1 & -\nu & -\nu \\ -\nu & 1 & -\nu \\ -\nu & -\nu & 1 \end{bmatrix}\begin{bmatrix} \sigma_{x,x} \\ \sigma_{y,y} \\ \sigma_{z,z} \end{bmatrix} \tag{1.37}$$

Worth noting is that the stress-strain relationship does not have to be Hookean or isotropic. $\boldsymbol{\varepsilon}$ can be re-written in this same form in terms of more complicated elasticity models.

[5] Only now am I realizing how much of my scientific worldview I've taken from Pierre-Gilles de Gennes. His 1994 Dirac Memorial Lecture was the first book I read when I started my graduate studies in 2014, and apparently it stuck with me. Particularly his observation that "Simulations and other numerical exercises are the analogue of photography... Thus I tend to compare our community of soft-matter theorists to the amateur painters of a hundred years ago" [79]

Shear stresses can also be added to this description. One alteration we need to make before we can bring our shear description into matrix form though, is with our definition of shear strain. In particular, we have been using *engineering* shear strain. Instead, we use the *true* strain, which differs by a factor of two[6]:

$$\gamma_{x,y} = 2\varepsilon_{x,y} = \frac{2(1+\nu)\sigma_{x,y}}{E}. \tag{1.38}$$

Including strain in all three Cartesian coordinates gives,

$$\begin{bmatrix} 2\varepsilon_{y,z} \\ 2\varepsilon_{x,z} \\ 2\varepsilon_{x,y} \end{bmatrix} = \begin{bmatrix} \gamma_{y,z} \\ \gamma_{x,z} \\ \gamma_{x,y} \end{bmatrix} = \frac{1}{E} \begin{bmatrix} 2+2\nu & 0 & 0 \\ 0 & 2+2\nu & 0 \\ 0 & 0 & 2+2\nu \end{bmatrix} \begin{bmatrix} \sigma_{y,z} \\ \sigma_{x,z} \\ \sigma_{x,y} \end{bmatrix}. \tag{1.39}$$

A full description incorporates both normal and shear strains, and combines both Equation 1.37 and Equation 1.39:

$$\begin{bmatrix} \varepsilon_{x,x} \\ \varepsilon_{y,y} \\ \varepsilon_{z,z} \\ \gamma_{y,z} \\ \gamma_{x,z} \\ \gamma_{x,y} \end{bmatrix} = \frac{1}{E} \begin{bmatrix} 1 & -\nu & -\nu & 0 & 0 & 0 \\ -\nu & 1 & -\nu & 0 & 0 & 0 \\ -\nu & -\nu & 1 & 0 & 0 & 0 \\ 0 & 0 & 0 & 2+2\nu & 0 & 0 \\ 0 & 0 & 0 & 0 & 2+2\nu & 0 \\ 0 & 0 & 0 & 0 & 0 & 2+2\nu \end{bmatrix} \begin{bmatrix} \sigma_{x,x} \\ \sigma_{y,y} \\ \sigma_{z,z} \\ \sigma_{y,z} \\ \sigma_{x,z} \\ \sigma_{x,y} \end{bmatrix}. \tag{1.40}$$

Equation 1.37 may appear big and intimidating, but really it's just the combination of all of the results we've seen so far. Better still, we can often simplify Equation 1.40 by considering the geometry of the system we are studying. In this thesis in particular, we can simplify Equation 1.40 significantly by treating certain dimensions as significantly smaller than others.

[6]The reason for this difference is historical. The matrix formulation of elasticity was developed long after engineers first started thinking about stresses and strains. At the time, engineering shear strain was an intuitive and simple way to define shears. This definition, however, does not give the correct relationship between stresses and strains when calculated in matrix notation. A better definition was developed that fixed this problem. Specifically, the true strain is the change in angle between two line elements which are initially perpendicular when undeformed. In short, the difference is a factor of two.

1.3.2 Slenderness and Plane Stress

The systems we study are three-dimensional, but sometimes we can pretend they're not. By treating a material as two-dimensional (or even one-dimensional), we can significantly simplify its stress and strain description by ignoring some components of Equation 1.40. Take for instance a thin, elastic sheet - something like the skin of a balloon.

A balloon is a great example of a stretchable, elastic material. Readers may recall the tactile memory of stretching and snapping a balloon like a rubber band, or the difficulty of blowing into a particularly stiff one that just wouldn't inflate. You may also recall the frustration of losing control of a balloon while blowing it up, sending it flying across the room and ending up back in its limp and floppy initial state. These experiences are made possible by the thin elastic skin of a balloon being much harder to stretch than it is to bend. This is not because of some sort of anisotropic stiffness or exotic material property but rather, it is due to the thinness of the elastic sheet.

In a sense, the thinness of an elastic sheet lets you bend it "for free", or at a much lower energetic cost compared to stretching it. In terms of geometry, we can develop a scaling argument to compare the energetic cost of bending a thin sheet to stretching the same sheet. Earlier (via Hooke's law in Section 1.1.1) we saw that stretching a three-dimensional material scales with its cross-sectional area, while bending energy scales with the material's second moment of area (via bending in Section 1.2.1),

$$\frac{E_{\text{stretch}}}{E_{\text{bend}}} \propto \frac{A_0}{I} = \frac{hw}{h^3 w} = \frac{1}{h^2}. \tag{1.41}$$

This result says that the balance of bending and stretching depends on the thickness of the material squared. Sometimes bending will be more difficult than stretching (when $h >> 1$). When $h << 1$, this expression tells us bending will be much easier than stretching. With a typical balloon, $h << 1$, and can be considered to experience "plane stress", named after the stresses that are dominant. In terms of Equation 1.40, $\sigma_{x,z} = \sigma_{y,z} = \sigma_{z,z} = 0$. This leads to a simplified

expression,

$$\begin{bmatrix} \varepsilon_{x,x} \\ \varepsilon_{y,y} \\ 2\varepsilon_{x,y} \end{bmatrix} = \frac{1}{E} \begin{bmatrix} 1 & -\nu & 0 \\ -\nu & 1 & 0 \\ 0 & 0 & 2+2\nu \end{bmatrix} \begin{bmatrix} \sigma_{x,x} \\ \sigma_{y,y} \\ \sigma_{x,y} \end{bmatrix}. \tag{1.42}$$

Taking these components individually, the set of constitutive equations are then,

$$\varepsilon_{x,x} = \frac{1}{E}(\sigma_{x,x} - \nu\sigma_{y,y}), \tag{1.43}$$

$$\varepsilon_{y,y} = \frac{1}{E}(\sigma_{y,y} - \nu\sigma_{x,x}), \tag{1.44}$$

$$2\varepsilon_{x,y} = \frac{1}{E}(2+2\nu)(\sigma_{x,y}). \tag{1.45}$$

Stresses in these directions then, in a sense, limit the sorts of deformations a thin sheet will experience. We will expand on this idea in the next section when we consider elastic instabilities and deformations via energy methods.

As a final note, a similar argument can be made for slender beams like fibers, hairs, or cables as well. With slender beams we assume the cross-sectional area is small compared to its length, then bending can happen readily. For example, in Chapters 3, 4, 5, we assume our thin fibers are a) inextensible, and b) buckle before experiencing significant compression. These are approximations we can make only after we have considered the relevant forces in the system, which can include more than just elasticity. The next section is dedicated to some of the other forces encountered in this thesis.

1.4 Capillarity and Other Forces

Here is a seemingly simple question: how do the stresses on the surface of an inflated balloon and the stresses on the surface of a soap bubble compare? Both are described by a sort of "tension" that resists increases to their surface areas, but do they work in the same way? I was caught under-prepared by this question during my M.Sc defence and subsequently "flubbed it". I bring it up now[7] because the question brings into focus an important point: elasticity and surface tension

[7] to bait a question for my PhD defense.

are similar, but are not the same. For instance, elasticity and surface tension often result in stresses that are different by orders of magnitude, but even this is not always the case. This question, and the competition between elasticity and surface tension is the focus of Chapter 4 and will be explained further in the following section.

1.4.1 Surface Tension, Capillarity, and Interfacial Energy

When you inflate a balloon its skin stretches causing a plane-stress over its surface. The more air you blow into it, the more the balloon inflates, which increases the stress. In general we can assume that the stress is uniform across the surface of the balloon, and provided the balloon's thickness is also uniform, the strain or stretching the balloon experiences at any point on its surface should be uniform too. A similar phenomenon occurs with a liquid bubble, but for different reasons. Liquids have a physical property called surface tension that describes the self-

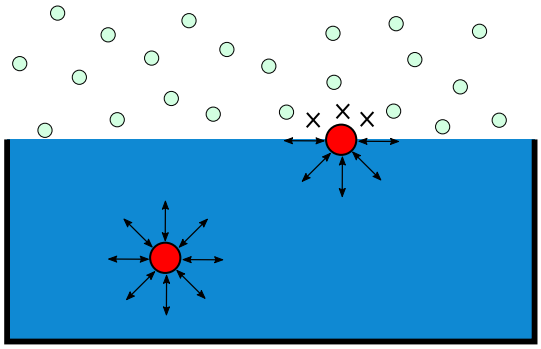

Figure 1.8: A schematic of the intermolecular interactions of liquid molecules within the bulk of the liquid compared to the surface. The molecules at the surface of the bath are in an energetically unfavorable state compared to the ones in the bath.

cohesion a liquid experiences [32, 80]. Liquids are made up of molecules held together by relatively weak inter-molecular forces. In the absence of these forces, a liquid may be free to dissociate into a vapor. Although the liquid molecules are relatively free to move within their bulk, in some ways surface tension imposes a sort of *elasticity* we would more often attribute to a solid. In particular, the surface tension of a liquid (or in general, the interfacial tension of a material) acts

to reduce the interface between itself and other materials by reducing its interfacial area, much like a rubbery sheet resists being stretched.

The exact origin of of the intermolecular interactions within liquids vary depending on the liquid. For molecules like water with powerful hydrogen bonds, each molecule's polarity causes a mutual attraction between oppositely charged poles. Non-polar molecules can experience attraction from van der Waals forces and the attraction from induced dipole moments at short ranges, and repulsion at short ranges from the electron clouds surrounding atoms [81]. The combination of the attractive and repulsive interactions between non-polar liquids is often modelled using a Lennard-Jones potential,

$$U_{LJ}(r) = 4\epsilon\left[\left(\frac{\sigma}{r}\right)^{12} - \left(\frac{\sigma}{r}\right)^{6}\right], \tag{1.46}$$

where r is the distance between molecules, ϵ is the potential energy minimum, and σ is the distance where $U_{LJ} = 0$.

A classic schematic explaining how the potential energy between liquid molecules relates to surface tension is shown in Figure 1.8. Liquid molecules are shown to each experience an attractive potential (arrows) for each other molecule that surrounds it [30]. Since there are fewer liquid molecules to surround those at the liquid-vapor interface, meaning these interfacial molecules will be at a higher potential energy than they would be in the bulk. It is from this unfavorable energy state at the liquid-vapor interface that surface tension effects originate.

The schematic in Figure 1.8 is useful for describing the origin of interfacial tension, but a better way to probe the analogy between interfacial tension and elasticity is through a simple thought experiment. In this experiment we imagine a liquid film (like a soap film) suspended across a rectangular wire frame with one of length L that can be slid along the frame. When the movable wire is a distance x along the parallel sides of the frame, the liquid film has a surface area $2Lx$, where the factor of two comes from the fact the film has both a top and bottom side. If a force F is applied to the movable wire so that it slides along the frame a distance $\mathrm{d}x$, the area of the liquid film will increase by $2L\ \mathrm{d}x$. However, increasing the area of the liquid film also increases the amount of liquid-air interface the film has.

Figure 1.9: A three-sided wire frame and a movable bar of length L support a liquid film. A force F is required to move the bar and increase the surface area of the liquid film by $2Ldx$.

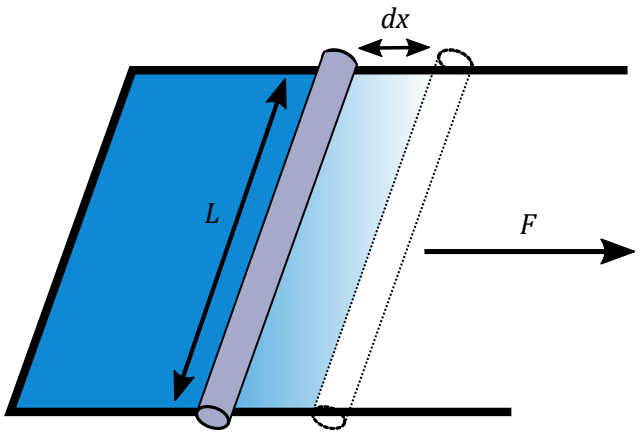

Since forcing liquid molecules to the liquid-air interface increases their potential energy, work needs to be done on the system. This work comes from F as the bar is moved by $\mathrm{d}x$. Equating the work done with the increase in energy of the liquid film,

$$F\mathrm{d}x = 2\gamma L\mathrm{d}x, \tag{1.47}$$

where γ is the surface tension of the liquid and has units of $\mathrm{J/m^2}$. It quantifies the work that it takes to increase the amount of interface a liquid has with another material, or how hard it is to increase the surface area of a liquid. The value of γ differs from material to material, and depends on what the material is sharing an interface with.

Another way to think of the experiment described above is to consider what would happen to the movable wire when the force F is released. In this scenario, the liquid film is free to reduce its own surface area. By doing this, the liquid releases some of its interfacial energy which is now able to pull the wire in the opposite direction. If one were to actually perform this experiment, they might find that the movable wire fires off the frame, giving the liquid the opportunity to coalesce on the remaining sections of frame. And as more and more liquid accumulates, gravity may eventually pull droplets of liquid off the frame. If we could observe these falling droplets in the absence of air resistance, what we'd find is that

they would continue to minimize their surface area, leading them towards forming perfect spheres. This is why, in micro-gravity environments like the International Space Station, water and other liquids can be seen forming beautifully spherical volumes.

The fact that liquids are driven to become spherical to minimize its surface area and interfacial energy leads directly to one of the more common ways of measuring a liquid's surface tension [32]. When a small volume of liquid is deposited on a smooth, flat surface, and providing other forces (like gravity) are minimal, the liquid will form a spherical cap like the one shown schematically in Figure 1.10 [26]. What happens to the liquid above the surface is not too surprising – to minimize

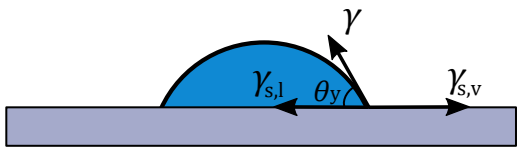

Figure 1.10: A liquid droplet sits atop a flat, smooth, non-deformable solid surface. In the absence of other forces, the droplet takes on the shape of a spherical cap with contact angle θ_y defined by the competition of interfacial energies.

its interface with air (or vapor), it takes on a spherical shape. However, the sphere is truncated where the liquid comes into contact with the solid. To be clear, forming a spherical cap does not result in a smaller surface area than forming a true sphere. What it actually does is minimize the interfacial energy of the *entire* system, including that of the solid-liquid and the liquid-vapor interfaces.

As a novice physicist, I attempted to solve for the final shape a volume of liquid would make with a smooth flat surface by minimizing the interfacial energies (surface areas times surface tension) of each of the three phases (solid, liquid, vapor) using a three-dimensional model. While certainly possible, a far more effective strategy is to identify the symmetry of the system (any way you slice it, each cross-section has the same contact angle and interfacial tensions) like the one shown in Figure 1.10) and model what happens at the point where the three phases meet. One way to think of this is to recognize that while surface tension has units of J/m^2, that is also equivalent to units of N/m. So in a sense, surface tension

acts like a force at this three-phase contact point, where the solid-vapor surface tension ($\gamma_{s,v}$) works to make the liquid spread across the surface, the solid-liquid surface tension ($\gamma_{s,l}$) pulls in the opposite direction to minimize the solid-liquid interface, and the liquid-vapor surface tension (γ) acts tangent to the surface of the spherical cap. By balancing these surface tensions in the direction parallel to the plane of the solid[8], we obtain Young's law:

$$\cos\theta_y = \frac{\gamma_{s,v} - \gamma_{s,l}}{\gamma}, \tag{1.48}$$

where θ_y is the "contact angle" a liquid makes with the underlying solid. As we can see from Equation 1.48, changing any of the three materials will affect the value of θ_y. In many everyday situations the vapor phase is simply room temperature[9] air. Keeping with that assumption, θ_y can be used as a good measure of a liquid's affinity for the underlying material. For example, the interfacial energy between water and a typical polytetrafluoroethylene coating (PTFE is a dominant component of Teflon coatings on cooking pans) is high, which leads to a large θ_y resulting in water forming nearly-spherical beads over its surface. On the contrary, cooking oil has a higher affinity for PTFE and thus a smaller θ_y when it makes contact with a PFTE surface.

Although we normally think of surface tension as being a liquid property, the same property can be more broadly described as *interfacial energy*, describing the amount of energy stored in a system at the interfaces between different materials [46, 82, 83]. Solids exhibit this property reciprocally with liquids, but also with vapor phases, just as a liquid does, though often the work required to increase the amount of interface between a solid and vapor is overshadowed by another property – elasticity. Often, the work required to stretch a material elastically is far greater than the work that needs to be done to increase the interface between a solid and another phase. To illustrate this separation of scales, we finally return to the balloon and the liquid drop (or soap bubble). Specifically, we ask, *"How much work does it take to inflate a balloon, and how does this compare to inflating*

[8] If we assume the solid is rigid and non-deformable, the vertical component of γ is compensated for by the elasticity of the solid.

[9] Yes, all of these surface tension values depend on temperature.

a soap bubble?"

Consider a spherical, elastic (Hookean) balloon with skin thickness h and a radius r. We can assume $r >> h$, which means we can use our plane-stress argument and consider the balloon to be stretching-dominated, thus ignoring the bending energy in the skin. When the balloon is inflated, it retains its spherical shape while its radius increases by $\mathrm{d}r$. This corresponding to a strain $\varepsilon = \mathrm{d}r/r$ that affects the surface of the balloon uniformly. For reasonably small deformations, the elastic energy in the balloon depends on the following scaling:

$$U_E \propto Eh\pi r^2\varepsilon^2. \tag{1.49}$$

On the other hand, inflating a soap bubble (which is a lot like a liquid droplet, the main difference being an additional factor of 2 due to the interior interface) is much simpler. Since we no longer need to consider elasticity, the surface energy only depends on the change in area of the bubble and its surface tension γ,

$$U_\gamma \propto 2\gamma\pi r^2. \tag{1.50}$$

Comparing the two types of "tension" (elastic and interfacial) for the type of balloon and soap bubble you might expect at a birthday party, we find that elasticity is typically much stronger than surface tension:

$$\frac{U_E}{U_\gamma} = \frac{Eh\varepsilon^2}{2\gamma} \approx 10^8, \tag{1.51}$$

where we have taken $E \sim 10$ MPa and $\gamma \sim 10$ mN/m, reasonable values for many rubbery materials and soapy water respectively.

Doing this calculation demonstrates two things. First, it emphasizes the difference in magnitude between surface tension and elastic tension. Despite having surface energy like a soap bubble, the balloon's mechanics are elasticity-dominated, which is generally true of all but the softest solids. The calculation also shows that surface tension and elastic tension exhibit different "scaling". Elasticity depends on the thickness of the elastic skin of the balloon as well as how much it has

been stretched, while surface energy depends only on the change of surface area[10]. Though typically $E >> \gamma$, the difference in scaling suggests that in some systems with particular geometric features (like slenderness) exist in a regime where elasticity and capillarity are comparable. This will be explored further in the next section.

1.5 Comparing Forces at Different Scales

If one considers the previous parts of this chapter as the introduction to an academic paper, Section 1.5 could be considered the "Conceptual Methods" section. The typical strategy employed in the original research presented in the following chapters begins with observing the system we wish to study, identify the dominant forces that define the system's mechanics, and discard lower-order effects. For instance, in the balloon example above, we may argue that the shape of the balloon is elasticity-dominated and therefore ignore the surface energy of the material when trying to describe its shape change. But there are in fact many systems where the magnitude of elastic effects are comparable to surface tension effects, and such a simplification would not be appropriate.

This chapter includes several examples of the strategy used throughout this thesis. By comparing the effect of gravity, elasticity, and surface tension in three different systems, we will see how these forces can work together (or opposite each other) at different scales to produce interesting and complicated effects. Likewise, as was hinted to in Section 1.3, the size and shape of the elastic solids we study as well as the way forces are applied to them can produce interesting competitions between modes of deformation. This will be introduced in Section 1.6.

Finally, the goal of this section is more than describing the conceptual methods used in this thesis. The examples are also intended to demonstrate the importance of size and scale when designing experiments. One of the benefits of working in

[10]This is a simplification. In crystals, it has been long understood that surface energy can be strain-dependent as stretching the bonds between atoms can also increases the interfacial energy of the material. Recently, it has been shown that this is also true of amorphous solids like polymers. This is called the Shuttleworth effect and while it is a small effect, it is in fact quite important in certain soft systems [46, 83]

the Dalnoki-Veress lab is having access to the kind of expertise that lets one develop unique experiments that use scale to their advantage. This section should emphasize that idea, and provide a good introduction to Chapter 2 which focuses on Experimental Techniques.

1.5.1 Surface Tension and Gravity

The first comparison we will make does not come up explicitly in the original work of the thesis but sets an upper limit on the size of the systems we explore in Chapter 5. An important assumption that is made throughout this thesis is that the force of gravity is much smaller than the other forces affecting the system such that it can be ignored. In Chapter 5, capillarity is the main driving force acting on an elastic material. In order to ensure that the force of gravity is either compensated for or negligibly small, we can ensure our experiments do not exceed the capillary length. The capillary length, l_c, is a characteristic length scale below which capillary forces are comparable in magnitude to the force of gravity acting on the system, and is defined as,

$$l_c = \sqrt{\frac{\gamma}{\rho g}}, \tag{1.52}$$

where γ is the liquid-vapor surface tension, ρ is the density of the fluid, and g is the gravitational acceleration acting on the fluid [32]. For a liquid with the surface tension and density of water, $l_c \sim 2.5$ mm, which is approximately the size of the meniscus visible in a typical glass of water. By keeping the scale of our surface tension experiments below this length, we can generally treat gravity as a negligible contribution to the system. On the other hand, systems with sizes on the order of l_c can exhibit some interesting and complicated phenomena. For example, you can look to a dewy spiderweb to see spherical water droplets decorate its lengths of silk. In isolation, a single droplet on a strand can either envelope the strand like a bulging, axi-symmetric cylinder (barrel orientation) or hang from one side of it (clam shell orientation); the orientation being a function of surface tension, fiber geometry, liquid volume, and gravitational forces [47, 51, 84–91]. Some other related effects include "capillary rise" in things like thin glass tubes or between

parallel fibers and films [86, 92], and when fibers are thin enough or droplets large enough, elastic deformations can complicate these effects further.

1.5.2 Elasticity and Surface Tension

As we saw with the balloon example, elasticity and surface tension are often separated by several orders of magnitude, owing to the geometry, scale, and material properties of the system. However, there are many examples of soft or slender solids that experience considerable "elastocapillary" deformations due to surface tension [29]. In recent years the study of elastocapillarity has blossomed into a rich and diverse, interdisciplinary field including biophysical systems, materials research, microfluidics, and all manner of engineering topics [25, 27, 28, 34, 93–95]. It was the subject of my Masters research, and is also the subject of Chapter 4 [45]. Therefore, as an introduction to elastocapillarity and ultimately Chapter 4, let's consider a liquid droplet on a solid surface.

As we have seen in Section 1.4.1, a liquid droplet in contact with a smooth, solid surface will form a spherical cap. This assumes that the force of gravity is small, and that the solid surface is non-deformable. However, a sufficiently soft or thin solid can in fact undergo measurable deformations [26, 33, 35, 40, 41, 82, 83, 96–100]. In principle, even a material with a high stiffness will undergo some amount of stretching or shear, though it may happen only on the smallest of scales. This length scale can be approximated by comparing the shear modulus G to the surface stress of the solid Γ, which includes the surface tension γ as well as any strain-dependent deviations to the surface energy. This results in a length scale known as the elastocapillary length,

$$l_s = \frac{\Gamma}{G}. \tag{1.53}$$

This is the length scale that sets the boundary below which one could observe capillary-induced shearing. An example of such a deformation is shown in Figure 1.11 a). It's important to note that l_s only depends on the surface energy of the system and the shear stiffness of the solid. This means that elastocapillary shearing may be observed in any system that is sufficiently soft, regardless of the size and shape of the underlying solid.

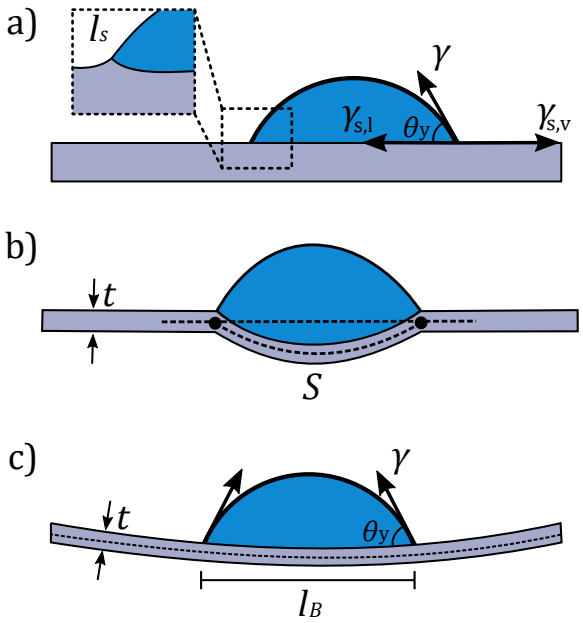

FIGURE 1.11: Elastocapillary deformations at different scales. a) Even stiff or thick solids can experience capillary-based shear, though the characteristic length scale of these deformations l_s may be small and isolated to the surface of the solid. Softer materials experience larger deformations. b) Compliant materials (which are not necessarily soft, but are thin) can experience stretching with characteristic strains S or c) bending with a length scale l_B.

Soft materials are not the only materials susceptible to elastocapillary deformations. Stiff materials can also undergo capillary-induced bending and stretching provided they are "compliant", or thin and flexible [17,38,39,41–45,47–54,101–106]. For instance, a sheet floating on the surface of a liquid will experience a force at the boundary of the sheet $\zeta = \gamma - \gamma_{sv} - \gamma_{sl}$ as the solid, liquid, and vapor phases attempt to minimize their surface energies [29]. If $\zeta > 0$ then the film experiences a tension which can result in a strain, $\varepsilon_\gamma = \zeta/Et$. From this, we can define a more generic but related parameter that quantifies the strain one can expect in a thin elastic material due to capillarity,

$$S = \frac{\gamma}{Et}. \tag{1.54}$$

For a material like plastic wrap that typically has a thickness of $t \sim 10^{-5}$ m, stretching can be extremely small, on the order of $S \sim 10^{-9}$. But the thin films

in Chapter 6 are considerably thinner ($t \sim 10^{-7}$ m) and thus considerably more compliant, which makes these films susceptible to capillary stretching. In the context of a liquid droplet sitting on a compliant solid like in Figure1.11 b), this kind of deformation can result in a stretching-dominated bulge in the solid below the surface of the liquid.

Capillary bending can also occur in sufficiently compliant elastic materials. For a beam with a cylindrical cross-section with radius r, a bending elastocapillary length scale l_B can be defined that balances capillary energy and bending energy,

$$l_B = \sqrt{\frac{Er^3}{8\gamma}}. \tag{1.55}$$

The exact definition of l_B depends on the geometry of the elastic solid, but is largely determined by the thickness of the deformed solid on account of the bending stiffness being related to the object's second moment of area (see Section 1.2.1). In Chapter 4 we will see how l_B can be used as a metric to relate experiments done at various length scales.

1.6 Elastic Instabilities

At last, we arrive at the main topic of the thesis. Now that we have developed a foundation in elasticity and discussed the types of forces that will drive the elastic deformations we observe in later chapters, we will explore how the geometry of a system and the way forces are applied to the system can generate interesting and non-trivial elastic deformations.

Elastic instabilities are one of those types of phenomena that are so ubiquitous that they can easily go overlooked. The wrinkle in your furrowed brow as you read this obtuse sentence, trying to guess the first example I will introduce, is in fact one of the types of instabilities that will become the topic of Chapter 5. Here, a competition between the compression caused by your forehead muscles (see Section 1.1.1), and bending (see Section 1.2.1) results in periodic undulations defined by the thickness, stiffness, and elasticity of your skin [57, 107–112]. The competition between compression and bending does not always result in something

beautiful like laugh lines though. If supporting columns are not designed to withstand high enough compressive loading, they too can undergo buckling though in this case, the result can be catastrophic mechanical failure as the columns lose a significant amount of compressive strength during buckling.

Torsion (see Section 1.2.3) can also cause unique and interesting deformations. Why, for instance, will a twisted headphone cable form loops and knots [21, 113]? Perhaps more marvelous, how did our bodies learn to bend, twist, and otherwise organize and cram massive strands of DNA into sub-cellular packages, like the aforementioned headphone cable jammed in a pocket [114–118]? Even though torsion may not seem like it would necessitate a compressive stress, we will find in Chapter 3 that tension can in fact stabilize a twisted beam from buckling and tangling, and removing that tension can allow a beam to take on a multitude of different orientations.

Although these examples cover a wide range of types of deformations across many different scales, there is a unifying principle that relates them all; each of these systems are put in a situation where they are presented with several different ways of relieving some of the stress and elastic energy that they are loaded with. Like we have seen in previous sections, many of these phenomena are in fact scale invariant, instead depending on the relative geometry of the system. This means that many of the phenomena we see in macroscopic systems can apply to microscopic systems as well, which can has allowed for biology-inspired flexible electronics and devices [119]. But the relationship goes in the other direction as well. As we will see in the following chapters, macroscopic experiments can also be used to model and understand prohibitively small systems as well. In this final section then, we will explore what this means exactly with regard to the systems we will encounter in the following chapters, and how we will approach characterizing these elastic instabilities.

Though there are a wide range of instabilities that we could cover, this section will be limited in scope to those encountered in this thesis. In particular, we will focus on instabilities caused in slender structures subjected to compressive and torsional loading, which typically lead to buckling. For a more complete look at

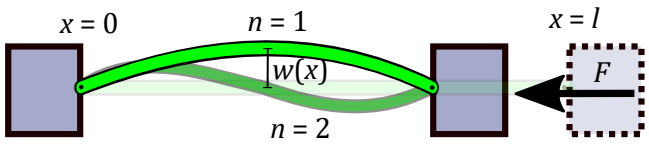

FIGURE 1.12: An elastic beam buckles in response to being subjected to a compressive force F.

elastic instabilities, Theory of Elastic Stability by Timoshenko and Gere is one of many textbooks that approaches the topic from an engineering perspective [120].

1.6.1 Buckling of Slender Structures: Critical Load and Stability

When an object is compressed, it has a tendency to decrease in length; we know this well by now. Imagine a beam of length L with a cylindrical cross-section of radius r held between two movable boundaries, shown schematically in Figure 1.12. If a force (or load) F is applied to the beam via the boundaries being forced together, the space the beam is able to occupy decreases. As a first guess, we may assume the beam will simply compress according to Hooke's law, storing an elastic energy $E_c = \int_0^{\varepsilon L} F(x)\mathrm{d}x = 1/2E\pi r^2\varepsilon^2$, where E is the beam's elastic modulus and ε is the compressive strain on the beam. But there are other ways for the beam to conform to its new, reduced boundary. Alternatively, the beam can *buckle*, or in other words, bend. Although the exact details of how the buckling occurs will depend on the boundary conditions, in essence, a sufficient compressive loading will create a situation where both compression and buckling can occur. How the beam responds will be determined by what orientation minimizes the energy of the system and what solutions are *stable*. Determining this involves building a model that can compare both bending and compression.

If the beam does not simply compress and instead buckles, we still need to be able to relate the applied force to the resulting deformation. This is more difficult than the pure compression case, as we will see, because there can be multiple solutions. Let's take our same beam from above and make the assumption that the ends of the beam are *pinned* to the boundaries (such that they can rotate but not slide). By equating the bending moment $M = EI\frac{\mathrm{d}^2w}{\mathrm{d}x^2}$ to the applied torque

$T = Fw(x)$ along the arclength of the beam, we get a differential equation,

$$Fw(x) = EI\frac{\mathrm{d}^2 w}{\mathrm{d}x^2}, \tag{1.56}$$

where w is the displacement of the beam in a direction perpendicular to $\hat{x}$. Equation 1.56 is an ordinary, second-order differential equation with the solution,

$$w(x) = A\cos(kx) + B\sin(kx), \tag{1.57}$$

where A and B are integration constants determined by the boundary conditions, and $k^2 = F/EI$. Applying our boundary conditions, we know that $w(0) = 0$ and $w(kl) = 0$, meaning $A = 0$. From here, we can have two sets of solutions. If $B = 0$ we get the case where no bending occurs, resulting in the simple compression scenario described above. If $B \neq 0$, our solution becomes,

$$w(x) = B\sin(kx). \tag{1.58}$$

Equation 1.58 defines a set of solutions that satisfy $kl = \pi n$, where n are integer values. The first several solutions are demonstrated in Figure 1.12.

So we have solutions defining the possible shapes an axially-loaded beam can take on. We can also use this information to calculate how much load the beam can take before it can take on one of these shapes. Using our definition of $k^2 = F/EI$, we get,

$$F_n = EI\frac{n^2\pi^2}{l^2}, \tag{1.59}$$

where F_n is the minimum force required to achieve each of the n solutions.

One important thing to note about this result is that applying a perfect axial load won't cause a buckle unless there is some sort of lateral perturbation. However, once a lateral perturbation is initiated, buckling will often occur readily. To illustrate this point, we can comparing the compression caused by a perfectly axial load to the deflection caused by the same load applied perpendicular to the axis

of the beam,

$$\frac{\Delta L}{\delta} = \frac{FL/\pi r^2 E}{FL^3/3EI} \propto \frac{r^2}{L^2} \tag{1.60}$$

where δ is the maximum lateral deflection at the end of a cantilever-style beam with a load applied perpendicular at its free end. This result shows that for the kind of long, thin beams used in this thesis where $r/L << 1$, lateral deflections happens much more readily. In fact, if we let the angle the applied force F makes with the axial length of the beam vary by an angle θ, we can find how much the angle of the applied force can deviate from perfectly axial such that the compression and deflection are of comparable magnitude:

$$\frac{\Delta L}{\delta} \propto \frac{r^2}{L^2} \cot\theta. \tag{1.61}$$

For an typical experiment described in any of the following chapters, $r/L \sim 10^{-4}$, meaning simply deviating by an angle $\theta \sim 10^{-9}$ radians could destabilize an axially-loaded beam at its buckling threshold.

The second important aspect of this result is that creating more buckles stores more energy in the beam, which means more work must be done on the beam, which is expressed in the fact that $F_n \propto n^2$. But the critical load applying the required amount of force is not all it takes to create multiple buckles. The way the beam is loaded, the energy stored in the system, and the stability of the system all contribute to determining how the beam buckles exactly.

1.6.2 Energy Methods

"Energy methods" are the predominant technique used in this thesis to predict the onset and stability of elastic deformations. This relatively vague term can refer to several different techniques, but here I use it to describe the strategy of comparing the energy stored in several possible states the system could be in, with the assumption that a system can release some of the stored energy in the form of motion in order to drive it towards a lower energy state.

For example, in Chapter 3, we consider elastic instabilities that also incorporate twisting. We compare the energy stored in a thin fiber where one side of the fiber

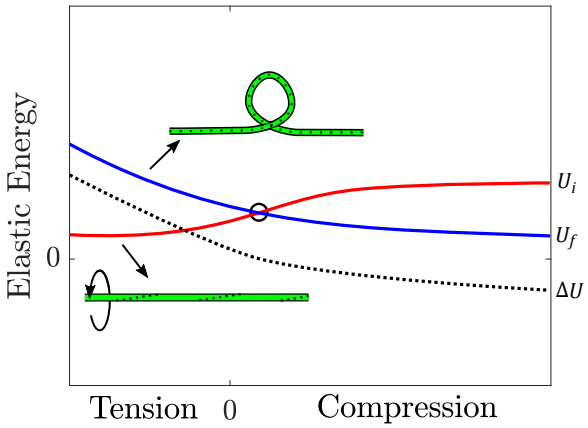

Figure 1.13: A schematic plot of the elastic energy in a fiber as a function of tension/compression for its initial twisted state (U_i) and final bent state (U_f). By calculating $\Delta U = 0$ (circled) we can predict at what point it becomes energetically favorable for the fiber to deform into its bent orientation.

has been subjected to some amount of rotation relative to the other side, and with variable amounts of tension or compression. Though twisting complicates the system some, many of the details and strategies remain the same. Namely, we present a model that calculates the energy stored in the system before and after an instability-driven deformation occurs, based on the orientations the fiber in the before and after states. By equating the energy stored in the system in each state, before and after our predicted deformation occurs, we calculate under what conditions our fiber will transition to the new orientation. This strategy is shown schematically in Figure 1.13, where a plot of a system's energy before (U_i) and after (U_f) an elastic instability occurs is plotted as a function of tension/compression. By setting $\Delta U = U_f - U_i = 0$, we can identify the conditions where it will be more energetically favorable for the system to transition to the new, deformed state.

In Chapter 4, a similar strategy is employed. The energies in the initial state are based purely on the interfacial energy between a fiber's material and the liquid bath it floats atop. The initial interfacial energy is compared to the interfacial energy between the same fiber and liquid after an air bubble has been injected below the fiber. Having a volume of air below the fiber ends up reducing the system's

interfacial energy, which drives the fiber to reorient and deform elastically. And finally, Chapter 5 combines the elastic responses of fibers and thin films, exploring how the size, shape, and orientations of buckles can be controlled by applying different stresses to the thin film.

Rather than take the approach described in Section 1.6.1 to determine the different orientations the fibers in these chapters will take on, much of the analysis in the following chapters are informed by experimental observations. This is one of the conveniences afforded by working in the Dalnoki-Veress lab. During my time in the lab, I benefited from many experimental techniques developed by myself and my colleagues to make small, uniform, and (relatively) easy-to-manipulate, idealized experimental systems which allowed me to try many different stress, strain, and loading experiments, making detailed observations of the resulting deformations along the way. In Chapter 2 I will elaborate on some of the techniques used throughout this thesis.

Chapter 2

Experimental Methods

The subject of Chapter 2 is the technical details of the experiments presented in Chapter 3, Chapter 4, and Chapter 5. Each of the papers contained in these chapters include their own experimental methods sections, so this chapter will serve as a supplement to those. The details contained in this chapter can be considered a how-to guide for future students who are interested in expanding on the results of this thesis, or using similar systems for their own studies. In general, the materials used in this thesis are polymer-based, and care has been taken in selecting the specific polymers for their material properties. These considerations will be covered in Section 2.1.1. The polymers are used to create micro and nanometric elastic structures like thin films and fibers. Section 2.1.3 and Section 2.1.2 will cover the details of producing these structures. Throughout this thesis, thin elastic structures were subjected to carefully controlled stresses. Controlling the stresses applied to such small structures required the development of several techniques which are described in Section 2.2. The main results contained in this thesis come from observations and measurements of these small structures as they respond to the applied stresses, which involved initial characterization of the elastic structures, imaging the geometry of the elastic structures take on in response to stresses, and measuring extremely small elastic forces. How this was accomplished is discussed in Section 2.3.

2.1 Sample Preparation

2.1.1 Polymers

The experiments featured in the following chapters focus on the elastic responses of a variety of simple, idealized structures like thin fibers and films. These structures were created with specific geometries in mind, and required consistent mechanical properties. Fabrication of fibers and films was achieved with carefully selected polymer materials, two which were physically cross-linked elastomers and one glassy polymer at room temperature. To create these structures, the polymer materials needed to be either made into a solution using a compatible solvent, or melted at high temperature.

For some applications, a physically cross-linked elastomer styrene-isoprene-styrene (SIS) triblock copolymer (Sigma-Aldrich) with a 14% styrene content was used. Typically, it would be dissolved in toluene (Fisher Scientific, Optima grade) at mass concentrations c ranging from 4% to 20%. Other applications required the SIS be dissolved at much higher but unspecific c. When made into a thin film or fiber, SIS exhibited a slightly sticky surface, a feature that was used in Chapter 5.

Another physically cross-linked elastomer used in this thesis was Elastollan. Solutions of Elastollan TPU 1185A (BASF) were made using cyclohexanone (Sigma-Aldrich, puriss p.a. >99.5%) with c ranging from 2% to 7%. Alternatively, Elastollan was also melted by bringing to to 240° C on a heating stage.

Finally, Polystyrene (PS) with a range of molecular weights and polydispersities (Scientific Polymer Products, see specific papers for details) was used. PS solutions were made by dissolving in toluene between c = 3% and c = 20%.

2.1.2 Fibers

A common feature of the experiments described in this thesis is the use of slender fibers. In all three papers, polymer fibers with cylindrical cross-sections and radii on the order of microns are used as the subject of some applied stress. The geometry of these fibers is simple and is nothing more than an idealized cylindrical beam of the kind described in Chapter 1, but the small scale and uniformity of

the fibers make them a fairly unique experimental system. This section explains the techniques used to fabricate these fibers. The fibers in this thesis are made through a manual process that involves "pulling" them from a liquid polymer melt or solution. Elastollan, PS, and SIS were each used to make fibers, and the pulling technique used for each of these polymers was similar between them. With PS and SIS, the polymer was first dissolved in toluene at a high solid concentration. The exact concentration was not recorded as the process required some amount of solvent evaporation, subsequent thickening of the solution, and trial and error. When the solution was sufficiently thick and viscous (similar to cold honey or a viscous oil), a droplet was placed on a small silicon wafer approximately 1 cm by 1 cm. A micropipette with tip diameter on the order of tens of microns was then dipped into the viscous droplet and pulled out rapidly, dragging a volume of solution along with it. As the polymer solution was removed from the droplet, it formed a thin cylindrical thread with a high surface area to volume ratio that solidified quickly as the solvent evaporated. This process resulted in long, slender, and solid polymer fibers that naturally adhered to the tip of the pulling micropipette. Lengths of fiber could easily span tens of centimetres and while the fibers varied in diameter along these lengths, smaller lengths of the fiber exhibited high uniformity with deviations to the diameter often being unmeasurable under a 50x optical objective. A nearly identical process was used to pull Elastollan fibers but instead of dissolving the polymer in a solvent, it was heated to 240° C on a heating stage before applying the dip and pull technique to the polymer volume. While the dip and pull technique is a relatively simple process[1], being successful with the technique takes some amount of trial and error and above all, patience. To reduce the stress of learning this technique, I have complied a list of tips and tricks to help guide a potential fiber puller to hone their technique.

1. I have not been able to pull fibers with exactly specified dimensions, however, multiple fibers can be pulled rapidly from the same setup. Having several micropipettes at the ready and pulling multiple fibers will allow you to select from a range of lengths and sizes.

[1]Fun fact: this is how cotton candy (candy floss) is made; sugar is heated until it melts, and thin filaments are lifted from the liquid. Typically these filaments are wound around a paper cone.

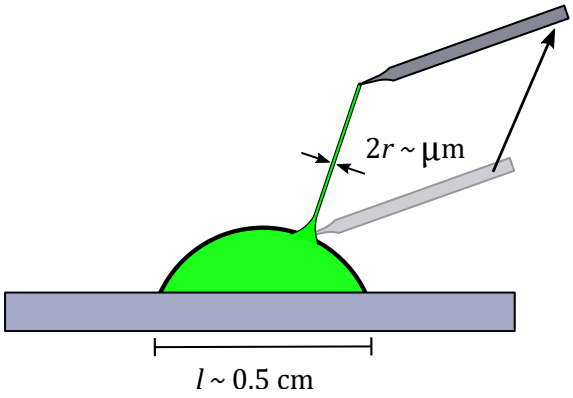

Figure 2.1: A micropipette is dipped into a liquid polymer and pulled out, resulting in thin fiber.

2. The pulling technique has a lot in common with dip coating, and much of the fine control of fiber thickness follows from this fact. Perhaps counter-intuitively, pulling a fiber faster will typically result in a thicker fiber, while slower pulling leads to thinner fibers.

3. The viscosity of the polymer melt or solution is critical and not only affects the thickness of the fiber that you pull, but also if a fiber can be pulled at all. If your polymer is too viscous, you will pull large globs of polymer from your silicon wafer. If this happens, dilute your solution with more solvent (or ensure your Elastollan is up to temperature and has time to melt). On the other hand, a polymer that is too inviscid will not entrain enough polymer onto the micropipette as you pull it out. Allow the polymer solution some time so that excess solvent can evaporate, or reduce the temperature of the Elastollan.

4. Since it takes some time for bulk polymer to dissolve in solvent, it is useful to pre-dissolve a volume of polymer at a high concentration and store it in a vial in the lab. From this volume you can produce your droplets and also re-dissolve polymer droplets that have become too viscous to pull fibers from.

5. Elastollan needs to be brought to a high temperature in order to pull fibers from it, but this also causes Elastollan to degrade over time. The first signs of degradation appears almost like a separation between a solid and liquid

portion of the polymer. A thicker, stiff volume of polymer may begin accumulating in the melt, leaving a thin lubricating layer between the polymer blob and the silicon wafer. Fibers can still be pulled from the polymer blob but they will tend to be thicker. After more time, the Elastollan sample will begin to yellow. At this point, the sample should be discarded and a new sample should be prepared.

Finally, while these fibers are useful as idealized elastic "beams", care must be taken to ensure they are not overly stressed. As a glassy polymer, PS is highly elastic but brittle and susceptible to breaking at small strains. It is not the ideal fiber for twisting experiments (see Chapter 3) since shear stress can easily cause kinks or breaks in the fiber. Additionally, PS fibers cannot undergo large extensions. However, of the three polymers discussed in this chapter, it exhibits the least amount of creep and hysteresis during extension-based experiments, and is not sticky or tacky. PS is best used for compression-based experiments and bending experiments where the radius of curvature of the fiber is large. SIS fibers, on the other hand, are very soft and do exhibit creep and significant extension-based hysteresis. For this reason, applied strains should be small (10% extension or less) and SIS fibers should not be left in a stressed state for long periods of time. It is also important to note that SIS fibers are sticky, though their small surface area limits how strongly an SIS fiber will adhere to another material. Like PS, SIS is useful during compression-based experiments, but can also be used in bending experiments where the radius of curvature is smaller. Twisting and shear-based experiments are not recommended. Elastollan fits in between SIS and PS in a lot of ways, and offers many attractive properties. It is a softer polymer than PS and is highly deformable like SIS. However, it is stiffer than SIS and does not exhibit any significant creep over a fairly wide range of extensions. Elastollan exhibits some amount of hysteresis during large extensions, but does not seem to flow like SIS. Elastollan is minimally tacky. Elastollan is essentially the workhorse of the polymer fibers and should be the first choice for the majority of fiber-based experiments whether they are extension-compression or shear-based. It also has an elastic modulus that is between PS and SIS, making them useful as comparison materials to Elastollan.

2.1.3 Films

Thin polymer films are a specialty of the Dalnoki-Veress lab and are used in Chapter 5 as a deformable, free-standing membrane. Films with thicknesses on the order of $\sim 100 - 500$ nm were made by spincoating a polymer solution onto a mica substrate which could be transferred from the mica substrate to a biaxial straining device (which will be described in Section 2.2.2). The spincoating process is shown schematically in Figure 2.2 a) and described below.

Spincoating is a process whereby a thin, uniform polymer film can be deposited on a smooth, flat substrate. This was done with a commercial spincoater (Headway Research Inc., Model PWM32) which featured a rotational stage that could achieve speeds of several thousand revolutions per minute. A fresh mica substrate was first cleaved to obtain an atomically-smooth surface which was then placed smooth-side-up on the rotating stage. A small volume of polymer-solvent solution was then placed on the mica surface before beginning the spinning cycle. During the spin cycle the polymer solution is accelerated outward, thinning the liquid layer and ejecting excess volume from the substrate. As the stage continues to spin, solvent evaporates from the residual polymer solution causing the film to further thin and increase in viscosity until a thin, solid film remains. At this point the film can be transferred to another surface using a float-and-stick technique shown in Figure 2.2 b) and c). The thin film and mica sample is dipped into a water bath at an angle so that the film begins to lift off the mica surface, remaining on the surface of the bath. Before the film is fully removed from the mica surface, it is gently removed from the bath which traps a thin layer of water between the film and the mica. The sample can then be placed film-side-down onto a new substrate where the mica can be peeled off due to the water layer. Finally, the residual water is allowed to evaporate, leaving behind only a thin, uniform polymer film.

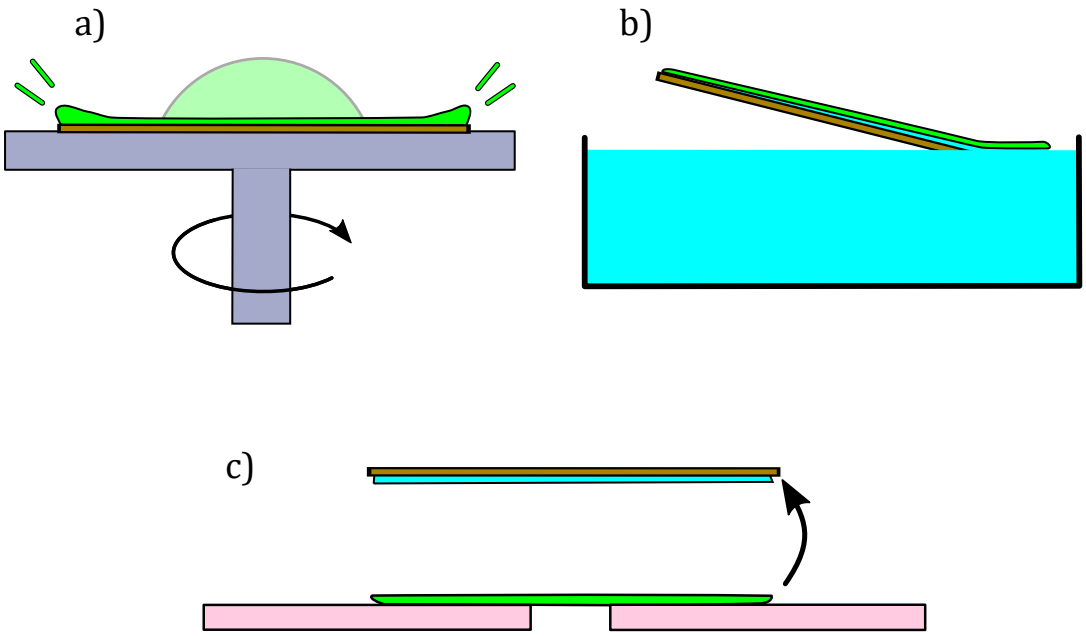

Figure 2.2: a) A thin polymer film is made by placing a polymer solution on a mica substrate and spun at several thousand revolutions per minute. b) The resulting polymer film is dipped into a water bath trapping water between the polymer film and the mica. c) The polymer sample is placed film-side-down on a new substrate. The mica is lifted away from the new substrate, leaving behind the polymer film which is now adhered to the new substrate.

2.2 Experimental Methods

2.2.1 Manipulating Fibers

In all three papers we investigate the deformation of fibers however, only in Chapter 3 do we manipulate the fibers directly. Rather, in Chapter 4 the fibers are deformed via surface tension and in Chapter 5 the fibers are deformed by the adhesive forces between fiber and film (which is described further in Section 2.2.2).

In Chapter 3, each end of a polymer fiber is wound around then glued to a post using a solvent-polymer solution, shown schematically in Figure 2.3. Gluing the fiber ends to the posts ensures that the fibers are unable to rotate and remain fixed to the posts, while winding ensures the fiber does not slip. It is important that the solvent used does not dissolve or swell the polymer fiber. When using Elastollan fibers, the glue solution was SIS and toluene.

More than serving as a fixed boundary for the fiber, the posts each served an additional purpose. One post consisted of a thin force transducer pipette (details in Section 2.3.2) capable of measuring tension in the fiber. The other was connected to a computer-controlled rotational motor which was also capable of acting as a computer-controlled translation stage (Newport Universal Motion Controller/Driver, Model ESP300).

The post with the force transducer pipette could be manually moved in three dimensions so that the ends of the fiber could be lined up before beginning each experiment. During the experiment, this post remained stationary so that the force transducer and the fiber could be imaged with a stationary optical microscope (see Section 2.3.1).

2.2.2 Manipulating Films

In Chapter 6 we explore the deformations of a fiber adhered to the surface of a thin polymer film that can experience biaxial strains. Though the fiber is not strained directly, manipulating the film caused various stresses to be transmitted to the fiber through their mutual adhesion. The system shown in Figure 2.4 was designed to create biaxial stress in the thin films.

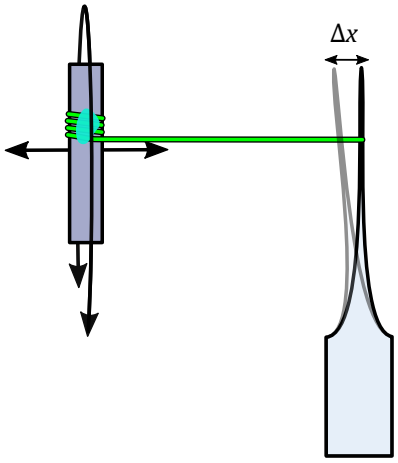

Figure 2.3: A polymer fiber is attached to two posts. The left post can be translated and rotated. The right post is a force transducer that deflects as a response to tension in the fiber.

The system consisted of an elastic sheet that was connected to four translation stages. The elastic sheet was thick (200 μm) compared to the films we were interested in, and were made from Elastosil (Wacker Chemie). A round hole with a radius of a few millimeters was punched out of the centre of this elastic sheet, which was where the thin film and fiber samples were transferred to in order to perform an experiment.

Once a film was transferred to the elastic sheet (which it adhered to on account of both materials being moderately sticky), the four translation stages could be moved independently to impose specific strains on the film which could be quantified by measuring the deformation of the circular hole in the elastic sheet.

2.3 Sample Measurements

2.3.1 Imaging

Most of the data collected and used in this lab was derived from optical imaging. Often, top-down microscopy images were collected and analysed using ImageJ or MATLAB.

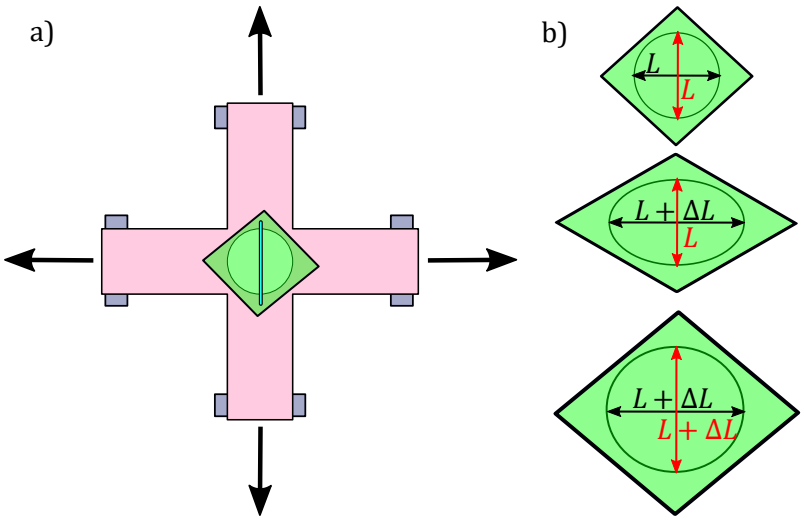

Figure 2.4: a) Top-down view of the biaxial strain device. An X-shaped elastic sheet with a hole in the centre is connected to four translational stages. A thin film adheres to the sheet and a polymer fiber adheres to the film. b) The translational stages allow for tunable biaxial stress.

A modified optical microscope, depicted in Figure 2.5, was used in Chapter 5 in order to take images of the fiber-film system at various angles. A computer-controlled, motorized ring-shaped stage (Newport Universal Motion Controller/Driver, Model ESP300) was used to mount a camera with optical tube and lens. The ring-stage was arranged such that the fiber-film sample was in line with the ring's centre, which allowed the camera to be rotated around the sample while maintaining the same distance and focus.

2.3.2 Measuring Forces

In Chapter 3, the tension in polymer fibers was measured. Because the fibers were so thin ($\sim 10^{-6}$ m), the magnitude of the tension in a typical experiment was very small ($10^{-}5$ N). To resolve these small forces, a micropipette deflection technique was used which is shown schematically in Figure 2.3 [121].

The micropipette deflection technique entails heating and pulling a micropipette with a diameter of 1.0 mm (World Precision Instruments, USA) with a pipette

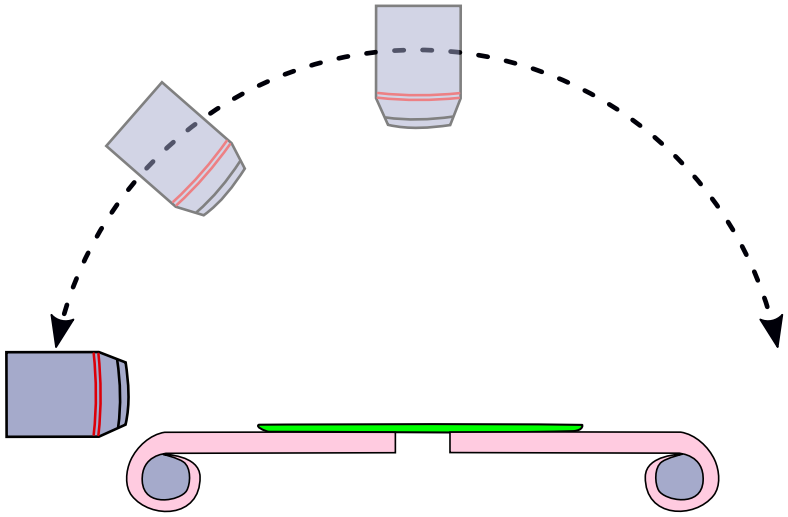

Figure 2.5: Side view of the biaxial strain device with rotating camera lens. The rotating lens can image the polymer film sample at multiple angles.

puller (Narishige, Japan) such that one end of the pipette would be stretched and tapered to a diameter of tens of micrometers. Because of the length and thinness of the pipette tip, and in spite of glass' high elastic modulus, pulling on a fiber glued to the micropipette would cause the pipette to deflect by a measurable amount Δx. By calibrating the size of deflection with several known masses, a spring constant k could be calculated for each micropipette according to $F = k\Delta x$. Knowing k allowed for visible deflections observed during an experiment to be converted to Newtons.

Finally, images of the experiment were taken rapidly and an automated MATLAB program was used to track the deflection of the pipette between frames. A cross-correlation algorithm was used to track the pipette to sub-pixel resolution which gave the force transducer system a lower limit on the order of tens to hundreds of pico-Newtons [121].

Chapter 3

Energy release by twisted, compressed fibers via hockling and writhing

The first paper included in the thesis is about the shapes a rod, fiber, or wire makes when subjected to twisting, tension, and compression. It has been accepted to be published in The European Physical Journal E.

It is known that fibers under small or no tension will form loops when twisted, and that increasing the twist causes loop to wind and "writhe", forming a double-helix-like structure called a *plectoneme*. This paper builds on the work of many engineers interested in the kinking and twisting of cables, where a hockle can mean a irreparable damage to the cable [22, 122–125]. Recently, the physics of hockling and writhing of "rods" has found application in describing the conformations of DNA [6, 7, 126–128].

In this paper we present a purely geometric theory that predicts the onset and removal of hockles in linear elastic fibers. This theory can be used to calculate the tension in the fiber when hockles form or are removed, or predict the size of the hockle at either point. We also explore the relationship between tension in a fiber and the onset and removal of plectonemes. We find that the tension during removal of plectonemes exhibits a non-monotonic behaviour that has gone unreported by

most of the literature. We develop a friction-based theory that accounts for this unexpected phenomenon.

The experiments, theory, and data analysis presented in this paper were designed and performed by myself, with assistance on the experimental side by undergraduate thesis student Elsie Loukechenko and theory contributions by Kari Dalnoki-Veress. The paper was written by myself and Kari Dalnoki-Veress.

Writhing and hockling instabilities in twisted elastic fibers

Adam Fortais,[1] Elsie Loukiantchenko,[1] and Kari Dalnoki-Veress[1,2,*]

[1] *Department of Physics and Astronomy, McMaster University, 1280 Main Street West, Hamilton, Ontario, L8S 4M1, Canada*
[2] *UMR CNRS Gulliver 7083, ESPCI Paris, PSL Research University, 75005 Paris, France.*

(Dated: October 3, 2021)

The buckling and twisting of slender, elastic fibers is a deep and well-studied field. A slender elastic rod that is twisted with respect to a fixed end will spontaneously form a loop, or *hockle*, to relieve the torsional stress that builds. Further twisting results in the formation of plectonemes – a helical excursion in the fiber that extends with additional twisting. Here we use an idealized, micron-scale experiment to investigate the energy stored, and subsequently released, by hockles and plectonemes as they are pulled apart, in analogy with force spectroscopy studies of DNA and protein folding. Hysteresis loops in the snapping and unsnapping inform the stored energy in the twisted fiber structures.

INTRODUCTION

Take a cord, twist one end with respect to the other, then relax the tension in the cord. We have all likely encountered the spontaneous looping and subsequent helix that will form with additional twisting. Hockling, or the buckling and looping of a twisted rod, is a well known and intensely studied phenomenon [1–16]. When a cord is twisted, a significant amount of elastic energy can be stored in the twists of the fiber. By introducing slack in the fiber, this stored energy can be released by untwisting, however, if the rotation at the ends of the cord are fixed, untwisting is accompanied by bending into a hockle or plectoneme (a double-helix structure terminating in a loop) since the ends are fixed. When this occurs, hockling is preceded by a modified Euler buckling that results in sinusoidal buckles, eventually coarsening into a single loop [2–4].

Because hockling can result in damage to cables, determining the criteria for hockling is of practical engineering concern. Research has focused on experiments using braided cables, nickel-titanium (nitinol) rods, and plastic fibers with thicknesses ranging from millimeters to centimeters [3, 4, 6, 10, 12, 13, 17–20]. However, performing these experiments at such large scales leads to complicating factors such as gravitational sagging, material defects, and non-uniformity. Furthermore, few experimental studies have explored the removal of hockles [10, 12, 19, 21, 22]. Additionally, the choice of material in these studies are often prone to plastic deformation at low strains, limiting the study of hockle removal to small degrees of twist.

Beyond hockling – the creation of the first loop – a highly twisted rod may begin writhing, where the associated rotation of the loop results in the formation of a plectoneme [2, 3, 6, 9, 13, 18, 23–32]. While this is less common in engineering applications, it occurs frequently in biological systems like DNA and plant tendrils [23, 33–41]. However, it is difficult to study this process *in-vitro*, and in the particular case of DNA, thermal fluctuations, and electrostatic interactions may both initiate plectoneme formation as well as introduce noise into any potential force measurements [25, 26, 28, 42–49]. Gaining a deeper understanding of twisted fibers could help in developing bio-inspired smart materials [9, 50, 51].

In this study, uniform, cylindrical, elastic fibers with diameters on the order of ~ 10 μm are used to experimentally investigate the hockling and writhing phenomena. Much like force spectroscopy measurements carried out with DNA and magnetic tweezers [43, 44], here on larger length scales we employ a micro-pipette deflection technique [52, 53] to quantify the tension, twisting, and bending energies in the system as a fiber hockles, writhes, and is pulled apart again. Extending the work of Ross and Yabuta, we first derive exact, material-independent hockling and hockle-removal criteria [12, 21]. The expression derived is purely geometric with no fit parameters, and accurately describes experiments performed with fibers of various sizes. We then focus on the formation and removal of plectonemes from a twisted fiber, with the latter revealing an especially rich force response.

EXPERIMENT

A cylindrical, elastic fiber with a radius of ~ 10 μm is attached to two thin glass capillary pipettes acting as posts. One glass post is mounted on a rotational stepper motor (1.8° resolution) and linear actuator, allowing precise control of tension, slack, and degree of twisting in the fiber. The other post, a capillary that acts as a sensitive force transducer, is capable of measuring the tension in the fiber directly. The force transducer pipette is mounted perpendicular to the length of the fiber to facilitate force measurement. A schematic of the experimental setup is shown in Figure 1a).

Both posts are made from glass capillary tubes with a diameter of 1.0 mm (World Precision Instruments, USA). The force transducer is made by pulling a capillary tube with a pipette puller (Narishige, Japan) to be long (∼

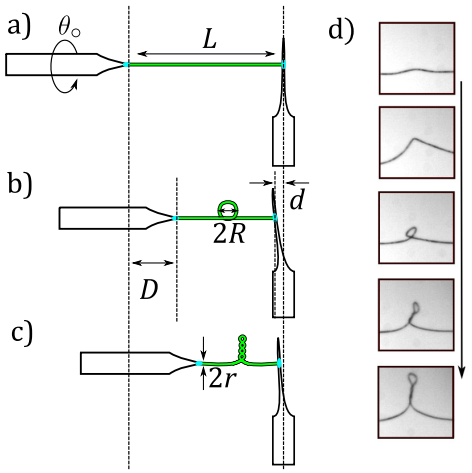

FIG. 1. a) A fiber with radius r and length L was glued to two posts, a mobile post (left) and a force-transducer post (right). The left post is rotated by an angle $\theta_\circ$, and moved toward the right post. b) As the posts move together, the fiber untwists with the formation of a loop. c) Upon further decreasing the distance a plectoneme forms. The process is then reversed and the glass pipettes are separated. Tension in the fiber is measured by observing the deflection d of the force-transducer pipette and $D >> d$. d) Optical image sequence of a $r \approx 10$ μm fiber during a typical experiment.

1 cm), thin ($\sim$ 10 μm) enough to deflect when tension was applied to the fiber. By calibrating this pipette, its spring constant k ($\sim$ 0.5 N/m) can be determined, allowing for force measurements as small as hundreds of pN by monitoring the deflection of the pipette d using cross-correlation image analysis [52, 53].

The fibers used in this experiment were made from Elastollan (Wacker Chemi AG), a commercially available elastomer with Young's modulus $E = 11 \pm 3$ MPa which was determined via extensional stress-strain tests performed on several different fibers with $r \approx 10$ μm (not shown). Fibers were made by heating a pellet of Elastollan to 240° C, dipping a glass pipette into the melt, then rapidly pulling the pipette out of the melt. The resulting fibers have uniform, cylindrical cross-sections with a diameters of ~ 10 μm. The fibers were inspected optically for uniformity, then glued across the posts with a dilute polystyrene-toluene solution. A droplet of the solution was placed at the contact point between the fiber and posts, and as the toluene evaporated, a layer of glassy polystyrene was left which holds the fiber in place. Toluene was selected as the solvent as it selectively dissolves polystyrene and not Elastollan.

In a typical experiment the fiber is rotated at one end by an angle of $\theta_\circ = 2\pi n$ corresponding to n full revolutions [Fig. 1a)], while the fiber of length L, is held at an initial tension such that the fiber remains straight and unbuckled. The tension is then released by moving the left post by a distance D and bringing the posts together at a speed of 30 μm/s [Fig. 1b)]. Strictly, the slack introduced into the fiber $\delta = D + d$, but since the distance the post is moved is $\sim 10^3$ times greater than the deflection of the force sensing pipette, we can take $\delta \approx D$. As the slack is increased, the fiber is observed and found to hockle and writhe as the elastic energy stored in the twisted fiber is converted into bending energy [Fig. 1c)]. An optical image sequence of the fiber during a typical experiment is shown in Fig. 1d). Since the fiber is radially symmetric, twisting in either direction is equivalent and experiments are repeated with an initial twist of $-\theta_\circ$ (note that $\theta_\circ$ is defined as positive). Repeating the experiment for $\theta_\circ$ and $-\theta_\circ$ compensates for any effects related to errors in defining $\theta_\circ = 0$ or radial non-uniformities. The deformations in the fiber as well as the deflection of the force transducer are simultaneously measured with optical microscopy.

RESULTS AND DISCUSSION

Formation and removal of a hockle

We consider the fiber as a slender rod with a large length to width ratio. We follow the argument outlined by Ross, which uses the results of Timoshenko and an analysis of the relevant energies in the system, to derive criteria for hockling related to the tension and torsion within a twisted fiber [12, 54, 55]. Notably, we find two different criteria for the creation and removal of a hockle, consistent with a bifurcated conformation pathway described by Neukirch *et al.* [56].

A twisted fiber will hockle and form a loop when the torsional energy stored in the fiber is large enough to overcome any stabilizing tension in the fiber. The bending energy within the resulting loop must be balanced by the work released as the ends of the fiber are brought together and the fiber untwists. To form a single loop, there are three energy contributions to consider: i) energy is required to bend the fiber into a loop; ΔU_b, ii) work is released as the two ends holding the fiber are brought closer, ΔW_T; and iii) energy stored in the twisted fiber is released, ΔW_M, because upon formation of a loop the fiber unwinds by one full rotation.

For the formation of a single loop, the bending energy is calculated assuming the fiber undergoes a linear elastic deformation into a perfect circle with radius R,

$$\Delta U_\mathrm{b} = \frac{EI}{2R^2} 2\pi R = \frac{\pi EI}{R}, \qquad (1)$$

where E is Young's modulus and I is the second area moment of the cylindrical fiber, $I = \pi r^4/4$. The work

done by bringing the two posts together is given by

$$\Delta W_{\mathrm{T}} = -T\Delta D, \tag{2}$$

where T is tension in the fiber, and ΔD is the change in the distance between the posts needed to form a loop (ΔD is defined as positive when the pipettes are brought together and negative as they are pulled apart). Lastly, the work done via untwisting, ΔW_{M}, is given by,

$$\Delta W_{\mathrm{M}} = 2\pi M, \tag{3}$$

where M is the twisting moment of the fiber, and 2π is the angle through which the fiber must unwind to form a single loop. Within the linear elastic regime, M varies linearly with the twist angle and is,

$$M = \frac{JG\theta_\circ}{L}, \tag{4}$$

where J is the torsional constant for a cylindrical fiber, $J = \pi r^4/2 = 2I$, and G is the shear modulus of the material (note that this assumption remains valid for large $\theta_\circ$ provided L is also large). The balance between the three energy contributions is then given by,

$$\frac{\pi EI}{R} + T\Delta D = 2\pi M. \tag{5}$$

Equation 5 can be applied to the formation of a loop as well as the removal of a loop, and each case will be considered in turn.

In the experiment presented here, a twisted fiber is stabilized against buckling by beginning in a state of tension. As the ends of the fiber are brought together, T decreases rapidly. For small values of $\theta_\circ$, the tension T at the point of hockling is minimal and we make the approximation that $T = 0$. This allows for Equation 5 to be simplified:

$$M = \frac{EI}{2R}. \tag{6}$$

From Equation 4 and Equation 6 we obtain,

$$\frac{JG\theta_\circ}{L} = \frac{EI}{2R}. \tag{7}$$

Making the generous assumption that the fiber outside the loop remains straight and all slack in the fiber goes into forming a perfect circle, we can define the slack as $\delta = 2\pi R$. We note that the assumption of a circular loop results in a small systematic error for small $\theta_\circ$ which will be discussed below. Equation 7 can then be written as,

$$\delta = \frac{\pi EI}{JG}\frac{L}{\theta_\circ}. \tag{8}$$

For a cylindrical fiber made from a material with a Poisson ratio of $\nu \approx 0.5$ (typical of elastomers), $E = 2G(1+\nu)$ and $J = 2I$, the amount of slack required to form a hockle is given by

$$\frac{\delta}{L} = \frac{3\pi}{2\theta_\circ}. \tag{9}$$

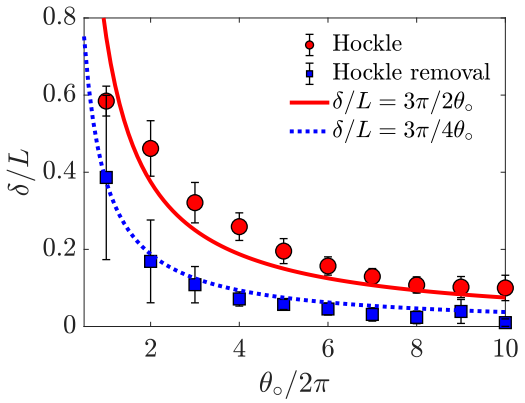

FIG. 2. Slack δ normalized by natural length L of fibers with initial twist $\theta_\circ$ at the point of hockling (circles, solid line) and removal of the loop (squares, dashed line) and their corresponding theoretical predictions. The data is the average of 10 fibers with lengths varying from $L = 6$ mm to 300 mm and radii varying from $r = 10$ μm to 1000 μm. Error bars are calculated as the standard deviation of the data.

We see from this expression that the amount of slack that needs to be provided in the fiber for loop formation is independent of the material properties of the fiber, and only dependent on geometry and how much the fiber is twisted. This result is to be expected since the formation of a hockle depends on equating the energy to form a loop with the energy stored in the twisted fiber, both of which depend on the modulus. In order to validate this expression, the slack required for a hockle to form for different values of $\theta_\circ$ was measured for 10 fibers with lengths varying from $L = 6$ mm to 300 mm and $r = 10$ μm to 1000 μm. The results are plotted in Figure 2 (circles). A systematic increase in δ/L for small values of $\theta_\circ$ can be seen, which is due to the assumption of a perfectly circular loop and straight fiber outside the loop. The assumption becomes increasingly valid at higher $\theta_\circ$. Interestingly, the results described above are consistent with the work of Strick *et al.* when the tension in the fiber approaches zero (hockle formation) [55]. Likewise, a comparable analysis using Crosserat rod theory has also been performed, yielding similar results by Neukirch and co-workers [56].

Having examined the formation of a hockle, we now turn to the removal of a hockle as the two ends of the fiber are pulled apart. If the ends of the fiber are pulled apart, R decreases, and the bending energy ΔU_{b} increases, until it becomes more energetically favorable to remove the loop and re-twist the fiber. In this case, T is no longer negligible and the work done in pulling apart the ends corresponds to the increase in bending energy in the increasingly small loop. The energy balance in Equation 5

then becomes $M = EI/R$. When compared to Equation 6, there is an extra factor of 2, which results in the prediction of δ (and size of the loop) when a hockle is removed,

$$\frac{\delta}{L} = \frac{3\pi}{4\theta_\circ}. \tag{10}$$

Again, there are no material parameters in the criterion for the removal of a hockle, and the data are shown in Figure 2 (squares). We note that, with the approximation of a circular hockle, the formation of a hockle requires twice as much slack in the fiber as does the removal of a hockle (compare Equations 9 and 10). In other words, the circumference of the loop which forms is twice as large as the circumference of the loop when the loop is removed. Since neither criteria depend on the material properties of the fiber, Equations 9 and 10 are valid for all uniform elastic rods with circular cross-sections within the linear elastic regime. Effects like sagging due to gravity which would affect large scale systems would modify this model.

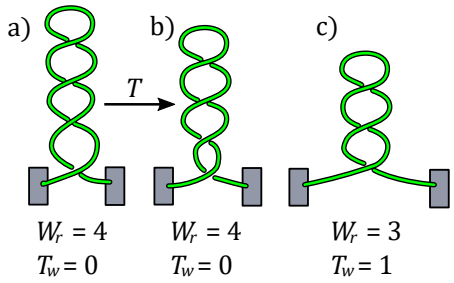

FIG. 3. Schematic of a plectoneme formed from a fiber with an initial twist angle corresponding to four full rotations ($\theta_\circ = 8\pi$). a) The stable plectoneme has minimal tension, and all of the energy stored in the twisted fiber is stored in the bends of the plectoneme. $L_k = 4$, $T_w = 0$, and $W_r = 4$. b) The tension is increased by separating the boundaries, and the bending energy in the loop at the base of the plectoneme increases. c) When the bending energy stored in the base loop is enough to destabilize the base loop, the twist in the fiber increases by one full rotation, and decrease the writhe number by 1: $T_w = 1$, and $W_r = 3$.

Plectoneme Growth and Removal

In the previous section we investigated the formation and removal of hockles. After a hockle forms in a highly twisted fiber, bringing the ends even closer together can allow a double-helix structure – a "plectoneme" – to form through a process called writhing. A plectoneme is shown schematically in Figure 3 (see also video in the Supplemental Information). Similar to destabilizing a hockle via tension, a plectoneme can also be destabilized, and this has been done in a number of studies on DNA using and magnetic tweezers [43, 57–60]. In this section we will investigate the growth and removal of plectonemes.

A plectoneme forms by exchanging the twist in the fiber for loops, resulting in points of self-contact as the fiber winds around itself. The "linking number", L_k, is defined as the sum of the "twist number" T_w and the "writhe number" W_r, both of which are integers [61, 62]. T_w counts the number of complete 2π radians of twist in the fiber, while W_r counts the number of self-contacts of the plectoneme [2, 18, 27, 28, 45]. If both ends of the fiber are unable to rotate, then $L_k = T_w + W_r$ is a constant. For example, a fiber with $\theta_\circ = 8\pi$ of twist and no self-contacts has $L_k = T_w = 4$, and $W_r = 0$. As expected, we observed that as the ends of the fiber were brought together, T_w decreased in steps of 1 with simultaneous increases in W_r. When $W_r = 1$, we observe a hockle in the fiber and when $W_r > 1$, a plectoneme is observed.

The results of a typical experiment are shown in Figure 4 where we plot T as a function of D (see movie in the SI [63]). The experiment proceeds as follows: a fiber is initially held under a small tension and twisted by $\theta_\circ$. At this point, $D = 0$, $W_r = 0$, and $L_k = T_w = \theta_\circ/2\pi$. One post is then translated with the motorized translation stage, increasing D (this sequence is labelled as *compression* in the figure). Small variations in the tension are observed as a plectoneme forms and W_r increases by forming self-contacts in a quantized manner. The process is then reversed (labelled as *extension* in the figure). Remarkably, a rich tension response emerges with much larger tension required to unwind a plectoneme compared to the formation. We observe large peaks in T, followed by sudden drops that are concurrent with decreases in the writhe number: $W_r \to W_r - 1$. The peaks increase in magnitude as W_r decreases, with the highest peak corresponding to the final removal of the hockle.

To understand the origin of the rich non-monotonic changes in tension, we now investigate what happens when $W_r \to W_r - 1$. Studies have found that a completely frictionless plectoneme experiences increased bending throughout the entire plectoneme structure [25, 26, 57]. Other studies, however, find that friction at fiber contact points plays an important role when a plectoneme is pulled apart [16, 64]. Our model is based on the importance of friction between fiber contacts for the discontinuous plectoneme unwinding. In the experiments shown, we observe that typically the self-contact at the base of the plectoneme slips, while the next self-contact sticks. Thus, as the tension is increased, the increase in bending is localized at the base of the plectoneme, and similar to pulling apart a hockle, the rotation of the plectoneme is a sudden event [see Fig. 3b) and c)]. While previous studies have sought to describe the bending energy contained in the plectoneme [2, 3, 6, 9, 10, 13, 18, 35, 38], we seek to understand this largely unreported phenomenon of discontinuous plectoneme unwinding: from the experiments

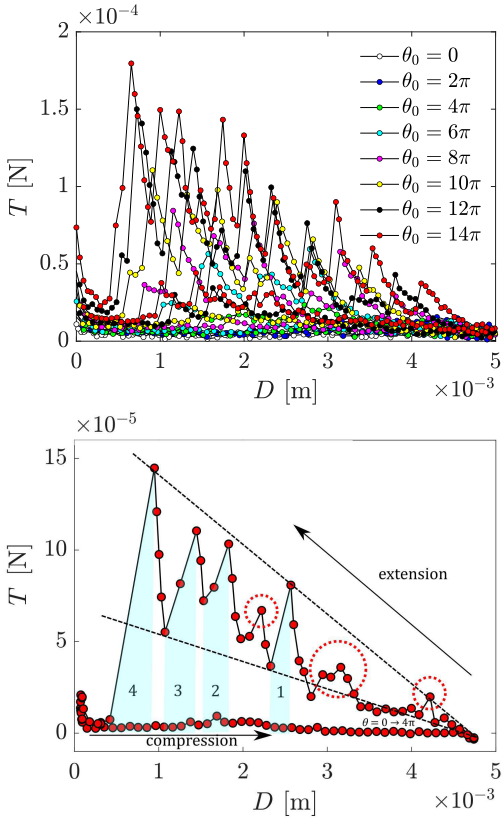

FIG. 4. a) T is measured in a twisted fiber with $L = 6$ mm and $r = 18$ μm for several values of θ_0 as its ends are brought together (compression) and then reversed (extension). b) For clarity, $\theta_0 = 12\pi$ has been plotted and annotated separately. As the fiber is compressed, small but distinct tension peaks are observed corresponding to an increase in the writhe number, W_r, until the tension vanishes within the resolution of the experiment. During extension T and M are initially small, allowing the plectoneme to unwind smoothly. After W_r decreases by 2, peaks and valleys in the tension corresponding to a reduction in W_r were observed (shaded area, numbered) and were determined by noting the image frames where the plectoneme begins rotating and where it stops rotating. Additional peaks (in dashed circles) are the result of stick-slip events as the fiber moved past itself that are not associated with a change in W_r. These stick-slip features are visible in the movie in the SI [63] when focussing on the vibrations of the right force-measurement pipette.

we observe that as tension is applied the plectoneme does not continuously unravel, rather, there are sudden and non-monotonic changes in the tension corresponding to the quantized decrease in W_r [25, 31, 64].

The schematic shown in Fig. 3 illustrates loops in the plectoneme. The size of these loops depend on the twist

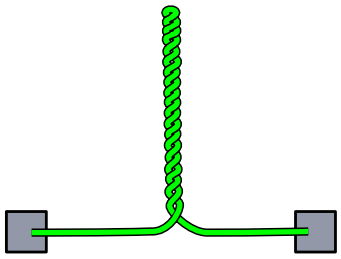

FIG. 5. Schematic of a plectoneme formed from a fiber with a high twist number and a correspondingly high twisting moment of the fiber M.

number: if the energy stored in twists is high compared to the energy required to bend the fiber, then tight loops form; conversely, a low twist number results in a low twisting moment, M, and open loops. In this study, M is low, and the experiments are carried out in a regime where loops form along the plectoneme. We find that the non-monotonic changes in the tension are coincident with the removal of a base loop. It is instructive to consider the limiting case of a fiber dominated by a high value of M with a plectoneme that is tightly wound as shown schematically in Figure 5, where the dominance of M means that we can ignore the contribution of bending energy. In this case, if we imagine pulling the boundaries apart then as the tension T increases, so does the twist angle, θ, in the fiber. In fact, any unit of length increase in the boundaries is directly proportional to an increase in θ. Thus $\theta \propto -\Delta D$ for separation of the boundaries (note the negative sign is the result of defining compression as positive). Next, the work done by tension goes into undoing the plectoneme and increasing the twisting energy of the fiber which scales as θ^2. We can then approximate $-T\Delta D \propto \theta^2$, which results in a linear change in the tension with separation of the boundaries like a Hookean spring, $T \propto -\Delta D$, for this continuum approach. Indeed the data shown in Figure 4 is bound by a linear envelope with the upper and lower boundaries in the tension corresponding to the transition from W_r to $W_r - 1$.

During the $W_r \rightarrow W_r - 1$ transition, the tension decreases suddenly from the initial value at the upper bound, to the final value after the transition at the lower-bound, T_i and T_f. We can understand this from the change in energy immediately before and immediately after the destabilization of the base-loop [see Fig. 3b) and c)]. Prior to destabilization, the tension increases and the work, $\int T(D)\mathrm{d}D$, increases the energy stored in bending at the base loop. A fraction of that bending energy is released when a loop is removed and a twist is added to the fiber: $W_r \rightarrow W_r - 1$ and $T_w \rightarrow T_w + 1$, resulting in a sudden decrease in the tension from T_i to T_f. As the tension decreases, the distance between the boundaries increases by some length roughly equal to the

slack created through the loss of the base-loop, l. Thus we have $(T_f - T_i)l \sim U_{b,f} - U_{b,i}$, where $U_{b,i}$ and $U_{b,f}$ are the bending energies before and after the destabilization of the base-loop. However, since the loss in bending energy is transferred into twist energy, we can write

$$-(T_f - T_i)l \sim \frac{JG}{L}(\theta_f^2 - \theta_i^2) = \frac{JG}{L}[4\pi(\theta_i + \pi)]. \quad (11)$$

We see that finally we obtain a linear dependence on the twist angle which bounds the maxima and minima in the tension given by this expression. Furthermore we see from Eq. 11, that $T_i - T_f$ increases with the degree of twist in the fiber, which is validated by the data since θ increases in Figure 4 as D decreases. Making the assumption, as in the continuum model above, that the variation in θ is linear in D, since each loop of the plectoneme is the same size, explains why the upper bound and lower bound are also linear in D.

We noted above that the discontinuous change in the tension associated with the quantized nature of destabilizing a plectoneme has been reported by few studies in the literature, while the sudden drop in tension associated with destabilizing a hockle is well known [25, 31, 64]. We attribute our success in measuring this effect to the small scale of our experiment. Since the magnitude of the tension peaks are linearly dependent on the twist angle θ (see Eq. 11), experiments for which $\theta_\circ$ is small may not exhibit large peaks until the final removal of a hockle. However, to stay within the linear elastic regime, $\theta_\circ/L$ must remain small. Because our fibers are exceedingly slender, we are able to perform experiments with relatively large $\theta_\circ$ while still remaining in the linear elastic regime. Finally, because our fibers are so small, sagging due to gravity is eliminated, facilitating the study of plectoneme formation and unravelling.

CONCLUSION

We have extended the energy analysis of Ross and Yabuta [12, 21] to predict the point at which the hockle is formed and destabilized, and validated both criteria with precise micron-scale experiments. The idealized system was also used to explore the formation and removal of plectonemes, observing multiple instabilities associated with the change in number of self-contacts within the plectoneme. The changes in tension observed with the experiments are well described by a simple model.

* dalnoki@mcmaster.ca

[1] T. Yu and J.A. Hanna. Bifurcations of buckled, clamped anisotropic rods and thin bands under lateral end translations. *Journal of the Mechanics and Physics of Solids*, February 2018.

[2] A. R. Champneys and J. M. T. Thompson. A multiplicity of localized buckling modes for twisted rod equations. *Proceedings of the Royal Society of London A*, 452(1954):2467–2491, 1996.

[3] J. M. T. Thompson and A. R. Champneys. From helix to localized writhing in the torsional post-buckling of elastic rods. *Proceedings of the Royal Society of London A*, 452(1944):117–138, 1996.

[4] J. Coyne. Analysis of the formation and elimination of loops in twisted cable. *IEEE Journal of Oceanic Engineering*, 15(2):72–83, 1990.

[5] M. A. Dias and B. Audoly. Wunderlich, Meet Kirchhoff: A General and Unified Description of Elastic Ribbons and Thin Rods. *Journal of Elasticity*, 119(1-2):49–66, April 2015.

[6] G.H.M. van der Heijden, S. Neukirch, V.G.A. Goss, and J.M.T. Thompson. Instability and self-contact phenomena in the writhing of clamped rods. *International Journal of Mechanical Sciences*, 45(1):161–196, January 2003.

[7] G. H. M. Van der Heijden and J. M. T. Thompson. Lock-on to tape-like behaviour in the torsional buckling of anisotropic rods. In *Localization And Solitary Waves In Solid Mechanics*, pages 133–156. World Scientific, 1999.

[8] N. Clauvelin, B. Audoly, and S. Neukirch. Matched asymptotic expansions for twisted elastic knots: a self-contact problem with non-trivial contact topology. *Journal of the Mechanics and Physics of Solids*, 57(9):1623–1656, 2009.

[9] M. Gazzola, L. H. Dudte, A. G. McCormick, and L. Mahadevan. Forward and inverse problems in the mechanics of soft filaments. *Royal Society Open Science*, 5(6):171628, June 2018.

[10] V. G. A. Goss, G. H. M. van der Heijden, J. M. T. Thompson, and S. Neukirch. Experiments on snap buckling, hysteresis and loop formation in twisted rods. *Experimental Mechanics*, 45(2):101–111, April 2005.

[11] D. M. Stump. The hockling of cables: a problem in shearable and extensible rods. *International journal of solids and structures*, 37(3):515–533, 2000.

[12] A. L. Ross. Cable kinking analysis and prevention. *Journal of Engineering for Industry*, 99(1):112–115, 1977.

[13] A. Ghatak and L. Mahadevan. Solenoids and plectonemes in stretched and twisted elastomeric filaments. *Physical Review Letters*, 95:057801, Jul 2005.

[14] M. Nizette and A. Goriely. Towards a classification of EulerKirchhoff filaments. *Journal of Mathematical Physics*, 40(6):2830–2866, June 1999.

[15] S. Neukirch and M. E. Henderson. Classification of the spatial equilibria of the clamped elastica: Symmetries and zoology of solutions. *Journal of Elasticity*, 68(1-3):95–121, 2002.

[16] M. K. Jawed, P. Dieleman, B. Audoly, and P. M. Reis. Untangling the mechanics and topology in the frictional response of long overhand elastic knots. *Phys. Rev. Lett.*, 115:118302, Sep 2015.

[17] H. Wada. Structural mechanics and helical geometry of thin elastic composites. *Soft Matter*, 12(35):7386–7397, 2016.

[18] W. B. Fraser and G. H. M. van der Heijden. On the theory of localised snarling instabilities in false-twist yarn processes. *Journal of Engineering Mathematics*, 61(1):81–95, May 2008.

[19] N. S. Ermolaeva, J. Regelink, and M. P.M. Krutzen. Hockling behaviour of single- and multiple-rope systems.

Engineering Failure Analysis, 15(1-2):142–153, January 2008.

[20] M. Habibi, N. M. Ribe, and D. Bonn. Coiling of Elastic Ropes. *Physical Review Letters*, 99(15), October 2007.

[21] T. Yabuta. Submarine Cable Kink Analysis. *Bulletin of JSME*, 27(231):1821–1828, 1984.

[22] N. Kojima. Cable Kink Analysis; Cable Loop Stability Under Tension. *Journal of Applied Mechanics*, 49:585, 1982.

[23] J. F. Marko and S. Neukirch. Competition between curls and plectonemes near the buckling transition of stretched supercoiled DNA. *Physical Review E*, 85(1), January 2012.

[24] W. B. Fraser and D. M. Stump. The equilibrium of the convergence point in two-strand yarn plying. *International journal of solids and structures*, 35(3-4):285–298, 1998.

[25] P. K. Purohit. Plectoneme formation in twisted fluctuating rods. *Journal of the Mechanics and Physics of Solids*, 56(5):1715–1729, May 2008.

[26] N. Clauvelin, B. Audoly, and S. Neukirch. Elasticity and Electrostatics of Plectonemic DNA. *Biophysical Journal*, 96(9):3716–3723, May 2009.

[27] S. Neukirch and J. F. Marko. Analytical Description of Extension, Torque, and Supercoiling Radius of a Stretched Twisted DNA. *Physical Review Letters*, 106(13), April 2011.

[28] I. M. Kulić, H. Mohrbach, R. Thaokar, and H. Schiessel. Equation of state of looped DNA. *Physical Review E*, 75(1), January 2007.

[29] J. F. Marko and S. Neukirch. Global force-torque phase diagram for the DNA double helix: Structural transitions, triple points, and collapsed plectonemes. *Physical Review E*, 88(6), December 2013.

[30] M.L. Smith and T.J. Healey. Predicting the onset of DNA supercoiling using a non-linear hemitropic elastic rod. *International Journal of Non-Linear Mechanics*, 43(10):1020–1028, December 2008.

[31] B. C. Daniels, S. Forth, M. Y. Sheinin, M. D. Wang, and J. P. Sethna. Discontinuities at the DNA supercoiling transition. *Physical Review E*, 80(4), October 2009.

[32] M. Chamekh, S. Mani-Aouadi, and M. Moakher. Stability of elastic rods with self-contact. *Computer Methods in Applied Mechanics and Engineering*, 279:227–246, September 2014.

[33] J. L. Silverberg, R. D. Noar, M. S. Packer, M. J. Harrison, C. L. Henley, I. Cohen, and S. J. Gerbode. 3D imaging and mechanical modeling of helical buckling in Medicago truncatula plant roots. *Proceedings of the National Academy of Sciences*, 109(42):16794–16799, 2012.

[34] S. J. Gerbode, J. R. Puzey, A. G. McCormick, and L. Mahadevan. How the Cucumber Tendril Coils and Overwinds. *Science*, 337(6098):1087–1091, August 2012.

[35] F. Tanaka and H. Takahashi. Elastic theory of supercoiled DNA. *The Journal of Chemical Physics*, 83(11):6017–6026, December 1985.

[36] B. D. Coleman, I. Tobias, and D. Swigon. Theory of the influence of end conditions on selfcontact in DNA loops. *The Journal of Chemical Physics*, 103(20):9101–9109, November 1995.

[37] K. A. Hoffman, R. S. Manning, and J. H. Maddocks. Link, twist, energy, and the stability of DNA minicircles. *Biopolymers: Original Research on Biomolecules*, 70(2):145–157, 2003.

[38] E. L. Starostin. Three-dimensional shapes of looped DNA. *Meccanica*, 31(3):235–271, 1996.

[39] M. M. Gromiha, M. G. Munteanu, A. Gabrielian, and S. Pongor. Anisotropic elastic bending models of DNA. *Journal of Biological Physics*, 22(4):227–243, 1996.

[40] A. G. Cherstvy. Looping charged elastic rods: applications to protein-induced DNA loop formation. *European Biophysics Journal*, 40(1):69–80, January 2011.

[41] I. V. Dobrovolskaia, M. Kenward, and G. Arya. Twist Propagation in Dinucleosome Arrays. *Biophysical Journal*, 99(10):3355–3364, November 2010.

[42] S. Goyal, N.C. Perkins, and C.L. Lee. Nonlinear dynamics and loop formation in Kirchhoff rods with implications to the mechanics of DNA and cables. *Journal of Computational Physics*, 209(1):371–389, October 2005.

[43] J. Lipfert, J. W. J. Kerssemakers, T. Jager, and N. H. Dekker. Magnetic torque tweezers: measuring torsional stiffness in DNA and RecA-DNA filaments. *Nature Methods*, 7(12):977–980, December 2010.

[44] F. Mosconi, J. F. Allemand, D. Bensimon, and V. Croquette. Measurement of the Torque on a Single Stretched and Twisted DNA Using Magnetic Tweezers. *Physical Review Letters*, 102(7), February 2009.

[45] J. F. Marko and E. D. Siggia. Statistical mechanics of supercoiled DNA. *Physical Review E*, 52(3):2912, 1995.

[46] D. M. Stump, W. B. Fraser, and K. E. Gates. The writhing of circular crosssection rods: undersea cables to DNA supercoils. *Proceedings of the Royal Society of London. Series A: Mathematical, Physical and Engineering Sciences*, 454(1976):2123–2156, 1998.

[47] M. Ganji, S. H. Kim, J. van der Torre, E. Abbondanzieri, and C. Dekker. Intercalation-Based Single-Molecule Fluorescence Assay To Study DNA Supercoil Dynamics. *Nano Letters*, 16(7):4699–4707, July 2016.

[48] H. Brutzer, N. Luzzietti, D. Klaue, and R. Seidel. Energetics at the DNA supercoiling transition. *Biophysical Journal*, 98(7):1267–1276, 2010.

[49] C. Maffeo, R. Schöpflin, H. Brutzer, R. Stehr, A. Aksimentiev, G. Wedemann, and R. Seidel. DNADNA interactions in tight supercoils are described by a small effective charge density. *Physical Review Letters*, 105(15):158101, 2010.

[50] A. R. Studart and R. M. Erb. Bioinspired materials that self-shape through programmed microstructures. *Soft Matter*, 10(9):1284–1294, 2014.

[51] N. Hu and R. Burgueño. Buckling-induced smart applications: recent advances and trends. *Smart Materials and Structures*, 24(6):063001, June 2015.

[52] M. J. Colbert, A. N. Raegen, C. Fradin, and K. Dalnoki-Veress. Adhesion and membrane tension of single vesicles and living cells using a micropipette-based technique. *The European Physical Journal E*, 30(2):117, Sep 2009.

[53] M Backholm and O Bäumchen. Micropipette force sensors for in vivo force measurements on single cells and multicellular microorganisms. *Nature Protocols*, 14:594–615, 2019.

[54] S. P. Timoshenko. *Theory of elasticity*. Engineering societies monographs. McGraw-Hill, 1987.

[55] T. R. Strick, M.-N. Dessinges, G. Charvin, N. H. Dekker, J.-F. Allemand, D. Bensimon, and V. Croquette. Stretching of macromolecules and proteins. *Reports on Progress in Physics*, 66(1):1–45, 2003.

[56] S. Neukirch, G.H.M van der Heijden, and J.M.T. Thompson. Writhing instabilities of twisted rods: from infinite

Chapter 4

Spontaneous elastocapillary winding of thin elastic fibers in contact with bubbles

The second paper included in the thesis is about elastocapillary. It has been accepted to be published in Physical Review Letters.

This paper builds on several articles studying the way thin fibers deform in and around liquid droplets via capillary forces [49, 50]. In it, fibers are found to wind and wrap around liquid bubbles, spontaneously forming unique fiber coils.

The experiments, theory, and data analysis presented in this paper were designed and performed by myself, with assistance on the experimental side by undergraduate thesis student Kathleen Charlesworth and theory contributions and helpful discussions with Kari Dalnoki-Veress and Rafael Schulman. The paper was written by myself and Kari Dalnoki-Veress.

Spontaneous elastocapillary winding of thin elastic fibers in contact with bubbles

Adam Fortais,[1] Kathleen Charlesworth,[1] Rafael D. Schulman,[1] and Kari Dalnoki-Veress[1,2,*]

[1] *Department of Physics and Astronomy, McMaster University, 1280 Main Street West, Hamilton, Ontario, L8S 4M1, Canada*
[2] *UMR CNRS Gulliver 7083, ESPCI Paris, PSL Research University, 75005 Paris, France.*

(Dated: September 29, 2021)

We study the elastocapillary interaction between flexible microfibers in contact with bubbles trapped at the surface of a liquid bath. Microfibers placed on top of bubbles are found to migrate to and wrap into a coil around the perimeter of the bubble for certain bubble-fiber size combinations. The wrapping process is spontaneous: the coil spins atop the bubble, thereby drawing in excess fiber floating on the bath. A two-dimensional microfiber coil emerges which increases the lifetime of the bubbles. A simple model incorporating surface and bending energies captures the spontaneous winding process.

Surface wetting is common to many natural and industrial processes like the clumping of wet hairs and fibers [1–5], and the spreading of liquids on surfaces [6–8], which can result in beautiful and useful elastic deformations of the solid surface [9–17]. Even simple systems consisting of a stiff fiber which is partially wet by a drop is more complicated than it may first appear, as it can take on two equilibrium states: an axisymmetric "barrel" where the fiber penetrates the drop, and non-axisymmetric "clam-shell" configuration where the droplet is sessile on one side of the fiber [6, 7, 16, 18–21]. More compliant fibers are able to buckle and collapse inside the drop when tension is reduced [5, 22–26]. In some cases this process has been shown to result in spooling a fiber within a liquid drop, and is used by some types of spiders in web construction [25]. Alternatively, a droplet may take on a clam-shell configuration when placed on a fiber if the liquid drop is small compared to the radius of the fiber, or if the fiber is less wettable [12, 20, 21, 27]. In the clam-shell configuration, capillary forces can be strong enough to induce large deformations in a thin strip or fiber [27], in some cases even causing the fiber to wrap entirely *around* the drop [12, 28].

In all of these elastocapillary systems, where capillarity and elasticity compete, a natural length-scale emerges which sets an approximate upper-bound on the size of elastic deformations caused by capillary forces [16, 17]. The bending elastocapillary length, l_b, represents the ratio between bending and capillary energies in a system, and for a fiber can be defined as, $l_b = \sqrt{EI/2\pi r\gamma}$, where EI is the bending stiffness of the elastic fiber, $2\pi r$ is the circumference of the fiber, and γ is the liquid-vapor surface tension [16]. EI, which depends on the Young's modulus of the fiber E and the second-moment of area I, has a strong dependence on the radius of the elastic fiber r. For a uniform, cylindrical fiber, $I = \pi r^4/4$, which explains why elastocapillary deformations are easily observed in slender objects like thin fibers.

Here we explore the elastic deformation of a fiber due to capillary forces at a liquid bath with an air-bubble. An elastic fiber is introduced at the liquid membrane at the top of an air bubble. If the fiber diameter is greater than the thickness of the film, the fiber bridges across the film, and, under some conditions causes the fiber to spontaneously wind around the circular periphery of the liquid membrane. The resulting coil is shown in Fig. 1 before (A) and after the air bubble bursts (B) (video in Supplemental Material (SM) [29]). The bridging mechanism is reminiscent of Pickering emulsions and techniques for bubble stabilization involving the absorption of solid inclusions at the liquid interfaces [30–38]. In short, the fiber has a lower free energy when bridging the liquid film on the top of the bubble, compared to that at the liquid interface, where less fiber is in contact with air. Using a simple model which balances the energy cost of bending the fiber against the reduction in the surface energy when the fiber bridges the liquid film, we predict the on-

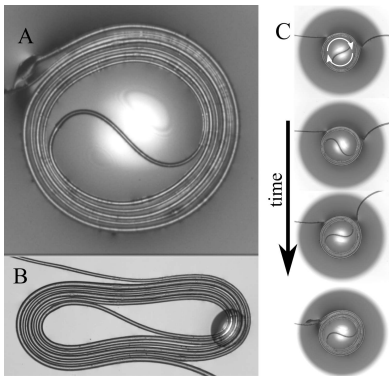

FIG. 1. An elastic fiber (SIS) with a radius $r = 5$ μm winds around the liquid film at the top of an air bubble at the interface of a glycerol bath before (A), and after (B), the bubble bursts (in this case a small air bubble remained trapped below the coils on the right side of (B). (C) A time sequence of the winding process. The fiber can coil spontaneously, forming structures like these in no more than 2-3 minutes. For scale, the diameter of the coil in (A) and (C) is ~ 500 μm.

set of winding. This coiled structure bears a striking resemblance to the packing of genetic material within viral capsids, a process that requires large lengths of fiber-like materials to pack and orient within small volumes [39–42]. We observe that the wound structure stabilizes air bubbles at the interface.

In the experiment a fiber with radius $r \sim 10^{-6}$ m is placed on the surface of a glycerol ($\gamma \approx 64$ mN/m) bath. Small air bubbles with radii ranging from approximately $R_\mathrm{b} \sim 10^{-4}$ to $R_\mathrm{b} \sim 10^{-3}$ m are introduced below the surface of the bath with a syringe connected to a micropipette. Buoyancy carries the air bubbles to the surface, lifting the fiber as the bath's surface deforms locally into a shape well approximated by a spherical cap. A schematic of the air bubble is shown in Fig. 2(A). The air bubble and fiber are observed with optical microscopy from above [see Fig. 2(B)-(G)]. Worth noting is that the bubble cap can be related to R_b through the Bond number, Bo, which relates the relative importance of gravity to surface tension, in our experiments is small. $\mathrm{Bo} = \rho g R_\mathrm{b}^2/\gamma$, where $\rho \approx 1.3 \cdot 10^3$ kg/m^3 is the difference in density between the air and the liquid, and g is gravitational acceleration. Here $\mathrm{Bo} << 1$, and a bubble at the surface of a liquid will remain nearly spherical and protrude only about $\sim 0.05 R_b$ above the surface of the liquid [46–48].

The polymer fibers used in the experiment are made from several materials: polystyrene (PS), a glass at room temperature with a molecular weight of M_n = 25000 kg/mol, polydispersity index of PDI = 1.04 (Polymer Source Inc.), Elastollan 1185A-10 (BASF Inc.), a polyether-based physically cross-linked elastomeric solid at room temperature, and styrene-isoprene-styrene (SIS), a triblock copolymer (14% styrene content, Sigma-Aldrich) which is a physically crosslinked elastomeric solid at room temperature. The elastic modulus of Elastollan is $E_\mathrm{elast} = 10 \pm 3$ MPa (determined via extensional stress-strain tests performed on fibers with $r \sim 10^{-6}$ m). The elastic moduli of PS and SIS are taken from the literature (E_PS = 3.4 GPa, E_SIS = 0.8 MPa) [43, 44]. Fibers are made by either melting or dissolving the polymer, dipping a glass pipette into the viscous polymer liquid, then rapidly pulling the pipette out of the polymer. PS and Elastollan were melted by heating a small sample (170°C for PS and 235°C for Elastollan), while the SIS was dissolved into toluene (Optima-grade, Sigma Aldrich) to form a viscous polymer solution. The resulting fibers have uniform, cylindrical cross-sections with diameters ~ 10 μm, which were inspected optically for uniformity.

When a fiber and bubble come into contact, depending on the size of the air bubble and fiber, one of two processes occur. Either the fiber remains at the apex of the liquid film until the bubble eventually ruptures, or the fiber begins to bend, thereby increasing curvature, and migrate down the cap toward the perimeter of the

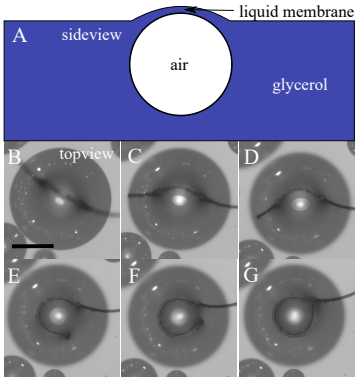

FIG. 2. (A) A schematic of an air bubble which deforms the surface of a liquid bath via buoyancy. (B-G) A SIS fiber spontaneously winding around an air bubble in a bath of glycerol over approximately 30 second. The scale bar is 200 μm.

bubble where it remains bridged but bounded by a membrane of increasing thickness. If the fiber migrates to the perimeter of the liquid film, the fiber winds around the portion of the bubble that is extended above the undeformed surface of the bath, and forms a coil. A sequence of the winding process taken with an optical microscope from above the experiment is shown in Fig. 2(B-G). For a fiber to spontaneously wrap around a bubble, the system must overcome the energy cost of bending around the perimeter of the liquid film atop the bubble, which is driven by a decrease in the system surface energy. We turn our attention first to the bending energy, before describing the surface energy.

When a fiber winds, it is observed to wind around the periphery of the bubble cap that extends above the surface of the liquid bath. We measure the radius of the bubble cap R_c by imaging the bubble from above with monochromatic light, resulting in a distinct light circle corresponding to the extended cap. An example of one of these images is shown in Fig. 3(A) and (B). Assuming linear elastic deformation of the fiber (typical strains < 0.02 [29]), the bending energy *per unit length* for a fiber can be described with Euler–Bernoulli beam theory,

$$E_\mathrm{b} = \frac{\pi E r^4}{8R^2}; \tag{1}$$

when the fiber bends to a radius of curvature R. As the fiber winds, it takes on a radius of curvature $R = R_\mathrm{c}$, resulting in an increase in bending energy.

Bending in the fiber will only proceed spontaneously if the system free energy is reduced. Here the bending is accompanied by a reduction of interfacial energy associated with the fiber bridging the liquid film at the apex of the bubble. The liquid membrane at the apex of the

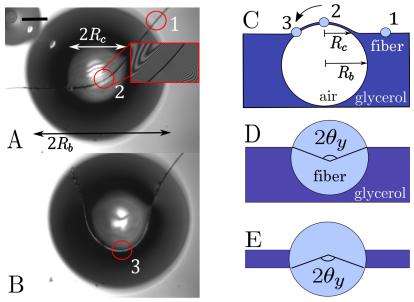

FIG. 3. (A) and (B) Top-down, monochromatic optical images of a fiber-bubble system before and after migrating to the perimeter of the bubble cap. Red circles are numbered 1-3 and correspond to the different states of a segment of fiber shown in (C). The scale bar is 250 μm, and the inset shows the interference fringes from the meniscus surrounding the bridged fiber. (C) Schematic of the fiber-bubble system side-on. The fiber is shown in light blue in position 1, 2, and 3, representing the unbridged, pre-winding and post-winding positions of the fiber. (D) and (E) are schematics of a fiber cross-section floating on a fluid bath (unbridged), and bridged across a fluid membrane respectively. The schematic in (E) omits the bridging meniscus for clarity.

air bubble is an air-glycerol-air film shown schematically in Fig. 3(C). The film is the region where the air bubble extends above the surface of the bath. The curvature of the membrane causes liquid to drain from the cap back into the bath, resulting in radial thinning of the cap. When the cap thins sufficiently, a fiber laid across the cap may "bridge" or straddle the liquid membrane, trading solid-liquid interface for liquid-vapor interface. This is observed experimentally as the fiber suddenly sinking into the liquid membrane, and the appearance of interference fringes resulting from a small meniscus that is created along the length of the fiber when viewed with monochromatic light. An example of these interference patterns are visible in the inset of Fig. 3(A), and an idealized schematic of a fiber before and after bridging is shown in Fig. 3(D) and (E). The bridging process occurs if there is a net reduction of interfacial energy *per unit length* of fiber which is given by,

$$\Delta E_{\rm s} = 2r\theta_y(\gamma_{sv} - \gamma_{sl}); \tag{2}$$

where θ_y is the glycerol/fiber contact angle, γ_{sv} is the solid-vapor interfacial tension, and γ_{sl} is the solid-liquid interfacial tension. The term on the right corresponds to the change in interfacial energy on the part of the fiber that bridges across the liquid membrane and goes from a solid-liquid interface to a solid-vapor interface. When $\gamma_{sv} - \gamma_{sl} < 0$, surface energy is reduced when the fiber bridges the liquid membrane. Using Young's law for partial wetting, $\gamma_{sv} = \gamma_{sl} + \gamma\cos\theta_y$, Equation 2 can be re-written,

$$\Delta E_{\rm s} = 2r\gamma\theta_y\cos(\theta_y). \tag{3}$$

Since the thickness of the liquid membrane defining the air bubble increases radially from the center of the bubble, there will be a point where the liquid membrane is too thick for the fiber to bridge. At this point, the change in surface energy per unit length of fiber ΔE_s results in a driving force, pulling more fiber on to the air bubble and into the bridged state. As more fiber is pulled on to the air bubble, the fiber must bend and reorient to accommodate this extra length. Wrapping around the perimeter of the liquid membrane allows more fiber to bridge. Fig. 3(A) and (B) show a top-view of a fiber-bubble system before and after the fiber migrates to the perimeter of the air bubble, immediately before the fiber begins to wind around the perimeter of the membrane. Thus, we have the remarkable result that a fiber will wrap itself around the capped film at the apex of the bubble when the increase in bending energy is less than the decrease in interfacial energy (see video [29]). Although the driving force causing this spontaneous winding comes from the bridging phenomenon, bridging alone is not sufficient to initiate winding, and many bridged samples do not proceed to wind. The energy released through bridging must be sufficient to overcome the increase in bending energy during the winding process.

We formulate a simple model by taking the initial state of the fiber as unbridged and straight [Fig. 3(D)], and comparing the energy to the the final state of the fiber which bridges the liquid film and is bent around the perimeter of the bubble cap [Fig. 3(E)]. The critical radius of the bubble cap, $\mathcal{R}_{\rm c}$, that distinguishes the non-winding regime, $R < \mathcal{R}_{\rm c}$, from the winding regime, $R > \mathcal{R}_{\rm c}$, is given by the point where the change in bending energy is balanced by change in surface energy: $\Delta E_{\rm s} + \Delta E_{\rm b} = 0$. We obtain $2r\gamma(\theta_y\cos\theta_y) = \pi E r^4/8\mathcal{R}_{\rm c}^2$. Re-arranging this expression allows one to calculate $\mathcal{R}_{\rm c}$ as a function of $l_{\rm b}$, and θ_y,

$$\mathcal{R}_{\rm c} = \frac{l_b}{\sqrt{2\theta_y\cos\theta_y}}. \tag{4}$$

Since θ_y is different for different polymer-liquid combinations, contact angle measurements were performed by placing small droplets of glycerol on films of each material. Droplets were imaged from the side to determine the contact angle θ_y for each polymer. The contact angles were $78^\circ \pm 2^\circ$, $82.5^\circ \pm 3^\circ$, and $67.5^\circ \pm 3^\circ$ for PS, SIS, and Elastollan respectively [29].

Equation 4 was tested by observing fibers and bubbles of various sizes as they were brought into contact. After bridging, if the fiber migrated to the perimeter of the cap and continued to pull more fiber onto the cap, it was considered to have begun winding, and the point was plotted in green (light grey) in Fig. 4. Otherwise, if the

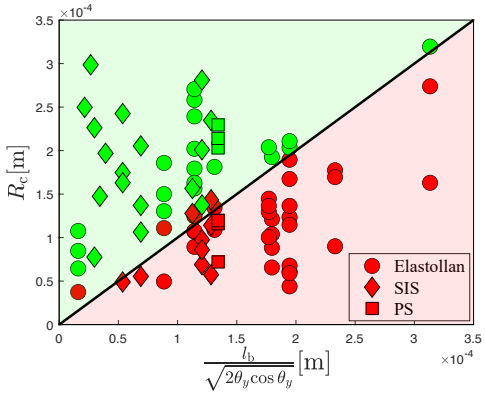

FIG. 4. Phase diagram of the winding criterion for Elastollan (circles), SIS (diamonds) and PS (triangles) fibers in glycerol. The slope defining the transition from Equation 4 is $m = 1$. Green (light grey) points designate fiber-bubble combinations which wind, red (dark grey) points designate those that do not wind.

fiber came to rest without winding around the perimeter, the point was plotted in red (dark grey). If any result was ambiguous (for example the bubble bursts while the fiber is migrating but has not begun to wind), the experiment was discarded. Notably, bubbles could be expected to burst prematurely if the time required to wind is longer than the typical lifespan of a bubble. Although the winding speed is expected to depend on the energy balance described above, the dynamics of the process is also related to the length of the fiber away from the bubble and the viscous drag this segment of fiber experiences. For this reason, the ability to see winding should be taken as an upper bound. By plotting R_c as a function of $l_b/\sqrt{2\theta_y \cos\theta_y}$ as suggested by Eq. 4, we obtain a winding phase diagram for all data with different bubble size, fiber radius, and three polymers spanning several orders of magnitude in modulus. The data is in excellent agreement with the model with a line passing through the origin and a slope of 1, defining the winding/no-winding boundary. The phase diagram indicates that winding is possible for bubbles with large radii and thin fibers, whereas thick fibers will not wind around a small radius.

Fibers which had completely wrapped around the bubble resulted in 2-dimensional coils as shown in Fig. 1(A) (video in SM [29]). By winding around the bubble cap, the fiber creates a spontaneous barrier which impedes drainage from the bubble cap to the bath. Thinning of the membrane is hindered, which enhances bubble stability. Though bubble stabilization depends on the viscosity of the liquid, winding speed, evaporation rate, and details as to how curved liquid membranes drain, we observe a qualitative increases of bubble lifetime. To test this, the

FIG. 5. A macroscopic demonstration of how the fiber coil can collapse to a flat surface, forming a unique, non-circular shape.

lifetime of 20 bubbles with radii between 170 – 600 μm was measured without coils and found to be 110±50 s. In contrast, for 22 similarly sized bubbles, fibers with radii between 2 – 11 μm were allowed to wind, and the wound bubbles were observed to have a lifetime of 440 ± 190 s, even *after* the winding was complete (a process which takes approximately 1 – 2 minutes). Since the winding process is dependent on the fiber thickness and bubble radius, the lifetime of wound bubbles presented should be taken as a lower bound. In fact, some bubbles survived hours, which is consistent with the stabilizing qualities of Pickering emulsions [45].

In instances when the fiber is thin, long, and the air bubble is large, the fiber migration process creates an S-shaped curve at the apex [see Fig. 1 (A)]. The S-shaped curve is formed when the length of fiber extending from both sides of the bubble are long. In that case, an S-curve must appear to satisfy the fiber lying on a 2D surface and winding in the same orientation (see the SM [29]). Fig. 1(B) shows the shape the fiber coil took after the bubble burst, and demonstrates another interesting aspect of the fiber coil geometry that is produced through winding. As a fiber completely surrounds a bubble cap, pulling more fiber onto the bubble perimeter requires the existing coil to be displaced. By migrating up the cap, more area around the perimeter of the cap can be liberated. The result is a coil which begins to trace the three-dimensional surface area of the spherical cap. When the bubble finally bursts, if there is low fiber-fiber adhesion, the coil will violently unwind in a process similar to the "entropic explosion" seen in viral capsids [39–42]. If there is sufficient adhesion between fiber surfaces, capillary forces pull the coil onto the surface of the bath, forcing the coil, which conforms to a spherical cap, to collapse onto an unfavourable flat surface. The deformation results in the unique shape shown in Fig. 1(B). One can replicate this easily by winding a rope around the apex of a sphere, and collapsing the structure onto a flat surface as shown in Fig. 5.

Here a unique self-assembly process is presented which occurs when thin polymer fibers are brought in contact with air bubbles located at the surface of a liquid bath. Fibers were found to bridge the liquid membrane defined by the air-liquid-air interface of the air bubble at the sur-

face of the bath. Doing so reduces the interfacial energy of the fiber-liquid system. The decrease in interfacial energy of the system comes at a cost of increasing the bending energy of the fiber as more fiber is pulled into the bridged state and forced to reorient on the bubble cap. A simple expression depending on the bubble size, bending elastocapillary length l_b, and liquid/solid contact angle of the fiber predicts the onset of this spontaneous winding process. This expression was confirmed experimentally for fibers of various sizes and materials in a bath of glycerol. By wrapping a bubble cap with a spiral of fiber, the flow of liquid from the cap back into the bath is impeded which significantly increases bubble lifetimes. The self-assembly process may be used in the fabrication of 2D microcoils, the production of metamaterials, or harnessed to stabilize or pattern micro-bubbles.

We gratefully acknowledge financial support by the Natural Science and Engineering Research Council of Canada.

* dalnoki@mcmaster.ca

[1] J. Bico, B. Roman, L. Moulin, and A. Boudaoud. Elastocapillary coalescence in wet hair. *Nature*, 432(690), 2004.
[2] C. Duprat, S. Protiére, A. Y. Beebe, and H. A. Stone. Wetting of flexible fibre arrays. *Nature*, 482(7386), February 2012.
[3] C. Duprat and S. Protiere. Capillary stretching of fibers. *Europhys. Lett.*, 111(5), 2015.
[4] A. Sauret, F. Boulogne, D. Cebron, E. Dressaire, and H. A. Stone. Wetting morphologies on an array of fibers of different radii. *Soft Matter*, 11, 2015.
[5] H. Elettro, A. Antkowiak, and S. Neukirch. The heavy windlass: Buckling and coiling of an elastic rod inside a liquid drop in the presence of gravity. *Mechanics Research Communications*, 93:58–61, October 2018.
[6] G McHale, N. A. Käb, M. I. Newton, and S. M. Rowan. Wetting of a High-Energy Fiber Surface. *J. Colloid Interface Sci.*, 186(2), 1997.
[7] B. J. Carroll. The equilibrium of liquid drops on smooth and rough circular cylinders. *J. Colloid Interface Sci.*, 97(1), 1984.
[8] D. Quéré. Fluid coating on a fiber. *Annual Review of Fluid Mechanics*, 31(1), 1999.
[9] O. Campás, T. Mammoto, S. Hasso, R. A. Sperling, D. O'Connell, A. G. Bischof, R. Maas, D. A. Weitz, L. Mahadevan, and D. E. Ingber. Quantifying cell-generated mechanical forces within living embryonic tissues. *Nat. Methods*, 11(2), 2014.
[10] J. B. Grotberg and O. E. Jensen. Biofluid mechanics in flexible tubes. *Annu. Rev. Fluid Mech.*, 36(1), January 2004.
[11] A. L. Hazel and M. Heil. Surface-tension-induced buckling of liquid-lined elastic tubes: a model for pulmonary airway closure. *P. R. Soc. A.*, 461(2058), June 2005.
[12] B. Roman and J. Bico. Elasto-capillarity: deforming an elastic structure with a liquid droplet. *J. Phys-Condens. Mat.*, 22(49), 2010.
[13] S. Shojaei-Zadeh, S. R. Swanson, and S. L. Anna. Highly uniform micro-cavity arrays in flexible elastomer film. *Soft Matter*, 5(4), 2009.
[14] R. W. Style, R. Boltyanskiy, Y. Che, J. S. Wettlaufer, L. A. Wilen, and E. R. Dufresne. Universal Deformation of Soft Substrates Near a Contact Line and the Direct Measurement of Solid Surface Stresses. *Phys. Rev. Lett.*, 110(6), 2013.
[15] A. Chakrabarti and M. K. Chaudhury. Direct Measurement of the Surface Tension of a Soft Elastic Hydrogel: Exploration of Elastocapillary Instability in Adhesion. *Langmuir*, 29(23), June 2013.
[16] J. Bico, É. Reyssat, and B. Roman. Elastocapillarity: When Surface Tension Deforms Elastic Solids. *Annual Review of Fluid Mechanics*, 50(1):629–659, January 2018.
[17] A. E. Cohen and L. Mahadevan. Kinks, rings, and rackets in filamentous structures. *Proceedings of the National Academy of Sciences*, 100(21):12141–12146, 2003.
[18] B. J. Carroll. The accurate measurement of contact angle, phase contact areas, drop volume, and Laplace excess pressure in drop-on-fiber systems. *J. Colloid Interface Sci.*, 57(3), 1976.
[19] G. McHale and M. I. Newton. Global geometry and the equilibrium shapes of liquid drops on fibers. *Colloids Surf., A*, 206(1-3), 2002.
[20] T. H. Chou, S. J. Hong, Y. E. Liang, H. K. Tsao, and Y. J. Sheng. Equilibrium phase diagram of drop-on-fiber: Coexistent states and gravity effect. *Langmuir*, 27(7), 2011.
[21] A. Sauret, F. Boulogne, K. Somszor, E. Dressaire, and H. A. Stone. Drop morphologies on flexible fibers: influence of elastocapillary effects. *Soft Matter*, 13(1):134–140, 2017.
[22] H. Elettro, F. Vollrath, A. Antkowiak, and S. Neukirch. Drop-on-coilable-fibre systems exhibit negative stiffness events and transitions in coiling morphology. *Soft Matter*, 13(33):5509–5517, 2017.
[23] P. Grandgeorge, A. Antkowiak, and S. Neukirch. Auxiliary soft beam for the amplification of the elasto-capillary coiling: Towards stretchable electronics. *Advances in Colloid and Interface Science*, 255:2–9, May 2018.
[24] Q. Liu and B. Xu. Liquid-Evaporation-Assisted Self-Folding of One-Dimensional Nanomaterials. *The Journal of Physical Chemistry C*, 122(5):3078–3090, February 2018.
[25] H. Elettro, S. Neukirch, F. Vollrath, and A. Antkowiak. In-drop capillary spolling of spider capture thread inspires hybrid fibers with mixed solid-liquid mechanical properties. *PNAS*, 113(22), 2016.
[26] H. Elettro, F. Vollrath, A. Antkowiak, and S. Neukirch. Coiling of an elastic beam inside a disk: A model for spider-capture silk. *Int. J. Nonlinear Mech.*, 75, 2015.
[27] A. Fargette, S. Neukirch, and A. Antkowiak. Elastocapillary Snapping: Capillarity Induces Snap-Through Instabilities in Small Elastic Beams. *Physical Review Letters*, 112(13), April 2014.
[28] R. D. Schulman, A. Porat, K. Charlesworth, A. Fortais, T. Salez, E. Raphaël, and K. Dalnoki-Veress. Elastocapillary bending of microfibers around liquid droplets. *Soft Matter*, 13(4):720–724, 2017.
[29] Additional information and a real-time video can be found in the Supplemental Materials at xxxx.xxxx.xxx (see https://youtu.be/u693UiQWb4E).
[30] G. Morris, K. Hadler, and J. Cilliers. Particles in thin liq-

uid films and at interfaces. *Curr. Opin. Colloid Interface Sci.*, 20(2):98–104, 2015.

[31] S. A. Ali, P. A. Gauglitz, and W. R. Rossen. Stability of Solids-Coated Liquid Layers between Bubbles. *Ind. Eng. Chem. Res.*, 39(8):2742–2745, 2000.

[32] T Horozov. Foams and foam films stabilised by solid particles. *Curr. Opin. Colloid Interface Sci.*, 13(3):134–140, 2008.

[33] G. Bournival, S. Ata, and E. J. Wanless. The roles of particles in multiphase processes: Particles on bubble surfaces. *Adv. Colloid Interface Sci.*, 225:114–133, 2015.

[34] I. Capron and B. Cathala. Surfactant-Free High Internal Phase Emulsions Stabilized by Cellulose Nanocrystals. *Biomacromolecules*, 14(2):291–296, February 2013.

[35] S. Lam, K. P. Velikov, and O. D. Velev. Pickering stabilization of foams and emulsions with particles of biological origin. *Current Opinion in Colloid & Interface Science*, 19(5):490–500, October 2014.

[36] A. M. Al-Qararah, T. Hjelt, A. Koponen, A. Harlin, and J. A. Ketoja. Bubble size and air content of wet fibre foams in axial mixing with macro-instabilities. *Colloids and Surfaces A: Physicochemical and Engineering Aspects*, 436:1130–1139, September 2013.

[37] I. Kalashnikova, H. Bizot, P. Bertoncini, B. Cathala, and I. Capron. Cellulosic nanorods of various aspect ratios for oil in water Pickering emulsions. *Soft Matter*, 9(3):952–959, 2013.

[38] T. Winuprasith and M. Suphantharika. Microfibrillated cellulose from mangosteen (Garcinia mangostana L.) rind: Preparation, characterization, and evaluation as an emulsion stabilizer. *Food Hydrocolloids*, 32(2):383–394, August 2013.

[39] A. S. Petrov and S. C. Harvey. Packaging Double-Helical DNA into Viral Capsids: Structures, Forces, and Energetics. *Biophysical Journal*, 95(2):497–502, July 2008.

[40] P. K. Purohit, M. M. Inamdar, P. D. Grayson, T. M. Squires, J. Kondev, and R. Phillips. Forces during Bacteriophage DNA Packaging and Ejection. *Biophysical Journal*, 88(2):851–866, February 2005.

[41] P. K. Purohit, J. Kondev, and R. Phillips. Mechanics of DNA packaging in viruses. *Proceedings of the National Academy of Sciences*, 100(6):3173–3178, March 2003.

[42] S. Tzlil, J. T. Kindt, W. M. Gelbart, and A. Ben-Shaul. Forces and Pressures in DNA Packaging and Release from Viral Capsids. *Biophysical Journal*, 84(3):1616–1627, March 2003.

[43] R. D. Schulman and K. Dalnoki-Veress. Liquid droplets on a highly deformable membrane. *Phys. Rev. Lett.*, 115:206101, Nov 2015.

[44] J. Brandrup, E. H. Immergut, and E. A. Grulke. *Polymer Handbook*. Wiley, 4th edition, 1999.

[45] Y. Yang, Z. Fang, X. Chen, W. Zhang, Y. Xie, Y. Chen, Z. Liu, W. Yuan. An Overview of Pickering Emulsions: Solid-Particle Materials, Classification, Morphology, and Applications. *Front. Pharma.*, 8:287, 2017.

[46] Y. Toba. Drop production by bursting of air bubbles on the sea surface (II) theoretical study on the shape of floating bubbles. *J. Oceanogr. Soc. Japan*, 15(3):121–130, 1959.

[47] C. T. Nguyen, H. M. Gonnermann, Y. Chen, C. Huber, A. A. Maiorano, A. Gouldstone, J. Dufek. Film drainage and the lifetime of bubbles. *Geochem. Geophys. Geosyst.*, 14(9):3616–3631, 2013.

[48] P. L. L. Walls, L. Henaux, J. C. Bird. Jet drops from bursting bubbles: How gravity and viscosity couple to inhibit droplet production. *Phys. Rev. E*, 92(2):021002, 2015.

Chapter 5

Buckling of elastic fibers confined to a thin elastic film

The third paper included in this thesis studies elastic instabilities that result from the combined effects of differentially-strained fibers and thin films.

This paper was inspired by work that considers the deformation of fibers embedded in elastic media [60, 64, 67, 74, 129, 130]. In particular, we explore the case where the fiber is much thicker than the elastic medium it is constrained by. Previous work has explored the way a fiber is able to buckle out of the plane of its elastic medium when the medium is very thin, or how it will be confined to buckling in plane if the medium is thick [107, 108]. Here we explore a system that can switch continuously from in-plane to out-of-plane buckling affecting the strain in the elastic medium in two dimensions.

The experiments, theory, and data analysis presented in this paper were designed and performed by myself, with theory contributions by Kari Dalnoki-Veress. The paper was written by myself and Kari Dalnoki-Veress.

Buckling of elastic fibers confined to a thin elastic film

Adam Fortais
Department of Physics and Astronomy, McMaster University, 1280 Main St. W, Hamilton, ON, L8S 4M1, Canada

Kari Dalnoki-Veress*
Department of Physics and Astronomy, McMaster University, 1280 Main St. W, Hamilton, ON, L8S 4M1, Canada
and
Laboratoire de Physico-Chimie Théorique, UMR CNRS Gulliver 7083, ESPCI, Paris, France
(Dated: December 16, 2021)

When an elastic beam is embedded in a deformable matrix which is then compressed, the beam may undergo "traction-based buckling". This buckling is a result of the friction forces between the beam and the matrix and is common in biological and technological systems like living cells containing microtubules, electrodes embedded in tissue, fiber-reinforced composites and stretchable, wearable electronics. Traction-based buckling typically results in periodic buckles with amplitude and wavelength determined by the geometry and stiffness of the beam and matrix. Work has been done on systems where the thickness of the embedding matrix is semi-infinite and much softer than the embedded beam, resulting in buckles with no preferred orientation. In this work we explore systems where an elastic fiber is adhered to a thin, compliant film. By altering the stress profile in the film and the thickness of either the film or the fiber, we are able to continuously control the orientation of the buckles with respect to the plane of the film.

I. INTRODUCTION

An unsupported elastic beam will buckle when subjected to a large enough compression, but by embedding it in another material, the beam can withstand a larger compressive load before buckling [1]. Beyond just stabilizing the beam, systems like this can also exhibit a wide range of interesting and unique morphologies that would otherwise be difficult to realize with a unsupported elastic beam [2–7]. For example, it has been shown that periodic buckling can develop in a supported beam where amplitude and wavelength of the buckles are determined by the relative stiffness and geometry of the beam and the embedding material [2, 8–14]. Being able to embed thin, fiber-like conductors within elastomeric substrates has been shown to be an effective way to design stretchable and wearable electronic devices [11, 15–19]. Standard conductive wiring is not typically stretchable but by taking advantage of strain-related deformations in thin fiber-like wires, wearable electronic devices can be designed such that the device can follow the elastic deformations of a user's skin without damaging the wiring; an important feature to consider when designing non-invasive, wearable medical devices [15, 17, 20, 21].

The way fiber-substrate systems deform and respond to stresses can be affected by a wide range of parameters. Material properties like the elastic modulus and Poisson ratio of both a fiber and its embedding substrate can determining the types of deformations that are possible in the system and likewise, the geometry of the fiber and substrate can be just as important [5–7, 12, 14, 22–25]. For example, when a fiber is embedded in an ideal semi-infinite substrate (with dimensions much larger than the radius of the fiber), there is a radial symmetry to the compression on the fiber that makes for no preferred orientation when buckles form [8, 10, 21, 26–33]. Several methods for breaking this symmetry and altering the orientation of buckles have been presented in the literature, specifically in ultra-thin films, the energetic cost of bending can be small compared to the bending energy in the fiber, and the buckles will form perpendicular to the film to minimize the stretching energy experienced by the film [14, 17, 22, 24, 34–42]. By increasing the thickness of the film, the energy cost of bending increases and the orientation of buckles were found to form to the undeformed film.

In the following experiments, we explore a similar system, now open to the possibility of bi-axial tension and continuous, reversible changes in the orientation of the buckles. By altering the stress parallel and perpendicular to the length of the fiber, we observe that a single sample can exhibit buckling that can be rotated continuously from perpendicular to parallel relative to the plane of the undeformed film. We present a simple theory that, through energy minimization of the fiber-film system, describes the orientation of buckles as a function of bi-axial

* dalnoki@mcmaster.ca

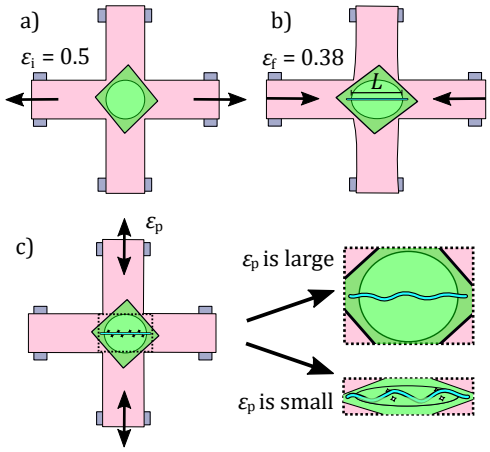

FIG. 1. a) An Elastollan film adheres to a "+-shaped" Elastosil sheet. A hole (diameter 1 cm) has been removed from the sheet. A strain $\varepsilon_i = 0.5 \pm 0.02$ is applied to the system. b) An Elastollan fiber (radius 10 μm) adheres to the film before the strain in the film is reduced to $\varepsilon_f = 0.38 \pm 0.02$ causing a compressive stress on the fiber. c) The fiber deforms in response to the compressive stress. Depending on ε_p, deformation can occur in the plane of the sheet (ε_p is large) or out of the plane of the sheet (ε_p is small).

tension.

II. EXPERIMENT

A. Methods

The following experiments use a strain-control device made with a 250 μm-thick Elastosil sheet (Wacker Chemie AG) cut into an "+" shape with a hole with a 1 cm diameter punched into the center. The arms of the sheet are fixed to four actuating posts that allow a controllable biaxial strain to be applied to the sheet. The device and the experimental method is shown schematically in Figure 1.

In each experiment, a thin elastic film is transferred to the hole at the center of the Elastosil sheet so that a 1 cm diameter circular section of the film would be free-standing. The film adheres to the sheet, and the biaxial strain applied to the sheet is in turn applied to the film. The strain can be measured by comparing the dimensions of the circular hole before and after the Elastosil sheet is stretched.

The Elastosil sheet (and thus the thin film) is first strained by $\varepsilon_i = 0.50 \pm 0.02$ while keeping the perpendicular direction fixed. An thin elastic fiber is then placed on the film along the direction of ε_i. Since Elastollan is somewhat sticky, bringing the fiber and film in contact caused them to adhere to each other.

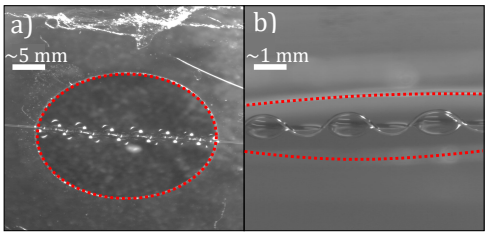

FIG. 2. Optical image of out of plane buckling by a fiber adhered to a film. The free-standing portion of the film is outlined (red dotted line). a) Top-down, the deformation in the fiber is hard to see, but the deformation causes reflective patches in the film, apparent as light spots along the length of the fiber. b) Side-on, the same fiber-film system is seen buckling out of plane of the sheet.

Once the fiber adheres to the film, strain in the film is reduced such that the new strain on the film is $\varepsilon_f = 0.38 \pm 0.02$. This creates a traction-based compression on the fiber sufficient for all fibers to buckle out of the plane of the film with wavelengths λ and amplitudes R that depends on the specific fiber-film combination. In the first experiment, this wavelength is measured for a variety of fiber and film thicknesses and an image of a typical experiment is shown in Figure 2.

In the second experiment, the same process is repeated after which the strain in the perpendicular direction ε_p is varied as $\varepsilon_f = 0.38$ is kept constant. When ε_p increases, the buckles are observed to rotate continuously, coming more in-plane with the film. The angle of rotation is measured by rotating an optical microscope in a circular orbit with it's center of rotation and focus fixed on the fiber. When the camera is imagining parallel to the amplitude of the buckles, the amplitude of the buckles appears to approach $R = 0$, providing a convenient way to determine the angle the buckles make with the film. $\theta = 0$ is defined when the buckles are perpendicular to the undeformed film while $\theta = \pi/2$ is when the buckles are oriented parallel to the plane of the film.

B. Materials

The thin elastic films in this work are made by first dissolving Elastollan, a commercial grade thermoplastic polyurethane elastomer (BASF Polyurethanes) into cyclohexanone (Sigma-Aldrich). This solution is spin-cast onto freshly cleaved mica sheets (Ted Pella Inc.) resulting in uniform films that that range in thickness, h, from 250 nm to 650 nm depending on spin-speed and solution concentration.

To determine the thickness of the spin cast films, one part of the film from each mica sheet is transferred to a silicon wafer and measured via ellipsometry (Accurion, EP3). The remaining parts of the film are used in the biaxial strain experiments.

The elastic fibers used in these experiments are made from Elastollan by dipping a micropipette into an Elastollan melt held at 240°C and then quickly pulling the pipette out again. Using this procedure, Elastollan fibers with cross-sectional radii, r, on the order of several micrometers can be made rapidly. Particularly uniform segments of the resulting fibers can then be cut out and used.

III. RESULTS AND DISCUSSION

A. Wavelength and amplitude of emerging buckles

A fiber adheres to the surface of a thin, pre-strained elastic film. When some of the strain is released it creates a compressive force on the fiber. Since the fiber is highly slender ($r/L \ll 1$), the fiber is prone to buckling, which it does out of the plane of the film. The lowest energy conformation is for the fiber to make one large-amplitude buckle however, the film resists large-amplitude deformations. As a result, the fiber forms multiple buckles with amplitude R and wavelength λ determined by a competition between bending energy in the fiber and stretching in the film,

$$E_B + E_S = 0 \tag{1}$$

Of course as the fiber bends the film follows, provided the bending happens out of the plane of the film. However, the film is much thinner than the fiber ($r/h \sim 10^3$) so the film's bending energy will be much smaller than that of the fibers. In the following experiments, r is several orders of magnitude larger than h, and we can neglect the bending energy in the film.

In the following experiments, we model the bending and stretching energies in the system as linear, and approximate the curvature of the beam as forming uniform, semi-circular arcs with a radius of curvature R,

$$\frac{EI}{R^2} = \frac{1}{2}EA(\varepsilon_f^2 - \varepsilon_i^2), \tag{2}$$

where $A = h\mathrm{d}L$ is a small cross-sectional area of the thin film. In the following experiment, $\varepsilon_f^2 - \varepsilon_i^2$ is kept constant while the thickness of the fibers and films are varied.

Approximating the buckles as uniform, circular arcs with radii of curvature R, and recognizing the length of the buckling fiber is fixed and bounded on either end by the much thicker Elastosil sheet, R can be related to the wavelength of the buckles, $\lambda = L/2n = 2\pi R$ where n are integer values, resulting in the following prediction for the wavelength of the observed buckles:

$$\lambda = \sqrt{\frac{2\pi^3 r^4}{hL(\varepsilon_f^2 - \varepsilon_i^2)}}. \tag{3}$$

Several fiber and film combinations were used to test this relationship and the results are shown in Figure 3. Intuitively, we would expect that a thick fiber or a thin film would result in a longer wavelength since in the limit of a fiber buckling with no film would result in a single buckle. Likewise, a very thin fiber or very thick film may stabilize the fiber such that it cannot buckle at all. Likewise, when ε_i is large, the stress in the film is also large which can act to suppress the amplitude of buckles.

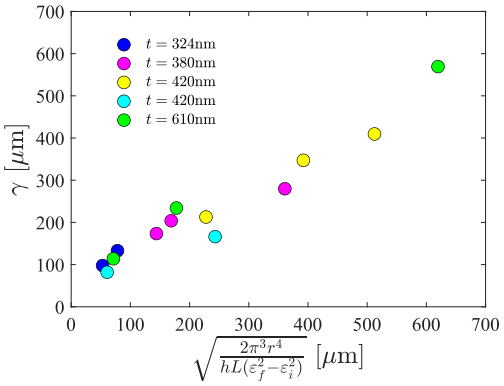

FIG. 3. Wavelength λ observed for fibers of various radii r after a 7% compression, normalized by the film thickness h according to Equation 2. In this experiment, $\varepsilon_f^2 - \varepsilon_i^2$ and L are kept constant between trials.

B. Biaxial Strain and the orientation of buckles

When perpendicular strain is applied to a film-fiber system with out of plane buckles, the out of plane amplitude of the buckles become suppressed. In general, the suppression can happen via a reduction in the amplitude of buckles or a rotation of the buckles. Like in the previous experiments, we fix the compression on the fiber by fixing the length of the film. Therefore, the buckles have two options: rotate to become more in-plane with the film to reduce out-of-plane stretching in the film, or spontaneously form another buckle. Since the rotation is a continuous process while the formation of another buckle requires overcoming a relatively large energy barrier, the rotation process is what we observe.

Beginning again from the stretching-bending energy balance from Equation 2 *after* the buckles emerge but this time the film can be strained in the direction perpendicular to the length of the fiber. When a strain ε_p is applied perpendicular to the length of the fiber, the buckles are observed to rotate by an angle θ with respect to their initial out-of-plane orientation. θ is measured as a function of ε_p, and the results are shown in Figure 4.

Additionally, the length of the film parallel to the fiber is kept fixed during the experiment, so increasing ε_p also increases the stress in the film parallel to the length of the fiber according to its Poisson ratio. This suppresses the

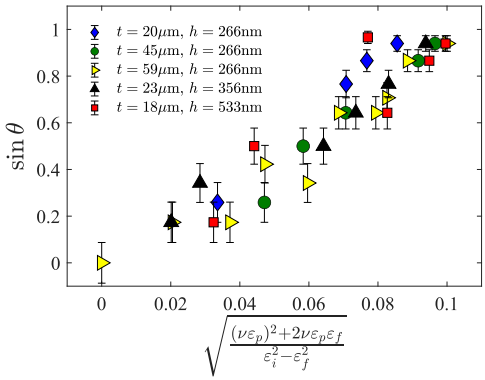

FIG. 4. Orientation of buckles defined by the angle θ the buckles make with the undeformed film as a function of perpendicular strain ε, normalized by the fiber radii r and film thickness h according to Equation 5.

amplitude of the buckles via rotation, and we model the out of plane portion of R as $\tilde{R} = R/\cos\theta$. Incorporating these additional pieces into Equation 2, we can calculate the angle of rotation as a function of ε_p,

$$\frac{EI}{(R/\cos\theta)^2} = -\frac{1}{2}EA((\varepsilon+\nu\varepsilon_p)_f^2 - \varepsilon_i^2). \tag{4}$$

Using the relationship found in the previous section (or by setting $\varepsilon_p = 0$ and $\theta = 0$) we find $R^2 \propto \frac{EI}{EA(\varepsilon_f^2-\varepsilon_i^2)}$) which sets the amplitude of buckles before a perpendicular strain is applied. This relationship leads to the following expression:

$$\sin\theta \propto \sqrt{\frac{(\nu\varepsilon_p)^2 + 2\nu\varepsilon_p\varepsilon_f}{\varepsilon_i^2 - \varepsilon_f^2}}. \tag{5}$$

In the context of an energy balance, we can think of the bending energy in the fiber as fixed for any given trial since the fiber is geometrically constrained. As ε_p is increased, the length of the film parallel to the fiber is held constant, so the elastic energy stored in the film increases and the energetic cost of maintaining an amplitude R increases as well. This extra stress is released when the fiber rotates. Because the fiber and film are made from the same materials, the only parameters the rotation depends on are ε_i, ε_f, and $\nu\varepsilon$.

IV. CONCLUSION

The buckling of a fiber embedded in an elastomeric substrate is a widely studied phenomena with exciting applications in stretchable and wearable electronics with

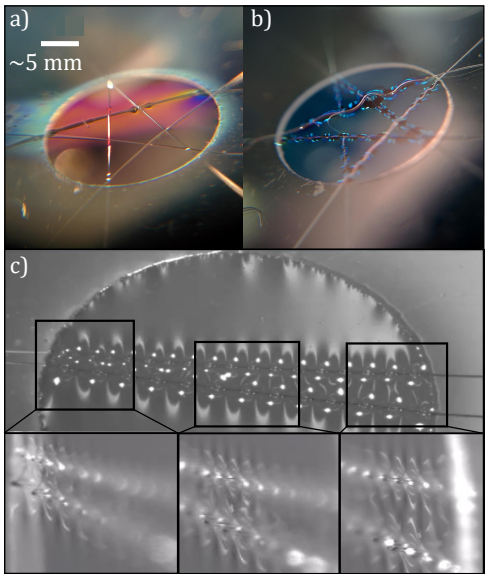

FIG. 5. Optical images of multi-fiber and film systems. a) Multiple fibers can be arranged on the same pre-strained film. The film appears pink because of the optical interference caused by the film. b) When tension in the film is released, the fibers and film deform. The film color changes to blue according to the small thickness change due to the Poisson effect. c) A different system showing the deformations of two nearly-parallel fibers. On the right of the image, the fibers are far enough apart that their deformations happen independently. On the left of the image, the deformation of the film caused by the fibers extend far enough that they begin to interact with the deformations caused by the other fiber. A technique like this could be used to create structures that would otherwise not be possible with a single fiber.

the majority of the focus on semi-infinite substrates []. However, embedding or adhering fibers to thin elastic films presents another type of system with its own unique modes of deformation []. Previous work has focused on the out of plane deformations the fiber-film systems make in response to compression, particularly in the case of uni-axial compression. In this paper we explore the deformations that occur when fiber-film systems are subjected to bi-axial stresses. The result is a highly tunable system where the amplitude, wavelength and orientation of buckles can be controlled. In particular, this work demonstrates that with thoughtful selections of fiber and film thicknesses and stiffness, along with a well-chosen pre-strain, a single system can be made to change the size, number, and orientation of buckles in a reversible manner.

While we explored the phase-space of buckles formed by a single fiber adhered to a thin film, we have not yet explored the range over which deformations caused by the fiber extend throughout the film. However, we have

seen that multiple fibers adhered to the same system can be made to influence each other *through* the film. This points to an even richer set of tunable deformations that can be produced by combining several fibers (or otherwise elastic support structures) throughout a film. One of the goals of such a system could be a collapsible structure that can take on any one of several spontaneously-forming geometries depending on how strains are applied and released.

Finally, while these experiments were performed with micron-scaled materials, the results are independent of scale. Though systems of the scale presented here may find use in stretchable, flexible, and wearable electronic devices, there is no reason larger or smaller structures could not be made following these results.

[1] S. Timoshenko and J. N. Goodier. *Theory of Elasticity*. McGraw-Hill Book Company, Inc., 2^{nd} edition, 1951.

[2] Stephen G. O'Keeffe, Derek E. Moulton, Sarah L. Waters, and Alain Goriely. Growth-induced axial buckling of a slender elastic filament embedded in an isotropic elastic matrix. *Int. J. Non Linear Mech.*, 56:94–104, 2013-11.

[3] Yan Zhao, Jing Li, Yan Ping Cao, and Xi-Qiao Feng. Buckling of an elastic fiber with finite length in a soft matrix. *Soft Matter*, 12(7):2086–2094, 2016. Number: 7.

[4] J. Xiao, H. Jiang, D.–Y. Khang, J. Wu, Y. Huang, and J. A. Rogers. Mechanics of buckled carbon nanotubes on elastomeric substrates. *J. Appl. Phys.*, 104(3):033543, 2008-08. Number: 3.

[5] Seung Yoon Ryu, Jianliang Xiao, Won Il Park, Kwang Soo Son, Yonggang Y. Huang, Ungyu Paik, and John A. Rogers. Lateral buckling mechanics in silicon nanowires on elastomeric substrates. *Nano Lett.*, 9(9):3214–3219, 2009-09-09. Number: 9.

[6] J Xiao, S Y Ryu, Y Huang, K-C Hwang, U Paik, and J A Rogers. Mechanics of nanowire/nanotube insurface buckling on elastomeric substrates. *Nanotechnology*, 21(8):085708, 2010-02-26. Number: 8.

[7] Hyemin Lee, Jung Gun Bae, Won Bo Lee, and Hyunsik Yoon. Mechano-responsive lateral buckling of miniaturized beams standing on flexible substrates. *Soft Matter*, 13(45):8357–8361, 2017. Number: 45.

[8] Youlong Chen, Yong Zhu, Xi Chen, and Yilun Liu. Mechanism of the transition from in-plane buckling to helical buckling for a stiff nanowire on an elastomeric substrate. *J. Appl. Mech.*, 83(4):041011, 2016. Number: 4.

[9] Nan Hu and Rigoberto Burgueño. Buckling-induced smart applications: recent advances and trends. *Smart Mater. Struct.*, 24(6):063001, 2015-06-01. Number: 6.

[10] A. Takei, F. Brau, B. Roman, and J. Bico. Stretch-induced wrinkles in reinforced membranes: From out-of-plane to in-plane structures. *EPL*, 96(6), 2011. Number: 6.

[11] Y. Sun, V. Kumar, I. Adesida, and J.A. Rogers. Buckled and wavy ribbons of GaAs for high-performance electronics on elastomeric substrates. *Adv. Mater.*, 18(21):2857–2862, 2006-11-03. Number: 21.

[12] Dan Wu, Huimin Xie, Yajun Yin, and Minjin Tang. Micro-scale delaminating and buckling of thin film on soft substrate. *J. Micromech. Microeng.*, 23(3):035040, 2013-03-01. Number: 3.

[13] André R. Studart and Randall M. Erb. Bioinspired materials that self-shape through programmed microstructures. *Soft Matter*, 10(9):1284–1294, 2014. Number: 9.

[14] Dong Yan, Kai Zhang, and Gengkai Hu. Wrinkling of structured thin films via contrasted materials. *Soft Matter*, 12(17):3937–3942, 2016.

[15] J. A. Rogers, T. Someya, and Y. Huang. Materials and mechanics for stretchable electronics. *Science*, 327(5973):1603, 2010. Number: 5973.

[16] Paul Grandgeorge, Arnaud Antkowiak, and Sébastien Neukirch. Auxiliary soft beam for the amplification of the elasto-capillary coiling: Towards stretchable electronics. *Advances in Colloid and Interface Science*, 255:2–9, 2018-05.

[17] Xin Li and Sang-Hu Park. Local wrinkle patterning with controlled morphologies on a membrane. *International Journal of Precision Engineering and Manufacturing*, 20(8):1415–1421, 2019-08.

[18] Xianhong Meng, Guanyu Liu, Zihao Wang, and Shuodao Wang. Analytical study of wrinkling in thin-film-on-elastomer system with finite substrate thickness. *Applied Mathematics and Mechanics*, 38(4):469–478, 2017-04.

[19] Martin Kaltenbrunner, Tsuyoshi Sekitani, Jonathan Reeder, Tomoyuki Yokota, Kazunori Kuribara, Takeyoshi Tokuhara, Michael Drack, Reinhard Schwödiauer, Ingrid Graz, Simona Bauer-Gogonea, Siegfried Bauer, and Takao Someya. An ultra-lightweight design for imperceptible plastic electronics. *Nature*, 499(7459):458–463, 2013-07.

[20] Yadong Zhou and Qingguo Fei. Evaluating deformation modes of sandwich serpentine structures for high stretchability. *Thin-Walled Structures*, 157:107087, 2020-12.

[21] Xin Li, Zhi-Jun Zhao, and Sang-Hu Park. Out-of-plane stretching for simultaneous generation of different morphological wrinkles on a soft matter. *Applied Physics A*, 122(7):705, 2016-07.

[22] Juner Zhu, Xiaowei Zhang, and Tomasz Wierzbicki. Stretch-induced wrinkling of highly orthotropic thin films. *International Journal of Solids and Structures*, 139-140:238–249, 2018-05.

[23] Luca Giomi. Softly constrained films. *Soft Matter*, 9(34):8121, 2013. Number: 34.

[24] L. Pocivavsek, R. Dellsy, A. Kern, S. Johnson, B. Lin, K. Y. C. Lee, and E. Cerda. Stress and fold localization in thin elastic membranes. *Science*, 320(5878):912–916, 2008-05-16. Number: 5878.

[25] Dong Choon Hyun and Unyong Jeong. Substrate thickness: An effective control parameter for polymer thin film buckling on PDMS substrates. *Journal of Applied Polymer Science*, 112(5):2683–2690, 2009-06-05.

[26] Yu-Cheng Chen and Alfred J. Crosby. High aspect ratio wrinkles via substrate prestretch. *Advanced Materials*, 26(32):5626–5631, 2014-08.

[27] Tomohiko G. Sano and Hirofumi Wada. Snap-buckling in asymmetrically constrained elastic strips. *Physical Review E*, 97(1), 2018-01-23. Number: 1.

[28] Florian Maurin. Solitary waves in longitudinally wrin-

kled and creased helicoids. *International Journal of Non-Linear Mechanics*, 89:133–141, 2017-03.

[29] Fei Liu, Fan Xu, and Chenbo Fu. Orientable wrinkles in stretched orthotropic films. *Extreme Mechanics Letters*, 33:100579, 2019-11.

[30] Hanqing Jiang, Dahl-Young Khang, Jizhou Song, Yugang Sun, Yonggang Huang, and John A. Rogers. Finite deformation mechanics in buckled thin films on compliant supports. *Proceedings of the National Academy of Sciences*, 104(40):15607–15612, 2007.

[31] David J. Schunter, Martin Brandenbourger, Sophia Perriseau, and Douglas P. Holmes. Elastogranular mechanics: Buckling, jamming, and structure formation. *Phys. Rev. Lett.*, 120:078002, Feb 2018.

[32] David J. Schunter, Regina K. Czech, and Douglas P. Holmes. Packing transitions in the elastogranular confinement of a slender loop. *Soft Matter*, 16:2039–2044, 2020.

[33] Valerie Choumet, Tarik Attout, Loïc Chartier, Huot Khun, Jean Sautereau, Annie Robbe-Vincent, Paul Brey, Michel Huerre, and Odile Bain. Visualizing non infectious and infectious anopheles gambiae blood feedings in naive and saliva-immunized mice. *PLOS ONE*, 7(12):1–13, 12 2012.

[34] Jun Young Chung, Adam J. Nolte, and Christopher M. Stafford. Surface wrinkling: A versatile platform for measuring thin-film properties. *Adv. Mater.*, 23(3):349–368, 2011-01-18. Number: 3.

[35] Qun Huang, Jie Yang, Wei Huang, Gaetano Giunta, Salim Belouettar, and Heng Hu. The boundary effects on stretch-induced membrane wrinkling. *Thin-Walled Structures*, 154:106838, 2020-09.

[36] Yinji Ma, Yeguang Xue, Kyung-In Jang, Xue Feng, John A. Rogers, and Yonggang Huang. Wrinkling of a stiff thin film bonded to a pre-strained, compliant substrate with finite thickness. *Proceedings of the Royal Society A: Mathematical, Physical and Engineering Sciences*, 472(2192):20160339, 2016-08.

[37] Rafael D. Schulman, John F. Niven, Michiel A. Hack, Christian DiMaria, and Kari Dalnoki-Veress. Liquid dewetting under a thin elastic film. *Soft Matter*, 14(18):3557–3562, 2018.

[38] Benjamin Davis-Purcell, Pierre Soulard, Thomas Salez, Elie Raphaël, and Kari Dalnoki-Veress. Adhesion-induced fingering instability in thin elastic films under strain. *The European Physical Journal E*, 41(3):36, 2018-03.

[39] John F. Niven, Gurkaran Chowdhry, James S. Sharp, and Kari Dalnoki-Veress. The emergence of local wrinkling or global buckling in thin freestanding bilayer films. *The European Physical Journal E*, 43(4):20, 2020-04.

[40] Jan Genzer and Jan Groenewold. Soft matter with hard skin: From skin wrinkles to templating and material characterization. *Soft Matter*, 2(4):310, 2006.

[41] E. Cerda. Mechanics of scars. *J. Biomech.*, 38(8):1598–1603, 2005-08. Number: 8.

[42] Dominic Vella, Jiangshui Huang, Narayanan Menon, Thomas P. Russell, and Benny Davidovitch. Indentation of ultrathin elastic films and the emergence of asymptotic isometry. *Phys. Rev. Lett.*, 114:014301, Jan 2015.

Chapter 6

Discussion and Conclusions

When I tell people that I am a physicist, they often assume I study the smallest particles, the biggest celestial bodies, or some breed of exotic material. When they find out that I play with elastic objects, they are usually quite surprised. I think the surprise comes from the fact that most people can picture what it means to deform elastic materials, meanwhile most untrained people's imaginations and intuitions fail when presented with some of the more extreme branches of physics. Even still, that elasticity theory feels more graspable than some of the topics covered by "modern physics" does not mean there are no more interesting questions in the field of elasticity. In fact, one could argue that the opposite is true; the more we learn about the natural world, the more soft, squishy and fluid systems we encounter, giving us more interesting problems that elasticity theory can be applied to.

All of the work presented in this thesis shares a common foundation - the phenomena we explored can be understood as types of small, linear, and elastic deformations. Bending, twisting, or stretching an object under these assumptions is not unto itself novel. But throughout this thesis, the combination and competition between these different modes of elastic deformation create unique, complicated, and –hopefully you agree– interesting effects with the potential to help us understand different aspects of the natural world.

In Chapter 3, we explored what happens when various amounts of tension or compression are applied to a thin, elastic fiber. Early studies of this type of system focused on applications to the kinking, twisting, and "hockling" (looping) of cables and wires [22, 131]. Later, researchers noted the similarity between the hockling

of cables and the beautifully complicated coiling of biological materials like vines, tendrils, and even strands of DNA [16, 20, 23]. The original work presented in Chapter 3 begins by expanding on and experimentally validating earlier theories that characterized the formation and removal of a single hockle as a competition between bending and twisting within a long, slender fiber. We demonstrated with great precision that this description of the hockling phenomenon works, and can be expressed as a fully geometric, material-agnostic description, provided we can assume the material behaves elastically. The work goes further, exploring a peculiar phenomenon that has gone unreported – the non-monotonic tension required to unwind a highly twisted "plectoneme".

A plectoneme is the structure formed when a fiber undergoes a large degree of twisting while under relatively low tension. The result is a double-helix-like excursion between the two free ends of the fiber, terminated by a single loop. These structures can be found at all length scales, from twisted wires and cables to the supercoiling of DNA [10, 22]. Many studies have considered the tension required to keep a twisted fiber from forming a plectoneme, or the tension required to pull one apart, and have either not observed or failed to characterize the sudden and non-monotonic changes in tension as the plectoneme forms or is removed. In our model, we explain this effect as a result of a friction-based self-interaction where the fiber meets in the plectoneme. In experimental studies using macroscopic fibers and cords, it is reasonable to assume frictional forces would be small in comparison to the tensions experienced by the fiber during plectoneme formation/removal. This would make the formation and removal processes appear to proceed smoothly with no significant jumps in tension. On the other hand, when similar experiments are performed on microscopic structures like DNA, thermal fluctuations and other sources of experimental noise can mask secondary effects like friction. Our experiments were performed on an intermediate scale with a force transducer that allowed tensions across a large range to be measured without a loss of resolution in the data. Using this system, we validate a model that treats the large changes in tension during the unwinding of a plectoneme as the transition between two linear, elastic regimes separated by a stick-slip friction event.

Though this experiment is essentially controlled by only two degrees of freedom

(rotation of one fixed end relative to the other, and tension/compression), there are plenty of other phenomena that this experiment can be used to explore. When a fiber is held under low tension and twisted, a hockle forms. When it is twisted further, a plectoneme forms. Both of these deformations can be thought of as out-of-plane excursions of the fiber; deformations that cause segments of the fiber to extend perpendicular to the length of the fiber. This is only possible because the tension in the fiber is low, and is also why increasing the tension in the fiber is a method of removing these features. Were one to perform the same experiment but with a higher tension, completely different structures form, called solenoids. These are corkscrew-like structures that form along the length of the fiber and to date, there is only a small amount of literature devoted to understanding the formation, removal, and applications of these structures [132]. Going even further, solenoids can be further twisted under different amounts of tension to form tertiary structures highly reminiscent of the disorganized and wild tangles of supercoiled DNA. Supercoiling is an important part of the way DNA stores and transfers DNA and has been studied extensively in-situ and computationally, but has only just begun to be explored with idealized, model experiments. It is possible that our experimental system could be used for this type of study.

Finally, I have only described fibers with no initial curvature. However, with the help of thesis student Michael Costa-Parke, we have begun exploring pre-coiled polymer fibers. Much of our work up to this point has been focused on fabricating these micro-coiled fibers, an example of which is shown in Figure 6.1. With the techniques in this thesis, the system could lead to some interesting and unexpected results.

In Chapter 4, we explored a system where a thin elastic fiber winds and wraps around the liquid membrane of a bubble. This is an example of an elastocapillary interaction, where surface tension acts as the driving force causing an elastic deformation. Because the size of the bubble defines the size of the fiber coils produced, larger bubbles allow fibers to form larger coils, requiring less bending of the fiber. Likewise, thinner and softer fibers will have a lower bending stiffness, which means it is easier to force the fiber to take on more bent orientations. We present a simple energy-based model that, based on the size of the bubble and bending stiffness of

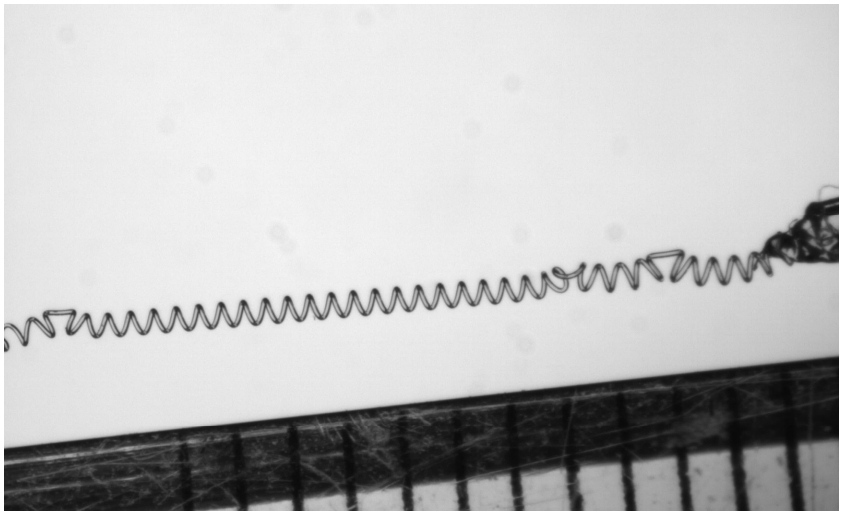

FIGURE 6.1: A polymer fiber with intrinsic curvature. A mm-scale ruler is included for scale.

the fiber, accurately predicts for what fiber-bubble pairs will exhibit the winding phenomenon and which will not.

This work is ripe for applications, as it presents a unique, spontaneous process for creating micron-scale structures. In particular, fabricating microfluidic or micron-scale devices can be difficult on account of their small sizes [119,133]. Using the unique self-assembly process described in Chapter 4 could be useful wherever micron-sized coils and loops are needed. To that end, it is worth noting that this technique does not depend on the fiber being made from polymers; the physics describes the way metal or any other flexible material would interact.

Besides the visually attractive coiling that is possible with this fiber-bubble system, there are more fundamental questions about the way fibers and bubbles interact. The way the fiber penetrates the liquid membrane of the bubble by bridging across the membrane seems to stabilize the bubble from popping. We speculate that this is a result of hindered drainage of the membrane due to the fiber cutting the cap off from the rest of the bubble. Exploring this bridged state and the way it influences fluid flow in the liquid membrane could be of interest to the bubbles and foams industry.

The coiling described in Chapter 4 also exhibited some variation that we did

not investigate. Exploring the ways the coils pack onto the surface of a bubble could result in even more control over the fabrication process of these micro-coils, or provide an experimental system for studying the way things like proteins pack into geometrically constrained environments.

In Chapter 5, thin elastic fibers are used as deformable struts, adhering to the surface of thin elastic membranes. The buckling is a competition between bending of the strut and stretching of the membrane, and when these struts are compressed, they form multiple buckles. Since the struts are confined to the membrane, the wavelength and amplitude of the buckles are intimately connected to the geometry of the membrane as well as any stresses that are applied to the membrane. Most notably, we show that the orientation (in-plane or out-of-plane of the membrane) of the emergent buckles can also be controlled within one single sample. While other studies in the literature explored the orientation of buckles with respect to the stiffness of the adherent membrane, we show that there are many fiber-membrane systems that can exhibit either in-plane or out-of-plane buckling depending on the stress applied to the membrane before the buckles form, that the buckling is reversible, and that a new orientation can be obtained by altering the applied stress before allowing the buckles to re-form.

Knowing that the orientation of buckles are sensitive to the pre-stress in the attached membrane, the next step would be to characterize the local stress throughout the membrane in real-time such that the resultant buckles could be exactly configured. In addition, having multiple fibers included on a single membrane means the local deformations in the membrane caused by a fiber will influence the surrounding fibers. These interactions could find utility in a new type of self-assembly process based on stretching, bending and twisting.

Reaching the end of this thesis, I am proud to look back on how a few simple (and sometimes silly) ideas have grown into a cohesive body of work. I am hopeful that the results contained – though an ending for me – become the beginning for someone else. But more than this, I am excited to see what completely new, weird, and wonderful (and why not funny?) ideas come from the students of the Dalnoki-Veress group.

Appendix A

Science Writing

Here is a statement I would not consider controversial: One of the more important parts of research is communicating the results of said research. But "communicating" research results can mean different things to different people. Securing financial support to pursue new research often depends on a well crafted and well argued presentation of the state of the literature in a field, the previous results achieved by the researcher's program, and what the funding agency (or society as a whole) stands to gain from funding this research. So in a very real sense, a scientist's ability to communicate their results can define their success as a researcher. But for others, communicating research can mean something different entirely; the public needs to know where their publicly-funded research dollars are going for a variety of reasons, so someone needs to fill them in.

Science is a process, but results get money. Communicating research publicly gives people a chance to satisfy their curiosity (entertainment), context for large-scale decisions (public policy), and can potentially improve the quality of life through a changed worldview for the consumers of this type of "product". In return, researchers stand to draw more attention to their work, prove to funding bodies that there is interest in the work (even if the utility of the results are unclear), and perhaps most importantly, provide an opportunity to emphasize the researcher's understanding of *process*, which can hopefully provide a little relief from the pressure of results-oriented funding decisions.

Throughout my graduate career, I've grown to appreciate the importance of

science communication and in fact found myself drawn to the challenge of absorbing, internalizing, and sharing the work of others to the point where I've begun to enjoy finding ways to communicate results more than actually producing the results. Thankfully I've been supported in this pursuit by the unflagging enthusiasm of my supervisor. As a result, I've had the chance to start building a portfolio of articles and blog posts for a variety of publications. Considering the importance of this work on my development as a scientist, researcher, and communicator, I have included an additional bibliography of the writing I have done for online and print publications. A new technique for crafting optical components: simple, easy, and cheap.
Cambridge CORE Blog (Journal of Fluid Mechanics), 2021

Weathering the storm at the Qingtu Lake observation array
Cambridge CORE Blog (Journal of Fluid Mechanics), 2021

Scientists capture the inner workings of the click beetle's explosive jumps.
MassiveSci.com – syndicated to Salon, 2021

The range of microbes in your sourdough starter affect its smell and rise.
MassiveSci.com, 2021

How to make sense of recent CERN finding that challenges the Standard Model of particle physics.
MassiveSci.com, 2021

Soft electronics with liquid-metal veins.
PhysicsToday.org, 2020

Physics in the pandemic: mailing lab kits to students enhances learning at home.
PhysicsWorld.com, 2020

All conferences should be virtual in a post-coronavirus world.
MassiveSci.com – syndicated to Salon, 2020

You can mimic the physics happening on the surface of the Sun in your kitchen.
MassiveSci.com, 2020

Coffee baristas were right all along — grinding coffee finer doesn't always produce a stronger cup of espresso coffee.
MassiveSci.com, 2020

Researchers play with elastic bands to understand DNA and protein structures.
Softbites.org, 2020

Mechanism of Contact between a Droplet and an Atomically Smooth Substrate.
Softbites.org, 2019

Elastogranularity and how soil may shape the roots of plants.
Softbites.org, 2018

Bibliography

[1] J. D. Moroz and P. Nelson. Torsional directed walks, entropic elasticity, and DNA twist stiffness. *PNAS*, 94(26):14418–14422, 1997.

[2] J. F. Marko and E. D. Siggia. Statistical mechanics of supercoiled DNA. *Phys. Rev. E*, 52(3):2912, 1995.

[3] P. U. Walker, W. Vanderlinden, and J. Lipfert. Dynamics and energy landscape of DNA plectoneme nucleation. *Phys. Rev. E*, 98:042412–042425, 2018.

[4] A. Worcel, S. Strogatz, and D. Riley. Structure of chromatin and the linking number of DNA. *PNAS*, 78(3):1461–1465, 1981.

[5] K. Ott, L. Martini, J. Lipfert, and U. Gerland. Dynamics of the Buckling Transition in Double-Stranded DNA and RNA. *Biophys. J.*, 118:1690–1701, 2020.

[6] J. F. Marko and S. Neukirch. Competition between curls and plectonemes near the buckling transition of stretched supercoiled DNA. *Phys. Rev. E*, 85(1), January 2012.

[7] H. Brutzer, N. Luzzietti, D. Klaue, and R. Seidel. Energetics at the DNA Supercoiling Transition. *Biophys. J.*, 98(7):1267–1276, April 2010.

[8] S. Neukirch. Extracting DNA Twist Rigidity from Experimental Supercoiling Data. *Phys. Rev. Lett.*, 93(19), November 2004.

[9] F. Mosconi, J. F. Allemand, D. Bensimon, and V. Croquette. Measurement of the Torque on a Single Stretched and Twisted DNA Using Magnetic Tweezers. *Phys. Rev. Lett.*, 102(7), February 2009.

[10] F. Tanaka and H. Takahashi. Elastic theory of supercoiled DNA. *J. Chem. Phys.*, 83(11):6017–6026, December 1985.

[11] L. F. Liu and J. C Wang. Supercoiling of the dna template during transcription. *PNAS*, 84, 1987.

[12] L. A. Freeman and W. T. Garrard. Dna supercoiling in chromatin structure and gene expression. *Crit. Rev. Eukaryotic Gene Express*, 2(2), 1992.

[13] C. Lavelle. Pack, unpack, bend, twist, pull, push: the physical side of gene expression. *Curr. Opin. Genet. Dev.*, 25:74–84, 2014.

[14] J. L. Silverberg, R. D. Noar, M. S. Packer, M. J. Harrison, C. L. Henley, I. Cohen, and S. J. Gerbode. 3D imaging and mechanical modeling of helical buckling in Medicago truncatula plant roots. *PNAS*, 109(42):16794–16799, 2012.

[15] A. Löf, P. U. Walker, S. M. Sedlak, S. Gruber, Obser T., M. A. Brehm, M. Benoit, and J. Lipfert. Multiplexed protein force spectroscopy reveals equilibrium protein folding dynamics and the low-force response of von Willebrand factor. *PNAS*, 116(38):18798–18807, 2019.

[16] S. J. Gerbode, J. R. Puzey, A. G. McCormick, and L. Mahadevan. How the Cucumber Tendril Coils and Overwinds. *Science*, 337(6098):1087–1091, August 2012.

[17] H. Elettro, S. Neukirch, F. Vollrath, and A. Antkowiak. In-drop capillary spolling of spider capture thread inspires hybrid fibers with mixed solid-liquid mechanical properties. *PNAS*, 113(22):6143–6147, 2016.

[18] E. Lauga. Floppy swimming: Viscous locomotion of actuated elastica. *Phys. Rev. E*, 75(4), 2007.

[19] Y. Forterre. Slow, fast and furious: understanding the physics of plant movements. *J. Exp. Bot.*, 64(15):4745–4760, 2013.

[20] J-S Wang, G. Wang, X-Q Feng, T. Kitamura, Y-L Kang, S-W Yu, and Q-H Qin. Hierarchical chirality transfer in the growth of towel gourd tendrils. *Sci. Rep.*, 3(1), 2013.

[21] W. B. Fraser and G. H. M. van der Heijden. On the theory of localised snarling instabilities in false-twist yarn processes. *J. Eng. Math.*, 61(1):81–95, 2008.

[22] A. L. Ross. Cable kinking analysis and prevention. *J. Eng. Indust.*, 99(1):112–115, 1977.

[23] D. M. Stump, W. B. Fraser, and K. E. Gates. The writhing of circular cross–section rods: undersea cables to DNA supercoils. *Proc. Math. Phys. Eng.*, 454(1976):2123–2156, 1998.

[24] K. Li and S. Cai. Wet adhesion between two soft layers. *Soft Matter*, 10(41):8202–8209, 2014.

[25] B Roman and J Bico. Elasto-capillarity: deforming an elastic structure with a liquid droplet. *J. Phys.: Condens. Matter*, 22(49):493101, 2010.

[26] A. Marchand, S. Das, J. H. Snoeijer, and B. Andreotti. Contact angles on a soft solid: From young's law to neumann's law. *Phys. Rev. Lett.*, 109(23), 2012.

[27] B. Andreotti, O. B aumchen, F. Boulogne, K. E. Daniels, E. R. Dufresne, H. Perrin, T. Salez, J. H. Snoeijer, and R. W. Style. Solid capillarity: when and how does surface tension deform soft solids? *Soft Matter*, 12(12):2993–2996, 2016.

[28] R. A Style, A. Jagota, C. Y. Hui, and E. R. Dufresne. Elastocapillarity: Surface tension an the mechanics of soft solids. *Annu. Reb. Condens. Matter Phys.*, 8:99:118, 2017.

[29] J. Bico, E. Reyssat, and B. Roman. Elastocapillarity: When surface tension deforms elastic solids. *Annu. Rev. Fluid Mech.*, 50(1):629–659, 2018.

[30] A. Marchand, J. H. Weijs, J. H. Snoeijer, and B. Andreotti. Why is surface tension a force parallel to the interface? *Am. J. Phys.*, 79(10):999, 2011.

[31] P.-G. de Gennes. *Scaling Concepts in Polymer Physics*. Cornell University Press, 1979.

[32] P.-G. de Gennes, F. Brochard-Wyart, and D. Quéré. *Capillarity and Wetting Phenomena: Drops, Bubbles, Pearls, Waves*. Springer, 2003.

[33] S. Karpitschka, S. Das, M. van Gorcum, H. Perrin, B. Andreotti, and J. H. Snoeijer. Droplets move over viscoelastic substrates by surfing a ridge. *Nat. Commun.*, 6:7891, 2015.

[34] J. W. van Honschoten, J. W. Berenschot, T. Ondarçuhu, R. G. P. Sanders, J. Sundaram, M. Elwenspoek, and N. R. Tas. Elastocapillary fabrication of three-dimensional microstructures. *Appl. Phys. Lett.*, 97(1):014103, 2010.

[35] R. W. Style and E. R. Dufresne. Static wetting on deformable substrates, from liquids to soft solids. *Soft Matter*, 8(27):7177, 2012.

[36] R. Pericet-Camara, G. K. Auernhammer, K. Koynov, S. Lorenzoni, R. Raiteri, and E. Bonaccurso. Solid-supported thin elastomer films deformed by microdrops. *Soft Matter*, 5(19):3611, 2009.

[37] J. Bae, T. Ouchi, and R. C. Hayward. Measuring the elastic modulus of thin polymer sheets by elastocapillary bending. *ACS Appl. Mater. Interfaces*, 7(27):14734–14742, 2015.

[38] C. Py, P. Reverdy, L. Doppler, J. Bico, B. Roman, and C. N. Baroud. Capillary origami: Spontaneous wrapping of a droplet with an elastic sheet. *Phys. Rev. Lett.*, 98(15), 2007.

[39] J. D. Paulsen, V. Démery, C. D. Santangelo, T. P. Russell, B. Davidovitch, and N. Menon. Optimal wrapping of liquid droplets with ultrathin sheets. *Nat. Mater.*, 14(12):1206–1209, 2015.

[40] E. R. Jerison, Y. Xu, L. A. Wilen, and E. R. Dufresne. Deformation of an elastic substrate by a three-phase contact line. *Phys. Rev. Lett.*, 106(18), 2011.

[41] N. Nadermann, C.-Y. Hui, and A. Jagota. Solid surface tension measured by a liquid drop under a solid film. *PNAS*, 110(26):10541–10545, 2013.

[42] R. D. Schulman and K. Dalnoki-Veress. Liquid droplets on a highly deformable membrane. *Phys. Rev. Lett.*, 115(20), 2015.

[43] R. D. Schroll, M. Adda-Bedia, E. Cerda, J. Huang, N. Menon, T. P. Russell, K. B. Toga, D. Vella, and B. Davidovitch. Capillary deformations of bendable films. *Phys. Rev. Lett.*, 111(1), 2013.

[44] J. Huang, M. Juszkiewicz, W. H. de Jeu, E. Cerda, T. Emrick, N. Menon, and T. P. Russell. Capillary wrinkling of floating thin polymer films. *Science*, 317(5838):650–653, 2007.

[45] A. Fortais, R. D. Schulman, and K. Dalnoki-Veress. Liquid droplets on a free-standing glassy membrane: Deformation through the glass transition. *Eur. Phys. J. E*, 40(7):69, 2017.

[46] R. D. Schulman, R. Ledesma-Alonso, T. Salez, E. Raphaël, and K. Dalnoki-Veress. Liquid droplets act as "compass needles" for the stresses in a deformable membrane. *Phys. Rev. Lett.*, 118(19):198002, 2017.

[47] A. Sauret, F. Boulogne, K. Somszor, E. Dressaire, and H. A. Stone. Drop morphologies on flexible fibers: influence of elastocapillary effects. *Soft Matter*, 13(1):134–140, 2017.

[48] A. Fargette, S. Neukirch, and A. Antkowiak. Elastocapillary snapping: Capillarity induces snap-through instabilities in small elastic beams. *Phys. Rev. Lett.*, 112(13), 2014.

[49] H. Elettro, F. Vollrath, A. Antkowiak, and S. Neukirch. Drop-on-coilable-fibre systems exhibit negative stiffness events and transitions in coiling morphology. *Soft Matter*, 13(33):5509–5517, 2017.

[50] R. D. Schulman, A. Porat, K. Charlesworth, A. Fortais, T. Salez, E. Raphaël, and K. Dalnoki-Veress. Elastocapillary bending of microfibers around liquid droplets. *Soft Matter*, 13(4):720–724, 2017.

[51] C Py, R Bastien, J Bico, B Roman, and A Boudaoud. 3d aggregation of wet fibers. *Europhys. Lett. (EPL)*, 77(4):44005, 2007.

[52] S. Mora, T. Phou, J-M Fromental, B. Audoly, and Y. Pomeau. Shape of an elastic loop strongly bent by surface tension: Experiments and comparison with theory. *Phys. Rev. E*, 86(2), 2012.

[53] S. Neukirch, A. Antkowiak, and J.J. Marigo. The bending of an elastic beam by a liquid drop: a variational approach. *Proc. Math. Phys. Eng. Sci. P ROY SOC A-MATH PHY*, 469(2157):20130066–20130066, 2013.

[54] C. Duprat, H. A. Stone, and S. Protière. Elastocapillary stretching of fibers. *Europhys. Lett.*, 2015.

[55] J. Bico, B. Roman, L. Moulin, and A. Boudaoud. Elastocapillary coalescence in wet hair. *Nature*, 432(7018):690–690, 2004.

[56] H. Elettro, F. Vollrath, A. Antkowiak, and S. Neukirch. Coiling of an elastic beam inside a disk: A model for spider-capture silk. *Int. J. Non Linear Mech.*, 75:59–66, 2015.

[57] E. Cerda. Mechanics of scars. *J. Biomech.*, 38(8):1598–1603, 2005-08.

[58] S. Armon, E. Efrati, R. Kupferman, and E. Sharon. Geometry and mechanics in the opening of chiral seed pods. *Science*, 333(6050):1726–1730, 2011.

[59] N. Hu and R. Burgueño. Buckling-induced smart applications: recent advances and trends. *Smart Mater. Struct.*, 24(6):063001, 2015-06-01.

[60] S. Y. Ryu, J. Xiao, W. I. Park, K. S. Son, Y. Y. Huang, U. Paik, and J. A. Rogers. Lateral buckling mechanics in silicon nanowires on elastomeric substrates. *Nano Lett.*, 9(9):3214–3219, 2009-09-09.

[61] Y. Sun, V. Kumar, I. Adesida, and J. A. Rogers. Buckled and wavy ribbons of GaAs for high-performance electronics on elastomeric substrates. *Adv. Mater.*, 18(21):2857–2862, 2006-11-03.

[62] J. A. Rogers, T. Someya, and Y. Huang. Materials and mechanics for stretchable electronics. *Science*, 327(5973):1603, 2010.

[63] Y. Chen, Y. Zhu, X. Chen, and Y. Liu. Mechanism of the transition from in-plane buckling to helical buckling for a stiff nanowire on an elastomeric substrate. *J. Appl. Mech.*, 83(4):041011, 2016.

[64] S. G. O'Keeffe, D. E. Moulton, S. L. Waters, and A. Goriely. Growth-induced axial buckling of a slender elastic filament embedded in an isotropic elastic matrix. *Int. J. Non Linear Mech.*, 56:94–104, 2013-11.

[65] J. Y. Chung, A. J. Nolte, and C. M. Stafford. Surface wrinkling: A versatile platform for measuring thin-film properties. *Adv. Mater.*, 23(3):349–368, 2011-01-18.

[66] A. R. Studart and R. M. Erb. Bioinspired materials that self-shape through programmed microstructures. *Soft Matter*, 10(9):1284–1294, 2014.

[67] H. Lee, J. G. Bae, W. B. Lee, and H. Yoon. Mechano-responsive lateral buckling of miniaturized beams standing on flexible substrates. *Soft Matter*, 13(45):8357–8361, 2017.

[68] S. Timoshenko and J. N. Goodier. *Theory of Elasticity*. McGraw-Hill Book Company, Inc., 2^{nd} edition, 1951.

[69] R. Hooke. *Lectiones Cutlerianae, or A collection of lectures, physical, mechanical, geographical & astronomical : made before the Royal Society on several occasions at Gresham Colledge [i.e. College] : to which are added divers miscellaneous discourses*. London : Printed for John Martyn, printer to the Royal Society, at the Bell in S. Pauls Church-yard, 1679.

[70] N.W. Tschoegl, W. G. Knauss, and I. Emri. Poisson's ratio in linear viscoelasticity – a critical review. *Mech. Time-Depend. Mater.*, 6(1):3–51, 2002.

[71] L. J. Hall, V. R. Coluci, D. S. Galvão, M. E. Kozlov, M. Zhang, S. O. Dantas, and R. H. Baughman. Sign change of poisson's ratio for carbon nanotube sheets. *Science*, 320(5875):504–507, 2008.

[72] J. Brandrup, E. H. Immergut, and E. A. Grulke. *Polymer Handbook*. John Wiley & Sons, Inc, 4^{th} edition, 1999.

[73] Z. Chen, X. Han, and H. Zheng. Residual stresses and poisson's effect drive shape formation and transition of helical structures. *J. Elast.*, 119(1):321–333, 2015.

[74] Y. Zhao, J. Li, Y. P. Cao, and X-Q Feng. Buckling of an elastic fiber with finite length in a soft matrix. *Soft Matter*, 12(7):2086–2094, 2016.

[75] J. Zhu, X. Zhang, and T. Wierzbicki. Stretch-induced wrinkling of highly orthotropic thin films. *Int. J. Solids Struct.*, 2018-02.

[76] M. Rubinstein and R. Colby. *Polymer Physics*. Oxford University Press, 2003.

[77] S. L. Garrett. *Elasticity of Solids*, pages 179–233. Springer International Publishing, 2020.

[78] R. J. Roark, W. C. Young, and R. G. Budynas. *Roark's Formulas for Stress and Strain*. McGraw-Hill Book Company, Inc., 7^{th} edition, 2002.

[79] P.G DeGennes. *Soft Interfaces: The 1994 Dirac Memorial Lecture*. Cambridge University Press, revised ed. edition, 2005.

[80] R. Di Leonardo, F. Saglimbeni, and G. Ruocco. Very-long-range nature of capillary interactions in liquid films. *Phys. Rev. Lett.*, 100(10), 2008.

[81] Jones R. A. L. *Soft condensed matter*. Oxford University Press, 2002.

[82] B. Andreotti and J. H. Snoeijer. Soft wetting and the shuttleworth effect, at the crossroads between thermodynamics and mechanics. *Europhys. Lett.*, 113(6):66001, 2016.

[83] R. D. Schulman, M. Trejo, T. Salez, E. Raphaël, and K. Dalnoki-Veress. Surface energy of strained amorphous solids. *Nat. Commun.*, 9(1):982, 2018.

[84] A. Sauret, A. D. Bick, C. Duprat, and H. A. Stone. Wetting of crossed fibers: Multiple steady states and symmetry breaking. *Europhys. Lett.*, 105(5):56006, 2014.

[85] S. Protière, C. Duprat, and H. A. Stone. Wetting on two parallel fibers: drop to column transitions. *Soft Matter*, 9(1):271–276, 2013.

[86] J. Bico, B. Roman, L. Moulin, and A. Boudaoud. Coalescence in wet hair. *J. Microelectromech. Syst*, 14:1083–1090, 2004.

[87] C. Duprat, S. Protiére, A. Y. Beebe, and H. A. Stone. Wetting of flexible fibre arrays. *Nature*, 482(7386):510–513, 2012.

[88] A. Sauret, F. Boulogne, D. Cébron, E. Dressaire, and H. A. Stone. Wetting morphologies on an array of fibers of different radii. *Soft Matter*, 11(20):4034–4040, 2015.

[89] D. Quéré. Fluid coating on a fiber. *Annu. Rev. Fluid Mech.*, 31(1):347–384, 1999.

[90] X-F Wu, M. Yu, Z. Zhou, A. Bedarkar, and Y. Zhao. Droplets engulfing on a filament. *Appl. Surf. Sci.*, 294:49–57, 2014.

[91] C. Fournier, Carmen L. Lee, R. D. Schulman, E. Raphaël, and K. Dalnoki-Veress. Droplet migration on conical fibers. *Eur. Phys. J. E*, 44(2):12, 2021.

[92] B. Miller, A. B. Coe, and P. N. Ramachandran. Liquid rise between filaments in a v-configuration. *Text. Res. J.*, 37(11):919–924, 1967.

[93] R. W. Style, Y. Che, S. J. Park, B. M. Weon, J. H. Je, C. Hyland, G. K. German, M. P. Power, L. A. Wilen, J. S. Wettlaufer, and E. R. Dufresne. Patterning droplets with durotaxis. *PNAS*, 110(31):12541–12544, 2013.

[94] Q. Liu and B. Xu. Liquid-evaporation-assisted self-folding of one-dimensional nanomaterials. *J. Phys. Chem. C*, 122(5):3078–3090, 2018.

[95] A. Zhu and A. Guo. Microfluidic controlled mass-transfer and buckling for easy fabrication of polymeric helical fibers. *Macromol. Rapid Commun.*, 37(5):426–432, 2016.

[96] G. R. Lester. Contact angles of liquids at deformable solid surfaces. *J. Colloid Interface Sci.*, 16:315–326, 1961.

[97] R. W. Style, R. Boltyanskiy, Y. Che, J. S. Wettlaufer, L. A. Wilen, and E. R. Dufresne. Universal deformation of soft substrates near a contact line and the direct measurement of solid surface stresses. *Phys. Rev. Lett.*, 110(6), 2013.

[98] C-Y Hui, A. Jagota, N. Nadermann, and X. Xu. Deformation of a solid film with surface tension by a liquid drop. *Procedia IUTAM*, 12:116–123, 2015.

[99] S. J. Park, B. M. Weon, J. S. Lee, J. Lee, J. Kim, and J. H. Je. Visualization of asymmetric wetting ridges on soft solids with x-ray microscopy. *Nat. Commun.*, 5, 2014.

[100] J. B. Bostwick, M. Shearer, and K. E. Daniels. Elastocapillary deformations on partially-wetting substrates: rival contact-line models. *Soft Matter*, 10(37):7361, 2014.

[101] N. Adami, A. Delbos, B. Roman, J. Bico, and H. Caps. Elasto-capillary collapse of floating structures-non-linear response of elastic structures under capillary forces. *arXiv preprint arXiv:1310.0329*, 2013.

[102] B. Audoly. Localized buckling of a floating elastica. *Phys. Rev. E*, 84(1):011605, 2011.

[103] T. Ohzono, H. Monobe, K. Shiokawa, M. Fujiwara, and Y. Shimizu. Shaping liquid on a micrometre scale using microwrinkles as deformable open channel capillaries. *Soft Matter*, 5(23):4658, 2009.

[104] M. Piñeirua, N. Tanaka, B. Roman, and J. Bico. Capillary buckling of a floating annulus. *Soft Matter*, 9(46):10985, 2013.

[105] Arthur A. Evans, Saverio E. Spagnolie, Denis Bartolo, and Eric Lauga. Elastocapillary self-folding: buckling, wrinkling, and collapse of floating filaments. *Soft Matter*, 9(5):1711–1720, 2013. Number: 5.

[106] A. Legrain, E. J. W. Berenschot, L. Abelmann, J. Bico, and N. R. Tas. Let's twist again: elasto-capillary assembly of parallel ribbons. *Soft Matter*, 12(34):7186–7194, 2016.

[107] D. Yan, K. Zhang, and G. Hu. Wrinkling of structured thin films via contrasted materials. *Soft Matter*, 12(17):3937–3942, 2016.

[108] A. Takei, F. Brau, B. Roman, and J. Bico. Stretch-induced wrinkles in reinforced membranes: From out-of-plane to in-plane structures. *EPL*, 96(6), 2011.

[109] H. Vandeparre, M. Piñeirua, F. Brau, B. Roman, J. Bico, C. Gay, W. Bao, C. N. Lau, P. M. Reis, and P. Damman. Wrinkling hierarchy in constrained thin sheets from suspended graphene to curtains. *Phys. Rev. Lett.*, 106(22), 2011. Number: 22.

[110] A. Concha, J. W. McIver, P. Mellado, D. Clarke, O. Tchernyshyov, and R. L. Leheny. Wrinkling of a bilayer membrane. *Phys. Rev. E*, 75(1), 2007. Number: 1.

[111] E. Cerda and L. Mahadevan. Geometry and physics of wrinkling. *Phys. Rev. Lett.*, 90(7), 2003. Number: 7.

[112] Q. Huang, J. Yang, W. Huang, G. Giunta, S. Belouettar, and H. Hu. The boundary effects on stretch-induced membrane wrinkling. *Thin Wall Struct*, 154:106838, 2020.

[113] B. Audoly, N. Clauvelin, and S. Neukirch. Elastic knots. *Phys. Rev. Lett.*, 99(16), 2007.

[114] R. Fulconis, A. Bancaud, J-F Allemand, V. Croquette, M. Dutreix, and J-L Viovy. Twisting and untwisting a single DNA molecule covered by RecA protein. *Biophys. J.*, 87(4):2552–2563, 2004.

[115] D. E. Smith, S. J. Tans, S. B. Smith, S. Grimes, D. L. Anderson, and C. Bustamante. The bacteriophage f29 portal motor can package DNA against a large internal force. *Nature*, 413:5, 2001.

[116] A. S. Petrov and S. C. Harvey. Packaging double-helical DNA into viral capsids: Structures, forces, and energetics. *Biophys. J.*, 95(2):497–502, 2008.

[117] P. K. Purohit, M. M. Inamdar, P. D. Grayson, T. M. Squires, J. Kondev, and R. Phillips. Forces during bacteriophage DNA packaging and ejection. *Biophys. J.*, 88(2):851–866, 2005.

[118] S. Tzlil, J. T. Kindt, W. M. Gelbart, and A. Ben-Shaul. Forces and pressures in DNA packaging and release from viral capsids. *Biophys. J.*, 84(3):1616–1627, 2003.

[119] R. Wu and T. Kim. Review of microfluidic approaches for fabricating intelligent fiber devices: importance of shape characteristics. *Lab Chip*, 21(7):1217–1240, 2021.

[120] S. Timoshenko and J. M. Gere. *Theory of Elastic Stability*. Courier Corp., 2^{nd} edition, 2012.

[121] Matilda Backholm, William S. Ryu, and Kari Dalnoki-Veress. Viscoelastic properties of the nematode caenorhabditis elegans, a self-similar, shear-thinning worm. *Proceedings of the National Academy of Sciences*, 110(12):4528–4533, 2013.

[122] J. M. T. Thompson and A. R. Champneys. From helix to localized writhing in the torsional post-buckling of elastic rods. *Proc. R. Soc. Lond. A*, 452(1944):117–138, 1996.

[123] N. Kojima. Cable kink analysis; cable loop stability under tension. *J. Appl. Mech.*, 49:585, 1982.

[124] J. Coyne. Analysis of the formation and elimination of loops in twisted cable. *IEEE J. Oceanic Eng.*, 15(2):72–83, 1990.

[125] G.H.M. van der Heijden, S. Neukirch, V.G.A. Goss, and J.M.T. Thompson. Instability and self-contact phenomena in the writhing of clamped rods. *Int. J. Mech. Sci.*, 45(1):161–196, 2003.

[126] S. Neukirch and J. F. Marko. Analytical description of extension, torque, and supercoiling radius of a stretched twisted DNA. *Phys. Rev. Lett.*, 106(13), 2011.

[127] J. Lipfert, J. W. J. Kerssemakers, T. Jager, and N. H. Dekker. Magnetic torque tweezers: measuring torsional stiffness in DNA and RecA-DNA filaments. *Nat. Methods*, 7(12):977–980, 2010.

[128] Y. Min and P. K. Purohit. Discontinuous growth of DNA plectonemes due to atomic scale friction. *Soft Matter*, 14(37):7759–7770, 2018.

[129] J. Xiao, H. Jiang, D.–Y. Khang, J. Wu, Y. Huang, and J. A. Rogers. Mechanics of buckled carbon nanotubes on elastomeric substrates. *J. Appl. Phys.*, 104(3):033543, 2008-08.

[130] J. Xiao, S. Y. Ryu, Y. Huang, K.-C. Hwang, U. Paik, and J. A. Rogers. Mechanics of nanowire/nanotube in-surface buckling on elastomeric substrates. *Nanotechnology*, 21(8):085708, 2010-02-26.

[131] T. Yabuta. Submarine cable kink analysis. *Bulletin of JSME*, 27(231):1821–1828, 1984.

[132] N. Charles, M. Gazzola, and L. Mahadevan. Topology, geometry, and mechanics of strongly stretched and twisted filaments: Solenoids, plectonemes, and artificial muscle fibers. *Phys. Rev. Lett.*, 123:208003, Nov 2019.

[133] S. Scott and Z. Ali. Fabrication methods for microfluidic devices: An overview. *Micromachines*, 12(3):319, 2021.